Defining the epithelial-to-mesenchymal transition and regulation of stemness in the ovarian surface epithelium

Lauren Carter
November 22th, 2018

Department of Cellular and Molecular Medicine
University of Ottawa
Ottawa, Ontario, Canada

This thesis is submitted as a partial fulfillment of the
Ph.D program in Cellular and Molecular Medicine.

Contributions

Manuscripts

- C.W. McCloskey, R.L. Goldberg, L.E. Carter, L.F. Gamwell, E.M. Al-Hujaily, O. Collins, E.A. Macdonald, K. Garson, M. Daneshmand, E. Carmona, B.C. Vanderhyden. (2014) A new spontaneously transformed syngeneic model of high-grade serous ovarian cancer with a tumor-initiating cell population. Frontiers in Oncology. *Frontiers in Oncology* 4: 53, 1–10.
- Vuong, N. H., D. P. Cook, L. A. Forrest, L. E. Carter, P. Robineau-Charette, J. M. Kofsky, K. M. Hodgkinson, and B. C. Vanderhyden. (In press) Single-Cell RNA-Sequencing Reveals Transcriptional Dynamics of Estrogen-Induced Dysplasia in the Ovarian Surface Epithelium. *PLoS Genetics* 14:11.
- L.E. Carter, D.P. Cook, O. Collins, L.F. Gamwell, H.A. Dempster, H.W. Wong, C.W. McCloskey, B.C. Vanderhyden. (2018) COX2 induction in the mouse and human ovarian epithelium promotes cell survival during ovulatory wound repair. *Biology of Reproduction* (Submitted).
    - Note - Sections of this manuscript are integrated into this thesis.
- L.E. Carter, D.P. Cook, C.W. McCloskey, T. Dang, O. Collins, L.F. Gamwell, H.A. Dempster, B.C. Vanderhyden. (2018) Transcriptional profiling of ovarian surface epithelial stem cells. *PNAS* (In preparation).
- A. Abedini, L.E. Carter, B.C. Vanderhyden. (2018) The opposing actions of *Wnt4* and *Wnt5a* in promoting ovulatory would repair. *Biology of Reproduction* (In preparation).

Book chapters

- L.E. Carter, D.P. Cook, B.C. Vanderhyden. (2018) Phenotypic Plasticity and the Origins and Progression of Ovarian Cancer. *The Ovary, Edition 3*, ed Peter C.K. Leung and Eli Y. Adashi. (Elsevier Academic Press), Chapter 33.
    - Note - Sections of this chapter are integrated into this thesis.

Students under supervision of Lauren Carter

1. David Cook → assisted with mOSE cell TGFB1 time course experiments and SB431542 experiments.
2. Holly Dempster → assisted in making the *Cox2* overexpressing mOSE cells and assessing their EMT status and stemness characteristics.
3. Howard Wong → assisted in assessing the pro-survival phenotype of *Cox2* overexpressing mOSE cells.

Other lab members

- David Cook → performed bioinformatics analysis for RNA-sequencing.
- Olga Collins → isolated OSE from mouse and human ovaries and performed hOSE sphere formation assays.
- Ken Garson → made the im*Snail* and i*GFP* mOSE cells and assisted in making the *Cox2* overexpressing mOSE cells.
- Curtis McCloskey → performed the BrdU pulse-chase experiments and the TGFB signalling targets PCR array.
- Lisa Gamwell → performed the stem cell PCR array.
- Tiffany Dang → assisted in assessing the stemess characteristics in *Brca1* knockout cells *in vitro*.

Contributions by collaborators

- Dr. Christopher Kennedy (University of Ottawa) → provided the *Ptger4*-floxed mice.

Contributions by core facilities

- McGill University and Génome Québec Innovation Centre, Montreal, Canada, for performing library preparation and sequencing associated with RNA sequencing.
- OHRI Core Facility, Ottawa, Canada, for performing the FACS sorting of CD44-positive mOSE cells.
- Ottawa Cell Biology and Image Acquisition Core Facility for providing access to the Essen Bioscience IncuCyte Zoom and accompanying analysis software.

Funding

- Canadian Institutes of Health Research (CIHR) grant
- Ontario Graduate Scholarship
- CIHR Reproduction, Early Development, and the Impact on Health Training Program

Thesis advisory committee members

- Dr. Jay Baltz
- Dr. Luc Sabourin
- Dr. Mike McBurney

Authorization

No authorization is required for the figures and tables presented in this thesis. There is no permission required to reproduce text and figures from the book chapter “Phenotypic Plasticity and the origins and progression of ovarian cancer”.

Abstract

The ovarian surface epithelium (OSE) is a monolayer of cells surrounding the ovary that is ruptured during ovulation. After ovulation the wound is repaired, however this process, and the mechanisms to maintain OSE homeostasis after the wound is repaired are poorly understood. We have shown the mouse OSE (mOSE) contains a stem cell population that is expanded by Transforming Growth Factor Beta 1 (TGFB1), a factor present in follicular fluid. These data suggest that components in the follicular fluid such as TGFB1 may promote wound repair and OSE homeostasis through maintenance of the OSE stem cell population. Additionally, TGFB1 may promote wound repair through induction of an epithelial-to-mesenchymal transition (EMT) and activation of pro-survival pathways, as seen in other tissues.

To elucidate the mechanism for TGFB1-mediated ovulatory wound repair, mOSE cells were treated with TGFB1, which induced an EMT seen with increased *Snai1* expression and cell migration. *Snai1* overexpression also increased cell migration and sphere formation (a stem cell characteristic). RNA sequencing results suggest this is at least in part through elevated collagen deposition in SNAI1 overexpressing cells. A TGFB signalling targets array identified *Cox2* induction following TGFB1 treatment. Constitutive *Cox2* expression did not promote an EMT, but enhanced sphere formation and cell survival. Finally, TGFB1 treatment decreased *Brca1* expression, which when deleted from mOSE cells also increased sphere formation. RNA sequencing results

suggest that *Brca1* deletion promotes stemness through activation of the stem cell genes *Ly6a* and *Lgr5*. RNA sequencing was also used to compare mOSE cells cultured as monolayers and as spheroids, with and without TGFB1. These results validate our findings that TGFB1 promotes an EMT partially through *Snail* induction and the upregulation of *Cox2*. mOSE cells cultured as spheroids acquire a mesenchymal transcriptional profile that is further enhanced with TGFB1 treatment.

These data suggest that TGFB1 may promote ovulatory wound repair and maintain OSE homeostasis through the induction of an EMT, maintenance of the stem cell population and activation of a pro-survival pathway. Interestingly, mOSE spheroids also decrease *Brca1* expression and upregulate cancer associated genes such as *Pax8* and *Greb1*. The induction of survival pathways, while simultaneously increasing stemness and repressing *Brca1* could render cells more susceptible to transformation. This work provides novel insights as to why ovulation is the primary non-hereditary risk factor for ovarian cancer.

Table of Contents

Contributions ii
Manuscripts ii
Book chapters ii
Students under supervision of Lauren Carter ii
Other lab members iii
Contributions by collaborators iii
Contributions by core facilities iii
Funding iii
Thesis advisory committee members iii
Authorization iv
Abstract v
Table of Contents vii
List of Tables xi
List of Figures xii
List of Abbreviations xv
Acknowledgments xviii
Chapter 1: Introduction 1
1.1: Phenotypic plasticity 1
Phenotypic plasticity in ovarian epithelial cells 2
1.2: The epithelial-to-mesenchymal transition 4
1.3: EMT and stemness 9
1.4: Stemness in the ovarian surface epithelium 10
Identification and characterization of stemness 10
Regulation of OSE stemness 12
1.5: Stemness in the fallopian tube epithelium 15
1.6: Phenotypic plasticity in ovulatory wound repair 19
Re-epithelialization 19
Inflammation 22
1.7: Potential consequences of cell plasticity 22
1.8: *Brca1* loss and its association with EMT, stemness and ovarian cancer risk 25

1.9: Rationale and specific aims 26
Rationale 26
Specific aims 27
Chapter 2: Materials and methods 28
2.1: OSE cell isolation and culture 28
2.2: PCR arrays 29
2.3: PGE2 ELISA 29
2.4: *Cox2* overexpressing mOSE cells 29
2.5: Inducible *Snail* expressing mOSE cells 32
2.6: Mouse superovulation 34
2.7: Quantitative reverse transcription-polymerase chain reaction (Q-PCR) 34
2.8: Western blot 37
2.9: Immunohistochemistry 40
2.10: Genotyping by PCR 40
2.11: Proliferation assay 41
2.12: Migration assay 41
2.13: Alamar Blue assay 41
2.14: Immunofluorescence 42
Actin 42
Bromodeoxyuridine (BrdU) 42
2.15: Primary sphere forming assay 43
Free-floating spheres 43
Spheres in methylcellulose 43
2.16: Secondary sphere forming assay 43
2.17: *Brca1* deletion in mOSE cells 44
2.18: BrdU pulse-chase 44
2.19: RNA sequencing (RNA-seq) 45
Sample Preparation 45
Monolayer conditions 45
Sphere forming conditions 45
Library preparation and sequencing 45
RNA-seq analysis 46
2.20: CD44 cell sorting 47

2.21: TGFBR1 inhibition 48
2.22: Statistical Analysis 48
Chapter 3: Results 49
3.1: TGFB1 induces an EMT, partially through increased *Snail* expression 49
TGFB1 induces an EMT in mouse OSE cells *in vitro* 50
TGFB1 increases *Snail* in a SMAD2/3 dependent manner 54
Forced *Snail* expression induces a partial EMT *in vitro* 56
RNA-seq of mOSE cells treated with TGFB1 reveals an upregulation of ECM deposition 59
TGFB1 induces an EMT in human OSE cells 62
Summary 64
3.2: TGFB1 increases COX2 expression to promote survival in the OSE 64
TGFB1 increases *Cox2* expression and PGE2 secretion *in vitro* 67
Forced *Cox2* expression induces a partial EMT 70
Forced *Cox2* expression increases OSE cell survival 72
COX2 is expressed during ovulatory wound repair in mouse ovaries 78
Summary 80
3.3: TGFB1 promotes stemness partially through *Snail* upregulation and *Brca1* downregulation 80
TGFB1 promotes stemness in the OSE 81
Snail expression promotes sphere formation in mOSE cells 95
COX2 expression promotes sphere formation in mOSE cells 100
Loss of BRCA1 promotes stemness in the OSE 103
Summary 113
Chapter 4: Discussion 114
4.1: Wound Repair and re-epithelialization 114
TGFB1 promotes re-epithelialization in the OSE by inducing an EMT, partially through *Snail* expression, and by promoting ECM remodelling 115
COX2 promotes cell survival during re-epithelialization 118
Potential consequences of *Cox2* induction 119
4.2: Stemness and ovarian homeostasis 120
TGFB1 promotes OSE stemness *in vitro* 121
CD44 is a marker of TGFB1-induced mOSE stemness 123

Transcriptional profile of mOSE spheres 126
Inherent stemness in mOSE cells 126
TGFB1-induced mOSE stemness 130
SNAIL overexpression and mOSE stemness 132
COX2 overexpression and mOSE stemness 133
BRCA1 loss promotes mOSE stemness 134
The OSE stemness continuum 136
OSE stemness, ovarian homeostasis and potential consequences 140
Chapter 5: Conclusion 143
References 147

List of Tables

Table Number	Table Description	Page Number
1	Overview of EMT/MET regulation in OSE and FTE cells.	13
2	Overview of the regulation of OSE and FTE stemness.	14
3	RT-PCR Primer Sequences.	35 – 36
4	Western blot antibody conditions.	38 - 39

List of Figures

Figure Number	Figure Description	Page Number
1	A schematic of the epithelial-mesenchymal transition and two models of the relationship between stemness and morphological characteristics associated with an EMT.	8
2	A timeline of publications describing putative stem cell populations of the ovarian and fallopian tube/oviductal epithelia.	18
3	WPI vector.	31
4	WPI-*Cox2* vector.	31
5	im*Snail* vector.	33
6	i*GFP* vector.	33
7	Epithelial-to-mesenchymal transition in mOSE cells treated with TGFB1 (10 ng/mL).	52
8	Gene expression analysis of mOSE cells treated with TGFB1 (10 ng/mL).	53
9	TGFB1-mediated increase in *Snail* expression is dependent on TGFBR1 signalling.	55
10	Forced *Snail* expression induces a partial EMT *in vitro*.	57
11	Forced *GFP* expression does not induce an EMT *in vitro*.	58
12	RNA sequencing results of TGFB1-treated mOSE cells (10 ng/mL) shows increased ECM deposition with treatment.	61
13	Human OSE cells treated with TGFB1 (10 ng/mL) acquire a mesenchymal phenotype and increased *SNAIL* expression.	63
14	TGFB1 Signalling Targets PCR array of mOSE cells treated with TGFB1 (10ng/mL, 96 hr).	65
15	mOSE cells treated with TGFB1 (10 ng/mL) increase *Cox2* expression and PGE2 secretion.	68

16	The TGFB1-induced increase in *Cox2* is dependent on TGFBR1 activity.	69
17	Human OSE cells treated with TGFB1 increase *COX2* expression.	69
18	WPI-*Cox2* mOSE cells have a similar amount of COX2 as mOSE cells treated with TGFB1 and exhibit a partial EMT.	71
19	Constitutive *Cox2* overexpression and PGE2 treatment activate AKT signalling in mOSE cells.	74
20	COX2 promotes a cell-survival phenotype in mOSE cells.	75
21	PTGER4 is necessary to maintain mOSE cell viability.	77
22	Immunohistochemistry detecting COX2 during ovulatory wound repair.	79
23	TGFB1 increases sphere formation in mOSE cells.	83
24	TGFB1 increases sphere formation in hOSE cells.	84
25	TGFB1 does not induce the expression of previously reported markers of OSE stemness in mOSE cells.	86
26	Stem cell PCR array of RNA extracted from mOSE cells treated with TGFB1 (10 ng/mL, 7 days).	88
27	mOSE cells treated with TGFB1 increase *CD44* expression.	89
28	mOSE cells enriched for *CD44* expression have enhanced sphere formation.	90
29	Transcriptional profiling of mOSE cells cultured as monolayer or in spheroid conditions, with or without TGFB1(10 ng/mL).	94
30	Inducible expression of *Snail* or *GFP* does not alter *Sca1* or *CD44* expression in mOSE cells.	96
31	Inducible *Snail* expression promotes sphere formation in mOSE cells.	97
32	Transcriptional profile of induced *Snail* expression in mOSE cells.	99
33	mOSE cells overexpressing COX2 have enhanced secondary sphere formation.	101

34	mOSE cells overexpressing COX2 do not have altered *CD44*, *Sca1* or *Snail* expression.	102
35	*Brca1* expression is decreased transiently by TGFB1 treatment, independent of *Snail* and *Cox2* overexpression.	104
36	*Brca1* knockout promotes *Sca1* expression and sphere formation in mOSE cells.	106–107
37	*Brca1* knockout decreases *Snail* expression in mOSE cells.	108
38	*Brca1* deletion increases label retention in mOSE cells *in vivo*.	110
39	Transcriptional profile of *Brca1* deletion in mOSE cells.	112
40	Combining the EMT and stemness continuums in mOSE cells.	139
41	Mechanism by which TGFB1 promotes ovulatory wound repair.	144

List of Abbreviations

ABC - ATP-binding cassette
Ad-*cre* - Adenovirus expressing *Cre recombinase*
Ad-*GFP* - Adenovirus expressing e*GFP*
ANCOVA – Analysis of covariance
ANOVA - Analysis of variance
APC - Allophycocyanin
bp - Base pair(s)
CD - Cluster of Differentiation
CDH1 - Cadherin-1/E-cadherin
CDH2 - Cadherin 2/N-cadherin
cDNA - Complementary DNA
ChIP-seq - Chromatin immunoprecipitation - sequencing
CLDN - Claudin
CO_2 - Carbon dioxide
DAB - Diaminobenzidine
DAPI - 4',6-diamidino-2-phenylindole
DMSO - Dimethyl sulfoxide
DNA - Deoxyribonucleic acid
dsDNA - Double stranded DNA
DSP - Desmoplakin
eCG - Equine chorionic gonadotropin
ECL - Enhanced chemiluminescence
ECM - Extracellular matrix
EGF - Epidermal growth factor
EMT - Epithelial-to-mesenchymal transition
FACS - Fluorescence-activated cell sorting
FBS - Fetal bovine serum
FGF - Fibroblast growth factor
FOX - Forkhead Box
FTE - Fallopian tube epithelium
GFP - Enhanced green fluorescent protein
GO - Gene ontology
hCG - Human chorionic gonadotropin
HEK293 cells - Human embryonic kidney 293 cells
hOSE - Human ovarian surface epithelium
hr - Hour(s)

HRP - Horseradish peroxidase
H_2O_2 - Hydrogen peroxide
IB - Intrabursal
IgG - Immunoglobulin G
IP - Intraperitoneal
ITSS - Insulin-transferrin-sodium-selenite solution
IU - International unit
KO - Knockout
LD50 - Lethal dose 50%
LoxP - Locus of X-over P1
LH - Luteinizing hormone
lncRNA - Long non-coding RNA
M - Molar
MET - Mesenchymal-to-epithelial transition
mg - Milligram(s)
min - Minute(s)
mL - Milliliter(s)
mM - Millimolar
mOSE - Mouse ovarian surface epithelium
M-PER - Mammalian protein extraction reagent
mRNA - Messenger RNA
NaOH - Sodium hydroxide
NCAM - Neural Cell Adhesion Molecule 1
ng - Nanogram(s)
OCLN - Occludin
OSE - Ovarian surface epithelium
PBS - Phosphate-buffered saline
PCR - Polymerase chain reaction
PFU - Plaque-forming units
PKPL - Plakophilin
pM - Pico molar
PVDF - Polyvinylidene difluoride
Q-PCR - Quantitative reverse transcription polymerase chain reaction
RNA - Ribonucleic acid
RNA-seq - RNA sequencing
ROS - Reactive oxygen species
RQ - Relative quantity
RT-PCR - Reverse transcription-polymerase chain reaction

rtTA - Reverse tetracycline-controlled transactivator
SB - SB431542
sec - Second(s)
S.E.M. - Standard error of the mean
SNAI1 - Snail family zinc finger 1/SNAIL
SOX - SRY Box
Stemness - stem cell characteristics
TF - Transcription factor
TGFB - Transforming Growth Factor Beta
TNF - Tumor Necrosis Factor
TPM - Transcripts per million
TRE - Tetracycline responsive element
VIM - Vimentin
WPI - pWPI
WT - wildtype
YFP - Enhanced yellow fluorescent protein
µg - microgram(s)
µL - microliter
µm - micrometer
°C - degrees Celsius

Acknowledgments

There are many people who have contributed to my success over the years and I am forever grateful. First, I would like to acknowledge Dr. Barbara Vanderhyden for her never ending support and encouragement. She is always there to challenge my experimental designs and my data interpretations, and without her I would not be the scientist I am today. I also attribute my mentoring skills to Barb's amazing guidance. I would never have foreseen myself mentoring 8 students throughout my studies if it weren't for Barb's support and encouragement.

My partner Tom Charlton has also supported me unquestionably throughout the years. He has always been there to celebrate my accomplishments, and more importantly, he has always been there to help me through my struggles. Graduate school is difficult, both mentally and emotionally, and I would not have asked to share this experience with anyone else.

My family has also been a huge support throughout this endeavor. Specifically, my parents Liane and Stuart, and my sister Kaci have only ever given me their love and support. Even though we all live in different countries, I can always count on you to be there whenever needed, and to support me through whatever challenges come my way.

People always say that success is because of a team effort and this could not be truer in Barb's lab. Everyone in the lab contributed to my success in some way or another. Thank you to everyone in the lab who has been there to bounce ideas off, to help me through my experimental failures and celebrate accomplishments with me. Specifically, thank you to Ken Garson, Olga Collins and Liz Macdonald for their training and support throughout the years. Rose Vuong, Pascale Charette, Dave Cook and Laura Forrest also need to be acknowledged. Thank you for always being there for me, not only in the lab, but also as friends. I could not imagine grad school without you and am forever grateful of your support. I have made lifelong friends in this lab and couldn't have asked for a better work environment.

It was not until grad school that I realized how important a balanced lifestyle is to my well being. Playing sports has not only helped me with my "lab rage" but has also provided me with a group of friends who I can confidently say have helped me through my studies. Specifically, with Biohazard, we might not be the best team physically, but we are definitely the best team in terms of spirit and support. I am fortunate to have played for this team during grad school and will be forever grateful for the friends I have made.

Finally, my guinea pigs Thelma and Louise deserve an acknowledgement. There is no better way to come home then to their undivided love and attention (although this might just be because they want food). They might not have contributed to my science, but they are always there to make me feel better when things aren't going my way.

Chapter 1: Introduction

1.1: Phenotypic plasticity

Cell plasticity—the ability for a cell to reversibly assume different phenotypes—is a common theme occurring throughout development, wound repair, and in cancer metastasis. It is often observed as an epithelial-to-mesenchymal transition (EMT), allowing an epithelial cell to acquire mesenchymal traits such as migration and invasion. This cell can then re-assume its epithelial phenotype through a mesenchymal-to-epithelial transition (MET), re-acquiring epithelial characteristics such as stable cell-to-cell junctions to maintain the epithelial barrier. Previously, this transition was considered a binary process where a cell could be either epithelial or mesenchymal; however, recently this transition has been thought of as a fluid transition, where cells can lie anywhere in the EMT spectrum and express combinations of epithelial and mesenchymal traits. The concept of increased stem cell characteristics, or stemness, has now been affiliated with the EMT, where cells exhibiting mesenchymal characteristics often display stem cell traits, such as the ability to form 3-dimensional clusters of cells, or spheres, *in vitro*. Although it has become increasingly apparent that the mesenchymal state coincides with stemness, a cell committing too far into the mesenchymal state loses these stemness traits, suggesting there is a window along the EMT spectrum that coincides with optimal stemness properties.

The ovarian surface and fallopian tube epithelia are two normal tissues displaying this cellular plasticity and have the capacity to gain stem cell characteristics when pushed towards the mesenchymal state. In the sections that follow, the phenotypic plasticity of these two epithelia and its importance for maintaining tissue homeostasis during ovulatory wound repair will be described. The potential consequences of this plasticity are also addressed, as both epithelia are putative origin sites for ovarian cancer. Plasticity may also reprogram the environment to promote cancer initiation and progression.

Phenotypic plasticity in ovarian epithelial cells

The ovarian surface epithelium (OSE) is a poorly differentiated simple epithelium surrounding the ovary. It is composed of flat-to-cuboidal epithelial cells derived from the coelomic epithelium during embryonic development (Auersperg et al. 2001). Initially the OSE was not thought to play a role in ovarian physiology so remained understudied until the late 1980s to early 2000s when studies emerged implicating the OSE as a tissue of origin for ovarian cancer (Auersperg et al. 2001). Since then, it has become well understood that the OSE is a layer of cells exhibiting both epithelial and mesenchymal characteristics and the cells composing the OSE layer have the capacity to interchange between each phenotype in response to environmental cues (Auersperg et al. 2001; Ahmed et al. 2007). The fallopian tube epithelium (FTE) is another accepted origin of ovarian cancer and is a layer of pseudostratified epithelial cells derived from the Mullerian duct (Stewart and Behringer 2012). Unlike the OSE, the FTE represents a

differentiated epithelium composed of ciliated and secretory cells. The ratio of ciliated and secretory cells is known to shift from ciliated cell dominance in the infundibulum to a secretory cell dominance in the isthmus (Stewart and Behringer 2012). This pattern of ciliated and secretory cells in the fallopian tube is not altered during the menstrual cycle, suggesting these cells comprise a more stable differentiated epithelium in contrast to the poorly differentiated OSE cells (Crow et al. 1994; Stewart and Behringer 2012). Ciliated FTE cells are not supported in cell culture conditions and over time result in a secretory FTE cell culture. Whether this is due to ciliated cells undergoing apoptosis or differentiating into secretory cells is unknown (Karst and Drapkin 2012). Taken together, the OSE represents a population of cells with the capacity to interchange between both epithelial and mesenchymal characteristics, whereas the FTE displays a more committed epithelial phenotype.

The ability to reversibly assume different cellular phenotypes has widely been studied in the context of an EMT, and the reverse MET, during embryonic development, cancer metastasis and wound repair. The epithelial state maintains tissue borders and acts as an epithelial barrier, whereas the mesenchymal state allows for cellular migration and invasion for growth or repair of tissues (Nieto et al. 2016; Lamouille et al. 2014; Savagner 2015). During embryonic development, epithelial cells transiently acquire a mesenchymal phenotype to allow for cellular migration. Once the cells have reached their destination, they revert to their previous epithelial state. This has classically been studied in gastrulation, neural crest cell migration, and heart morphogenesis (Savagner

2015). In the context of cancer metastasis, epithelial cancer cells assume a mesenchymal phenotype to allow for migration and invasion into neighbouring tissues where they revert back to their epithelial phenotype to establish a metastatic site (Thiery et al. 2009).

This epithelial-mesenchymal plasticity is also observed in wound repair. In the repair of an epithelial layer, cells assume a mesenchymal phenotype surrounding the injured site to allow for migration and secretion of new extracellular matrix proteins to close the wound and mediate a process referred to as re-epithelialization (Shaw and Martin 2016). The OSE layer also displays this plasticity where cells exhibiting an epithelial phenotype help maintain OSE structure and during ovulatory wound repair, these cells acquire a mesenchymal phenotype to repair the wound (Auersperg et al. 2001; Ahmed et al. 2007).

1.2: The epithelial-to-mesenchymal transition

The EMT is the process of an epithelial cell acquiring the phenotype of a mesenchymal cell. This process was first described in the primitive streak of chick embryos by Elizabeth Hay in 1995 and defined as an epithelio-mesenchymal transformation (Hay 1995). This event was later reclassified as a transition to emphasize the reversibility of this process and to differentiate it from cell transformation, a process related to cancer initiation. During the EMT process, epithelial cells lose their apical-basal polarity and acquire a front-rear polarity (Kalluri and Weinberg 2009; Lamouille et al. 2014; Savagner

2015). Epithelial cell-cell junctions are lost and cell cytoskeletal reorganization occurs, resulting in the acquisition of a spindle-like shape, characteristic of mesenchymal cell morphology (Kalluri and Weinberg 2009; Lamouille et al. 2014; Savagner 2015). Functionally, cells undergoing an EMT have enhanced migration and invasion and show resistance to apoptosis (Kalluri and Weinberg 2009; Savagner 2015). Gene expression changes commonly associated with an EMT include loss or decrease in *CDH1* (E-cadherin), *CLDN* (Claudins), *OCLN* (Occludins), *DSP* (Desmoplakin) and *PKP1* (Plakophilin) genes, all leading to a loss in epithelial barrier function (Lamouille et al. 2014). Mesenchymal gene expression commonly gained during an EMT include *CDH2* (N-cadherin), *NCAM* (Neural Cell Adhesion Molecule 1) and *VIM* (Vimentin), although specific genes can vary based on tissue type (Lamouille et al. 2014). There have been several transcription factors (TFs) identified as master EMT-driving proteins such as the SNAIL family, basic helix-loop-helix and ZEB family of TFs (ex: *SNAI1*, *TWIST1*, *ZEB1* respectively) (Lamouille et al. 2014; Savagner 2015). These traditional TFs are tightly regulated by mechanisms that have been evolutionarily conserved, highlighting their importance in normal cellular processes (Peinado et al. 2007). Additional TFs have been found to work in conjunction with the master EMT TFs such as Forkhead Box (FOX), GATA and SRY Box (SOX) TF families (Lamouille et al. 2014). Additional drivers of EMT have been studied, such as alternatively spliced mRNA of genes such as *Cluster of Differentiation (CD) 332* and *p120-catenin* and non-coding RNAs (microRNAs and lncRNAs) such as *miR-34* and *H19,* respectively (Lamouille et al. 2013; Díaz-López et al. 2014; Warzecha and Carstens 2012; Liang et al. 2015). With the emergence of high-

throughput techniques such as RNA-Seq and ChIP-Seq, more complex regulation of the EMT process is being uncovered and increasingly more interactions being identified as regulators of this program.

Recently, many studies have demonstrated that the EMT is best represented by a spectrum with the epithelial phenotype at one end, the mesenchymal phenotype at the other end, and a range of intermediate, or partial EMT in between (Lamouille et al. 2014; Nieto et al. 2016; Jolly et al. 2015; Savagner 2015). In the intermediary states, also referred to as “metastable” states, cells can possess varying levels of both epithelial and mesenchymal traits (Nieto et al. 2016). Huang et al. (2013) used 43 ovarian cancer cell lines to demonstrate the range of EMT states. Using EMT-related gene expression, they classified these tumor cell lines into 4 categories: epithelial, intermediate epithelial, intermediate mesenchymal and mesenchymal represented by 20.9%, 41.9%, 18.6% and 18.6% of cell lines, respectively (Huang et al. 2013). They found that different EMT-TFs peaked in expression levels in these categories, suggesting these EMT-TFs have different weights in dictating where the cell line falls within the EMT spectrum (Huang et al. 2013). The next year, Tan et al. (2014) developed an EMT scoring method using gene expression profiles of a variety of cancer cell types to quantitatively estimate where a particular tumor or cell line falls within this EMT spectrum. Most recently, Jolly et al. (2017) introduced the concept that the EMT spectrum is multidimensional and different EMT modulators contribute to different EMT characteristics on this spectrum. For example, the EMT characteristics migration and invasion can be represented as different

branches on the EMT spectrum and are regulated by different sets of EMT-TFs. Taken together, it is becoming increasingly apparent that the EMT is a fluid state regulated by numerous factors and cells have the capacity to shift their positioning on the spectrum based on their environmental cues (Figure 1A).

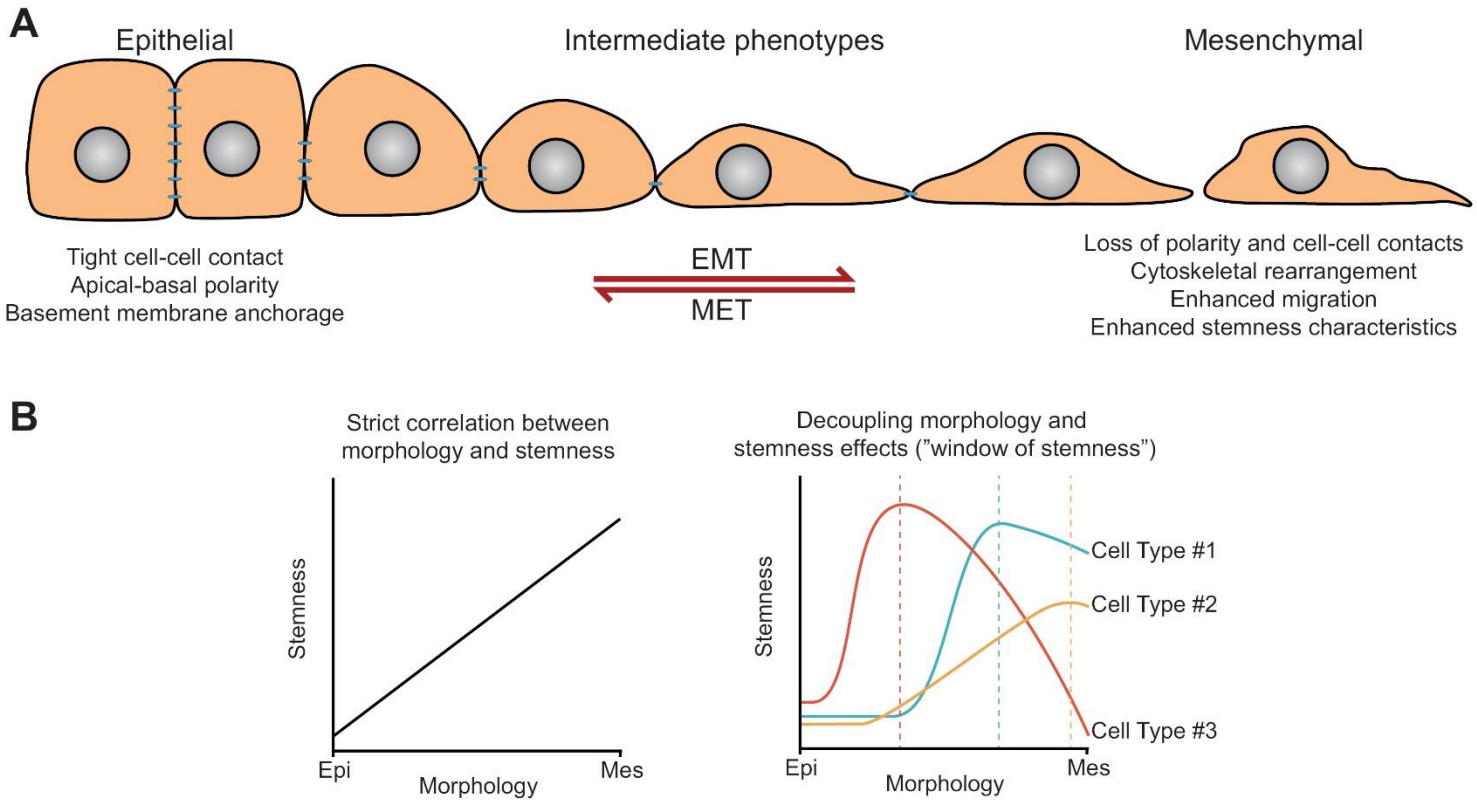

Figure 1. A) A schematic of the epithelial-mesenchymal transition, highlighting a continuous transition from an epithelial to a mesenchymal state, along with characteristics associated with each state**. B)** Two models of the relationship between stemness and morphological characteristics associated with an EMT. Historically, these traits have been thought to correlate quite strongly (left model), however recent work suggests that stemness is often optimal in an intermediate state which may be context-dependent (“window of stemness” model; right).

1.3: EMT and stemness

To further the EMT spectrum complexity, it has been demonstrated that cells undergoing an EMT can acquire stem cell characteristics (stemness) (Mani et al. 2008; Guo et al. 2012; Morel et al. 2008; Schmidt et al. 2015). Mani et al. were the first to publish this finding in 2008 using non-transformed cells. Immortalized human mammary epithelial cells induced to undergo an EMT via Transforming Growth Factor Beta (TGFB) 1 treatment or using ectopic expression of *TWIST* or *SNAIL* were found to acquire stem cell marker expression and increased mammosphere formation, which are two characteristics of stem cells (Mani et al. 2008). Guo et al. (2012) further characterized this phenomenon using transient ectopic expression of *Slug* (another EMT-TF), showing these stem cells were functional *in vivo* in a mammary gland reconstitution assay. This efficiency was enhanced when another EMT-TF commonly associated with stemness, *Sox9*, was also expressed (Guo et al. 2012). This study suggests that regulators of EMT can drive this stemness phenotype synergistically (Guo et al. 2012). In 2015, Schmidt et al. showed that constitutive *Twist1* expression induced an EMT in mammary epithelial cells, however transient expression was required to promote stemness. The authors observed that removal of *Twist1* did not fully restore cells to an epithelial state, but maintained cells in a partial EMT state where they were "primed" for stemness, suggesting there is a window of stemness within the EMT spectrum (Schmidt et al. 2015). This concept has also been inferred by Jolly et al. (2014) using a theoretical modeling of an EMT where both limits of the EMT spectrum have cells exhibiting less stemness than the intermediate zones. The authors further elaborated upon this idea by

showing that the positioning of the window of stemness on the EMT spectrum is not universal for all cell types and this positioning can be set using EMT driving factors, but "fine-tuned" using modulating factors such as Ovo Like Transcriptional Repressors (OVOL). OVOL couples with traditional EMT-driving factors to inhibit a full mesenchymal phenotype but simultaneously enhances the stemness phenotype (Jolly et al. 2015). This concept of a stemness window within the EMT spectrum has been shown in ovarian cancer cell lines where those in an intermediate EMT state possess enhanced capacity for spheroid formation and are anoikis resistant, both stemness characteristics (Huang et al. 2013). Taken together, it appears that within the EMT spectrum there is a window of stemness whose specific location is modulated by EMT-driving factors that work together to regulate where this window lies (Figure 1B).

1.4: Stemness in the ovarian surface epithelium

Identification and characterization of stemness

OSE cells are thought to contain a stem cell population that is present to maintain tissue homeostasis (Ng and Barker 2015). Since 2008, several studies have evaluated common stem cell characteristics to identify this population of cells. DNA label retention has been used to identify slow-cycling somatic stem cells that exhibit asymmetric division and retain a label for long periods of time. In comparison, lineage-committed daughter cells (which proliferate more rapidly) dilute out the label as they proliferate. Szotek et al. (2008) were the first to report a population of stem-like mouse OSE cells using this

technique. Side population analysis is another common technique used to identify a population of stem cells and can be identified using the ATP-binding cassette (ABC) pump inhibitor, Verapamil. ABC pumps are abundant in stem cells and are therefore able to efflux dyes such as Hoechst dye efficiently, whereas differentiated cells have a limited ability to do so. Szotek et al. (2008) found their population of label-retaining cells was enriched when isolating the side population present in mouse OSE cells. The following year, Bowen et al. (2009) published microarray and immunohistochemical data of human OSE cells, showing activation of stem cell quiescence and regulation pathways as well as expression of stem cell markers within these cells, suggesting these putative stem cells exist in both mouse and human ovaries. From 2012 - 2014, several publications further characterized this stem cell population in both mouse and human using *in vitro* assays such as sphere formation, and i*n vivo* assays such as lineage tracing and label retention (Gamwell et al. 2012; Flesken-Nikitin et al. 2013; Ng et al. 2014; Auersperg 2013; Suster et al. 2017). There have even been reports of OSE stem-like cells with the capacity to differentiate into additional cell types, including oocyte-like structures (Zou et al. 2009; Virant-Klun et al. 2008, 2009; Pacchiarotti et al. 2010; White et al. 2012; Johnson et al. 2004). Although many studies have identified stem cell characteristics in the OSE, there has yet to be a consensus on which marker(s) accurately represent this population of cells. One possible reason for this discrepancy in stemness markers, may be that the OSE does not have a fixed stem cell population but a transient one, that can be induced or expanded based on environmental cues.

Regulation of OSE stemness

Isolating OSE stem cells based on their gene expression may enrich for stem cell characteristics; however, there has not been any demonstration that combining stem cell marker expression purifies this population of cells, like it does in the hematopoietic system—a hierarchical stem cell model. This suggests the OSE stem cell population is best represented as a state rather than a defined population of cells, where these cells have the capacity to interchange between a "less differentiated state" exhibiting stem cell characteristics and a "more differentiated" cell state exhibiting more committed epithelial cell characteristics. Gamwell et al. (2012) showed that culturing mouse OSE cells negative for a stem cell marker *Stem Cell Antigen 1* (*Sca1/Ly6a*) in the presence of TGFB1 could convert them to a *Sca1*-positive state, exemplifying the plasticity of this cell state. Furthermore, the authors found that treating mouse OSE cells with TGFB1 (a known EMT inducer) increases stem cell characteristics, such as sphere formation, indicating this cell state is regulated by factors such as those driving an EMT. Studies examining EMT regulation and the stemness phenotype in OSE are summarized in Tables 1 and 2.

Table 1: Overview of EMT/MET regulation in OSE and FTE cells.

Cell Type	*In vitro* / *In vivo*	Species	Treatment	EMT / MET Characteristics	Ref.
OSE	*In vitro*	Human (primary culture)	Epidermal growth factor (EGF)	Mesenchymal morphology ↑ Motility ↑ Secretion of pro-matrix metalloproteinases ↑ ERK, ILK, AKT and GSK-3 signalling	(Ahmed et al. 2006)
OSE	*In vitro*	Human (immortalized cells)	Exogenous E-cadherin expression	Epithelial morphology ↑ Adherens and tight junctions ↑ Keratin expression	(Auersperg et al. 1999)
OSE	*In vitro*	Human (primary culture)	EGF + hydrocortisone	Mesenchymal morphology ↓ Keratin expression ↑ Collagenous extracellular matrix	(Salamanca et al. 2004)
OSE	*In vitro*	Human (primary culture)	Bone Morphogenetic Protein 4 Noggin	No change in cell motility	(Thériault et al. 2007)
OSE	*In vitro*	Human (primary culture)	TGFB1	Prevented formation of epithelial barrier ↓ E-cadherin, Claudin 1, Occludin, Crumbs 3 ↑ Snail, N-cadherin, Slug	(Zhu et al. 2010)
OSE	*In vitro*	Mouse (primary culture)	Exogenous *Pax8* expression	Mesenchymal morphology ↑ Migration ↑ N-cadherin and Fibronectin	(Rodgers et al. 2016)
OSE	*In vitro*	Human (primary culture)	Collagen gels	Mesenchymal morphology	(Kruk et al. 1994; Ohtake et al. 1999)
FTE	*In vitro*	Mouse (primary culture)	*Pax8* knockdown	No changes in migration or apoptosis	(Rodgers et al. 2016)
FTE	*In vitro*	Mouse (primary culture)	TGFB1	Mesenchymal morphology ↑ Migration ↑ Snail and ↓ E-cadherin	(Alwosaibai et al. 2017)

Table 2: Overview of the regulation of OSE and FTE stemness.

Cell Type	*In vitro* / *In vivo*	Species	Treatment	Stemness Characteristics	Ref.
OSE	*In vitro*	Human (primary culture)	Follicular fluid	Formation of primitive oocyte-like cells positive for alkaline phosphatase and markers of pluripotency (*SOX2*, *SSEA4*, *OCT4A*, *NANOG*, *NANOS*, *STELLA*, *CD9*, *LIN28*, *KLF4*, *GDF3*, and *MYC*)	(Virant-Klun et al. 2011)
OSE	*In vitro*	Mouse (primary culture)	Follicular fluid TGFB1 LIF	↑ stem cell marker expression (*Sca1*) ↓ proliferation, ↑ sphere formation, ↑ *Sca1* expression, converts SCA1- to SCA1+ cells ↑ sphere formation, ↓ *Sca1* expression	(Gamwell et al. 2012)
OSE	*In vivo*	Mouse	Ovulation	Label retaining cells (stem cells) are proliferative post-ovulation	(Szotek et al. 2008)
OSE	*In vivo*	Mouse	Ovulation	Ovulating OSE regions exhibit mitotically active LGR5+ cells (stem cells) LGR5+ cells respond to local Wnt signals	(Ng et al. 2014)
OSE	*In vivo*	Mouse	*miR-34* family and *miR-376b*	↓ in the stem cell population (ALDH+ cells)	(Flesken-Nikitin et al. 2013)
OSE	*In vitro*	Mouse (primary culture)	Exogenous *Pax2* expression	↓ sphere formation and stem cell marker expression (*CD44*, *Sca1*, *Lgr5*)	(Alwosaibai et al. 2017)
FTE	*In vitro*	Mouse (primary culture)	Serum	Label retaining cells ↑ expression of endometrial, proximal and distal oviductal specific genes	(Y. Wang et al. 2012)
FTE	*In vitro*	Mouse (primary culture)	TGFB1 *Pax2* knockdown	↑ stem cell marker (*CD44* expression) ↑ stem cell markers (*CD44*, *Sca1*, *CD133*) ↑ sphere formation	(Alwosaibai et al. 2017)

To this date, there have not been any direct studies in the OSE relating EMT and stemness, but this relationship has been established in other tissues as described above. As there is no agreement or coordination of stemness markers in the OSE, but there are clear stem cell phenotypes, perhaps the window of stemness is best represented by adding a second dimension to the EMT spectrum, where cells lie within the EMT spectrum based on their epithelial/mesenchymal genes and are shifted into the stemness dimension based on their stemness gene expression. This theory would allow for cells to exhibit similar functional readouts, while expressing different genes and would explain the discrepancy in some experimental findings (Figure 1B).

1.5: Stemness in the fallopian tube epithelium

Like the OSE layer, the FTE is also thought to contain a stem cell population that is present to maintain tissue homeostasis, although less is known about this population of cells. Wang et al. (2012) identified a population of label retaining cells located in the epithelium of the distal end of the mouse fallopian tube (oviduct). These cells formed spheres *in vitro* and were able to differentiate into glandular structures expressing mature Mullerian epithelial cell markers (Wang et al. 2012). The ability of these cells to contribute to FTE homeostasis was not assessed, but these cells were able to be differentiated into cell lineages of the endometrium, proximal and distal oviduct (Wang et al. 2012). Paik et al. (2012) identified a population of stem-like cells in the distal end of the human fallopian tube expressing the stem cell marker *CD44* and lacking expression of ciliated and secretory cell markers. These cells also had sphere forming

potential, suggesting this population of stem-like cells exists in the human fallopian tube as well (Paik et al. 2012). Patterson and Pru (2013) also demonstrated label retention in the distal end of the mouse oviductal epithelium. Additionally, there has been a population of cells exhibiting stem cell characteristics located at the hilum region of the mouse ovary, where the OSE and oviductal epithelium meet, that is slow cycling, expresses stem cell markers and is capable of sphere formation (Flesken-Nikitin et al. 2013). Additional stem cell markers have been found in the distal end of the mouse oviductal epithelium, such as *Lgr5* (Ng et al. 2014); however, further characterization of these cells and their regulation has not been carried out. Recently, a study from our lab showed that the stem cell characteristics in the oviductal epithelium can be enhanced with *Pax2* knockdown or TGFB1 treatment, which works in part by decreasing *Pax2* expression (Alwosaibai et al. 2017). This study directly implicates an EMT in the acquisition of stemness in the oviductal epithelium. Overviews of the characterization of EMT and stemness in the FTE are presented in Tables 1 and 2. These studies show that both OSE and FTE are capable of interchange between epithelial and mesenchymal phenotypes and when in a more mesenchymal state, exhibit stemness characteristics.

Constructing a timeline of discoveries on OSE and FTE stemness (Figure 2) emphasizes a surge in studies between 2012 - 2014, exploring the putative stem cell population in both of these epithelia. Despite this, however, momentum was lost as no further studies have been published since, with the exception of one from our lab, Alwosaibai et al. (2017), who found that knockdown of the transcription factor *Pax2* in oviductal

epithelial cells increased stem cell characteristics and forced expression in OSE cells reduced the features of stemness. This lull in activity since 2014 may be random, or perhaps it reflects the time taken to collect experimental findings. It may also reflect the recent shift the field has taken to focus on the FTE as the origin of ovarian cancer, and since *in vitro* culturing methods of FTE ciliated cells have not been optimized, progress is slowed.

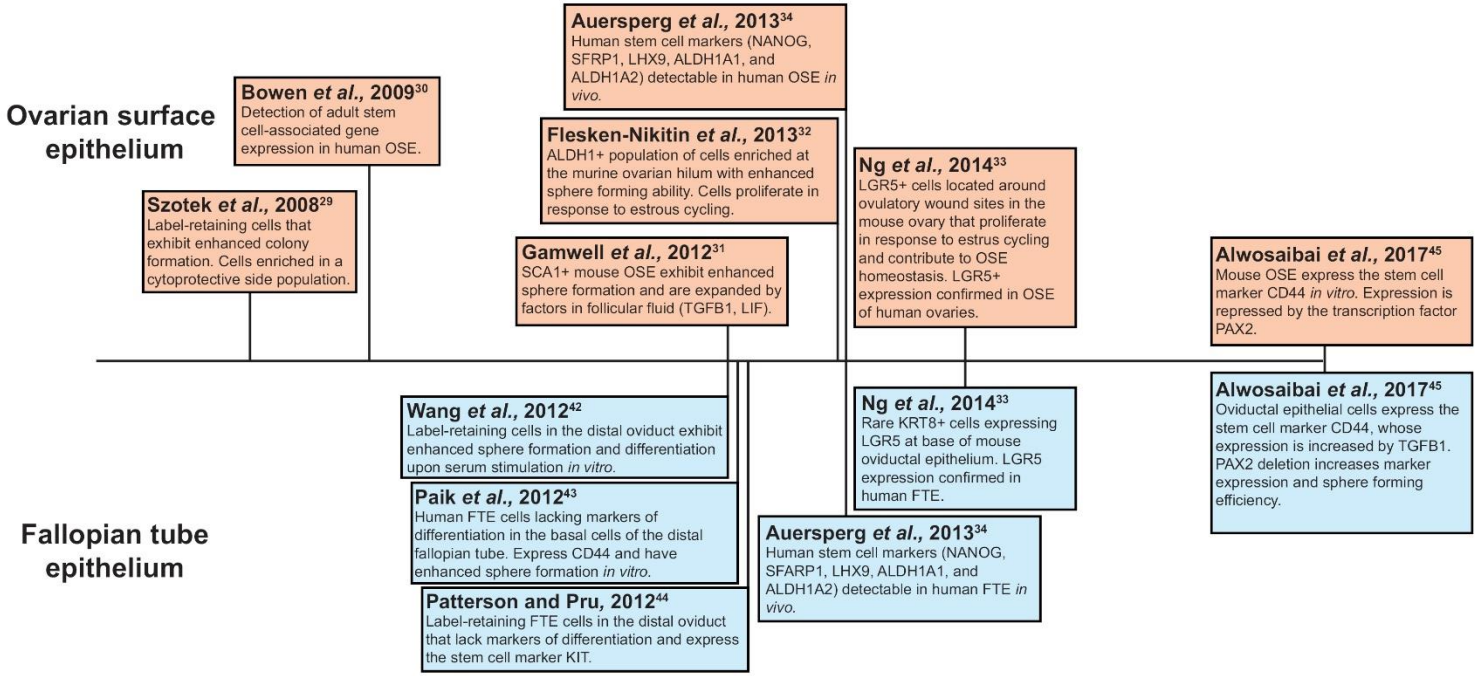

Figure 2. A timeline of publications describing putative stem cell populations of the ovarian and fallopian tube/oviductal epithelia. The field experienced a burst of activity between 2012-2014, however this has been followed by several years of inactivity.

1.6: Phenotypic plasticity in ovulatory wound repair

Ovulation, the process where the mature oocyte leaves the ovary for fertilization in the fallopian tube, is a cyclic process that is composed of three stages: the pre-ovulatory, ovulatory and post-ovulatory phases. In the pre-ovulatory phase, the dominant follicle continues to develop to the antral or Graafian stage where it is ready for ovulation. During this development, the follicle size is dramatically increased producing a stigma in the ovarian tissue overlying the follicle. In the events leading up to ovulation, the OSE layer surrounding the stigma proliferate to accommodate this change in ovarian size, whereas the OSE cells overlying non-ovulating sites remain non-proliferative (Gaytán et al. 2005; Burdette et al. 2006). Ovulation is triggered by a surge in luteinizing hormone (LH). The LH surge induces OSE cells to produce proteases, such as urokinase type plasminogen activator, which activates a proteolytic cascade that degrades extracellular matrix proteins and induces apoptosis at the apex of the ovarian stigma (Murdoch and McDonnel 2002). This epithelial cell breakdown facilitates the rupture in the OSE layer, allowing for ovulation to proceed. Once the cumulus-oocyte complex is released from the ovary, the ovulatory wound is repaired in as little as 12 hours in mice (Tan and Fleming 2004; Burdette et al. 2006).

Re-epithelialization

Wound repair is a complex event which requires synergy of multiple components to be successful. Re-epithelialization is one step in this process where cells on the edge of the wound site migrate to re-establish the damaged epithelium (Nieto et al. 2016). After

ovulation, OSE cells surrounding the wound site continue to proliferate and assume a mesenchymal phenotype, allowing for the secretion of collagen and extracellular matrix proteins (Murdoch and McDonnel 2002). Cell plasticity is also important for re-epithelialization of the OSE layer. OSE cells need to assume a mesenchymal morphology to facilitate the repair, however require the ability to re-establish their epithelial phenotype once the repair is completed to form the epithelial barrier. Recently, studies in the skin have shown that a partial EMT is induced during wound repair (Shaw and Martin 2016). This transient reprogramming of the wound edge cells facilitates their migration and invasion into the wound site as a cohesive cohort and not as individual cells (Savagner 2015). During this transient reprogramming, intermediate filaments are retracted, breakdown of the basement membrane occurs, and epithelial cells lose their polarity. Once cell migration has taken place, these cells re-form their cell-substrate contacts (Savagner et al. 2005). During this repair process, cells maintain their cytokeratin expression and desmosomes, further implying these cells undergo a partial EMT (Savagner 2015). This partial EMT can be seen in the OSE cell layer which maintains expression of Keratin 8 and E-cadherin throughout ovulatory wound repair (Singavarapu et al. 2010).

During ovulatory rupture, follicular fluid from the antral follicle bathes the OSE layer surrounding the rupture site. A recent study assessed the composition of human follicular fluid and found proteins belonging to several functional groups such as insulin growth factor (IGF) and insulin growth factor binding protein families, growth factors

and related proteins, receptor signalling, defense/immunity, anti-apoptotic proteins, matrix metalloprotease-related proteins, and complement activity (Zamah et al. 2015). The authors found that once ovulation was induced (following human chorionic gonadotrophin treatment), the composition shifted to include more proteins belonging to the protease inhibition, inflammation, and cell adhesion families (Zamah et al. 2015). Many of these follicular fluid components are known inducers of an EMT such as TGFB1 and IGF. These components may help facilitate the transient reprogramming of the remaining OSE cells to an EMT state to aid in wound repair.

OSE undergoing re-epithelialization around the wound site also gain expression of the stem cell marker *Lgr5,* suggesting this partial EMT allows for re-epithelialization and also induces stemness, necessary to maintain homeostasis (Ng et al. 2014). Furthermore, Gamwell et al. (2012) showed that treating OSE cells with follicular fluid enhances their stem cell characteristics, suggesting ovulatory wound repair expands this population (Gamwell et al. 2012). The concept that ovulation changes the OSE stem cell profile partially explains why there has not been agreement on the gene markers for this population of cells. Different factors produced in the surrounding ovarian tissue likely interact with the OSE layer to promote this stem-like state to maintain tissue homeostasis. Since these factors are complex and transient within the ovary, it is not probable that one marker of stemness will be found that represents all stem cells, but it is possible to describe these cells as a state within the spectrum.

Inflammation

Another important player in wound repair is the immune system. In adult tissues, wound repair relies heavily on a functional immune response. Wound repair is hindered when the immune response is impaired (Shaw and Martin 2016). For example, inhibiting macrophage function has been shown to delay tissue repair in rabbits and mice (Leibovich and Ross 1975; Lucas et al. 2010). Inflammation occurring after an epithelial wound recruits primarily neutrophils and macrophages to the wound site which work together to clear the wound debris (Shaw and Martin 2016). In the ovary, these immune cells home to the forming corpus luteum after ovulation in the mouse, rat and human (Brannstrom et al. 1994; Brannstrom et al. 1994; Cohen et al. 1997). Inflammation also supports re-epithelialization through the secretion EMT-driving factors such as TGFB1 and Tumor Necrosis Factor (TNF) alpha, which act on the epithelial cells surrounding the wound site (Shaw and Martin 2016; López-Novoa and Nieto 2009; Karin and Clevers 2016). As mentioned above, human follicular fluid also becomes more proinflammatory at ovulation, suggesting follicular fluid contributes to the inflammatory response (Zamah et al. 2015). Taken together, inflammation occurring during wound repair is important to facilitate this repair by altering the ovarian niche to be more inflammatory and promote an EMT in the repairing epithelium.

1.7: Potential consequences of cell plasticity

Ovulation is a cyclic event, occurring once every 28 days in women of reproductive age. It is also the primary non-hereditary risk factor for ovarian cancer, with the number of

ovulatory cycles being proportional to ovarian cancer risk (Jayson et al. 2014). This suggests that ovulation, or ovulatory wound repair, can lead to ovarian cancer initiation. During each cycle, the repairing OSE layer proliferates and undergoes a partial EMT. During this time, the cells surrounding the wound site also interact with the inflammatory agents present in the follicular fluid. Cells exhibiting a mesenchymal phenotype display resistance to apoptosis and therefore can survive harsh environmental conditions; however, this cell survival may allow the accumulation of DNA damage over time. Murdoch and Martinchick assessed the surviving OSE cells surrounding the ovulatory rupture site and found 8-oxoguanine modifications in these cells, indicating DNA damage (Murdoch and Martinchick 2004). As these cells undergoing an EMT also have enhanced stemness characteristics, it is conceivable these cells may develop DNA mutations that are propagated over time and can lead to ovarian cancer initiation.

The inflammation accompanying wound repair is tightly regulated since its dysregulation could have severe consequences. Improper wound repair in other tissues such as the liver, kidney and lung results in tissue scarring and fibrosis, leading to chronic inflammation (Nieto et al. 2016). This chronic inflammation results in persistent secretion of EMT-driving factors and maintenance of the EMT state in the epithelium (Kalluri and Weinberg 2009). As EMT is related to stemness characteristics, chronic inflammation in the ovary could also increase the stem cell characteristics in the OSE and distal FTE, which over time could transform into a cancer initiating cell. Briley et al.

(2016) reported that fibrosis in the mouse ovary increases with age and number of ovulatory cycles. Although this has yet to be established in humans, ovarian fibrosis is known to be associated with reduced fertility in women with polycystic ovarian syndrome (Zhou et al 2017). It is possible that fibrosis in the human ovary increases with age and the associated chronic inflammation could promote both an EMT and stemness in the OSE and FTE. This combination of events theoretically could provide a microenvironment conducive to cell transformation and the development of neoplastic lesions. This hypothesis could help to explain why the median age of ovarian cancer detection is post-menopausal, after the age-associated accumulation of post-ovulatory repair events results in ovarian fibrosis and inflammation (Jayson et al. 2014).

The FTE is another site of origin for ovarian cancer and is also affected by ovulation. The follicular fluid that is expelled from the ovary comes into contact with the distal FTE cells. Like in the OSE layer, the follicular fluid components may drive an EMT phenotype, induce DNA damage and promote stemness in the FTE. This concept is supported by Alwosaibai et al. (2017) who found that treating FTE cells with TGFB1, a component of follicular fluid, induced an EMT and increased the expression of stem cell markers. Interestingly, these effects were mediated in part by downregulation of *Pax2*, a transcription factor commonly lost in serous tubal intraepithelial carcinomas, a precursor lesion for ovarian cancer. Furthermore King et al. (2011) detected pro-inflammatory macrophages in the oviduct of superovulated mice as well as increased levels of phospho-gH2A.X, a marker of DNA damage, in the oviductal epithelial cells.

Taken together, the plasticity exhibited during wound repair by both the OSE and FTE layers may enable wound repair to take place and work to maintain tissue homeostasis. Under the inflammatory conditions of wound repair, however, it may change the ovarian niche to result in more DNA damage and promote transformation.

1.8: *Brca1* loss and its association with EMT, stemness and ovarian cancer risk

Brca1/*2* loss is the primary genetic risk factor for ovarian cancer, where *Brca1*/*2* mutations account for 95% of hereditary ovarian cancers (Reid et al. 2017). BRCA1 loss is also present in up to 30% of sporadic ovarian cancers due to epigenetic regulation such as promoter methylation (Turner et al. 2004). BRCA1 functions as a DNA repair enzyme, playing a role in regulating signal transduction during homologous recombination (Lord and Ashworth 2016; Starita and Parvin 2003). It is also known to have functions as a chromatin remodeler and transcriptional regulator, and has ubiquitin ligase activity (Lord and Ashworth 2016; Starita and Parvin 2003). There have been many reports suggesting BRCA1 loss promotes stem cell characteristics and induces an EMT in the normal and transformed mammary epithelium (Molyneux et al. 2010; Lim et al. 2009; Proia et al. 2011; Bai et al. 2013, 2014). Most recently, Bai et al. (2014) found that in the mammary epithelium, BRCA1 suppresses an EMT and dedifferentiation of luminal stem cells. They proposed that BRCA1 negatively regulates an EMT and stemness by binding the promoters of mesenchymal transcription factors such as *Twist* and *Foxc1*. Whether *Brca1* regulates stemness or an EMT in the ovarian surface epithelium is unknown,

however if this relationship does apply, then a dysregulation of DNA repair in a population of cells with enhanced stem cell characteristics, may lead to a transformation event and support the incessant ovulation hypothesis for ovarian cancer initiation that postulates that ovulation plays a role in the development of ovarian cancer by contributing to OSE transformation (Fathalla 1971).

1.9: Rationale and specific aims

Rationale

Gamwell et al. (2012) found that culturing OSE cells in the presence of follicular fluid enhanced their stem cell characteristics. When exploring the factors present in follicular fluid, they found TGFB1 to be a key component, that when added to mouse OSE (mOSE) cultures, also increased these stem cell characteristics. As TGFB1 is known to be a strong inducer of an EMT, we hypothesize that TGFB1 increases OSE stemness through the induction of an EMT. A TGFB1 signalling targets PCR array was used to determine the targets of TGFB1 treatment that may induce an EMT and increase stemness in OSE cells. *Cyclooxygenase 2* (*Cox2*) was the gene found to be most increased (8-fold) by TGFB1 treatment. *Cox2* has been implicated in stem cell maintenance, inducing an EMT as well as promoting cell survival in other tissues, and therefore may play a role in promoting ovulatory wound repair and maintenance of OSE homeostasis (Guo and Dipietro 2010; Aoudjit et al. 2006). **We hypothesize that at ovulation, TGFB1 induces an EMT, expands**

the stem cell population, and promotes a survival phenotype through *Cox2* expression in the OSE to mediate ovulatory wound repair and to maintain OSE homeostasis.

Specific aims

Three aims were used to address this hypothesis.

(1) To evaluate the signalling pathway of a TGFB1-induced EMT in OSE cells.

(2) To determine the role of TGFB1-induced COX2 in the OSE.

(3) To characterize the OSE stem cell population and its response to TGFB1 treatment.

Chapter 2: Materials and methods

2.1: OSE cell isolation and culture

mOSE cells were isolated from mouse ovaries as previously described (Gamwell et al. 2012). Briefly, ovaries were isolated from randomly cycling, 6-week-old FVB/N mice. Ovaries were incubated in 0.25 % Trypsin/PBS (Invitrogen) at 37 °C, 5% CO_2 for 30 min to remove the OSE layer. mOSE cells were isolated via centrifugation and plated onto tissue-culture plates (Corning) in mOSE media consisting of a-Minimum Essential Medium (Corning) supplemented with 4% FBS, 0.01 mg/mL insulin-transferrin-sodium-selenite solution (ITSS; Roche), and 2 μg/mL EGF (R&D Systems). Human OSE (hOSE) cells were isolated from one ovary from each of 5 different women as previously described (Tonary et al. 2000). Briefly, ovaries were obtained from women undergoing surgery for reasons other than ovarian pathology. OSE cells were scraped from the ovarian surface using a scalpel blade and transferred into hOSE media that was purchased from Wisent Bioproducts and supplemented with 10% FBS. OSE cells were isolated via centrifugation and plated onto tissue culture plates (Corning). All mouse and human OSE cells were passaged 2-3 times prior to experimental use and experiments were conducted with cells of a passage number less than 25.

2.2: PCR arrays

mOSE cells (1x10^6 cells) were plated 24 hr prior to treatment with TGFB1 (10 ng/mL, R&D Systems). For the TGFB1 signalling targets PCR array, RNA was collected 96 hr post-TGFB1 treatment (RNAeasy Kit, Qiagen). RNA was collected for the Stem cell PCR array 7 days post-TGFB1 treatment. cDNA synthesis was performed using RT^2 First Strand Kit (Qiagen) and run on the RT^2 Profiler Array - TGFB (TGFB signalling targets PCR array) or RT^2 First Strand Kit (Stem cell PCR array) (Qiagen). The arrays were run in triplicate (N=3) and analyzed using the DataAnalysis Excel platform provided with the array kits.

2.3: PGE2 ELISA

Media was collected from mOSE cell cultures in TGFB1-treated (10 ng/mL, R&D Systems) or untreated conditions and diluted 1:500 using fresh mOSE media. PGE2 concentrations were determined using the Prostaglandin E2 EIA Kit - Monoclonal (Cayman Chemical) as per manufacturer's directions. Analysis was performed using the excel platform provided with the kit and values were expressed as concentration of PGE2 in media per cell number.

2.4: *Cox2* overexpressing mOSE cells

The vector pWpi (referred to as WPI, Figure 3) was given as a gift from Didier Trono (Addgene plasmid # 12254). WPI encodes enhanced *GFP* (referred to as *GFP*) regulated by the *EF1-alpha* promoter. Murine *Cox2* cDNA was cloned from mOSE cells using the In-

Fusion PCR Cloning Kit (Clontech) following the manufacturer's protocol and then used to generate the lentivirus expression vector WPI-*Cox2*-IRES-*GFP* (referred to as WPI-*Cox2*, Figure 4). Lentiviral vectors were prepared by transfecting human embryonic kidney 293 (HEK293) cells (American Type Culture Collection). Viruses were harvested by collecting the media from the transfected cells 48 hr post-transfection and filtered using a 45 µm filter. mOSE cells were infected with 200 µL of either the WPI-*Cox2* or WPI virus. Infected mOSE cells were isolated using fluorescence-activated cell sorting (FACS) for GFP expression.

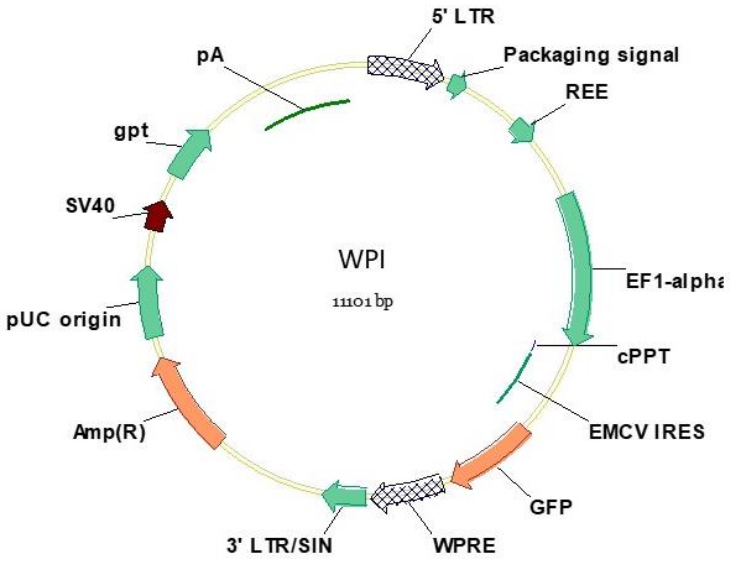

Figure 3: WPI vector.

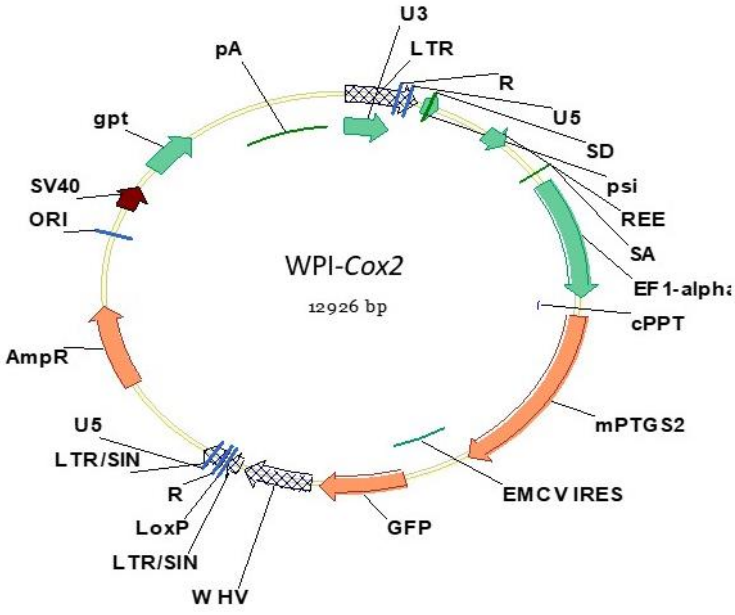

Figure 4. WPI-*Cox2* vector.

2.5: Inducible *Snail* expressing mOSE cells

mOSE cells were transduced with the lentiviral vector pEF1-tet and selected with G418 to generate the cell line mOSE-tet. pEF1-tet is a derivative of pLVX-Tet-On Advanced (Clontech) utilizing the human *EF1-alpha* promoter to drive the expression of reverse tetracycline-controlled transactivator (rtTA) and neomycin resistance. The mOSE-tet cell line was subsequently transduced with the lentiviral vector im*Snail* (Figure 5) and selected in hygromycin B. im*Snail* is a derivative of pLVX-Tight-Puro (Clontech) designed to express the murine *Snai1* under the control of the doxycycline inducible promoter (TRE) and hygromycin resistance under the control of the *PGK* promoter. As a control, the mOSE-tet cell line was transduced with the lentiviral vector i*GFP* (Figure 6) and selected in hygromycin B. i*GFP* is a derivative of pLVX-Tight-Puro (Clontech) designed to express the *eGFP* under the control of the doxycycline inducible promoter (TRE) and hygromycin resistance under the control of the *PGK* promoter.

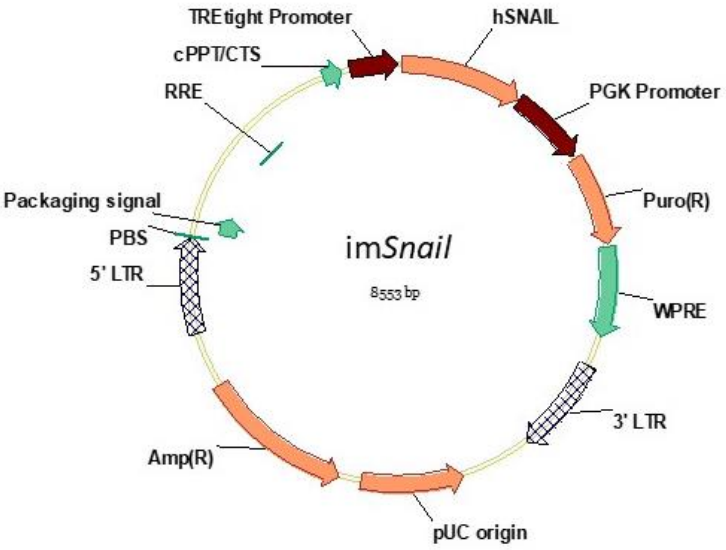

Figure 5. im*Snail* vector.

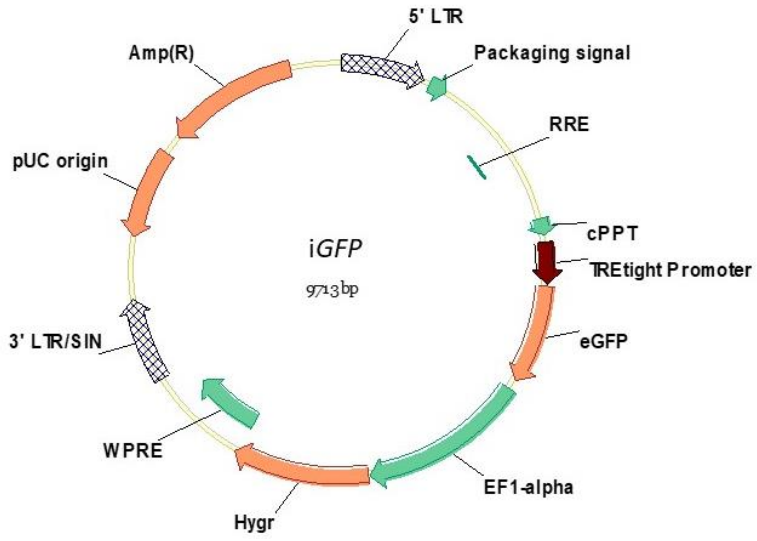

Figure 6. i*GFP* vector.

2.6: Mouse superovulation

FVB/N female mice were injected intraperitoneally (IP) with 5 IU of equine chorionic gonadotropin (eCG; Calbiochem) followed by 5 IU of human chorionic gonadotropin (hCG; Sigma) 46 hr later. Ovaries were collected 14-18 hr after hCG injection in order to assess ovulatory wound sites in these ovaries. They were fixed overnight in 10% formalin and paraffin embedded.

2.7: Quantitative reverse transcription-polymerase chain reaction (Q-PCR)

RNA extraction, cDNA synthesis and Q-PCR was performed as previously described (McCloskey et al. 2014). Briefly, RNA was extracted using the RNeasy Mini Kit (Qiagen) and cDNA was synthesized using the OneStep RT-PCR Kit (Qiagen). The ABI 7500 FAST qRT-PCR machine (Applied Biosystems) was used for Q-PCR using the Taqman gene expression (Life Technologies) and SsoFast gene expression (Bio-rad) assays. *Tbp* was used as an endogenous control for the assays. Primer sequences are listed in Table 3. RQ (relative quantity) was determined using the cycling threshold for the gene of interest in control or untreated samples compared to the cycling threshold in experimental samples, calculated using the Applied Biosystems 7500 FAST v2.3 software.

Table 3: RT-PCR Primer Sequences.

Gene	Species	Primer Sequence (5'-3')
Snail	Mouse	Forward - GTC TGC ACG ACC TGT GGA A Reverse - CAG GAG AAT GGC TTC TCA CC
Krt19	Mouse	Forward - TGA CCT GGA GAT GCA GAT TG Reverse - CCT CAG GGC AGT AAT TTC CTC
Zeb1	Mouse	Forward - GCC AGC AGT CAT GAT GAA AA Reverse - TAT CAC AAT ACG GGC AGG TG
Alcam	Mouse	Forward - AAA CTC CCT GAA TGT CTC TGC Reverse - AGA CCA ACG ACA ATT CCC AC
Twist	Mouse	Forward - AGC TAC GCC TTC TCC GTC T Reverse - TCC TTC TCT GGA AAC AAT GAC A
Cox2	Mouse	Forward - CAA AAG AAG TGC TGG AAA AGG T Reverse - GGA TGA ACT CTC TCC GTA GAA GA
TBP	Mouse	Forward - GGC GGT TTG GCT AGG TTT Reverse - GGG TTA TCT TCA CAC ACC ATG A
CD44 (total)	Mouse	Forward - CAC CAT TTC CTG AGA CTT GCT Reverse - TCT GAT TCT TGC CGT CTG C
CD44 (v1)	Mouse	Forward - GCC TCA ACT GTG CAC TCA AA Reverse - GTT GTG GGC TCC TGA GTC TG
CD44 (v2)	Mouse	Forward - GAT GAC CAC CCC TGA AAC AC Reverse - GGC ATC TTC GTT GTT GTA TGA A
CD44 (v3)	Mouse	Forward - GGA GTC AAA TAC CAA CCC AAC Reverse - ATC ATC ATC AAT GCC TGA TCC
CD44 (v4)	Mouse	Forward - GCA AGT ACT CCA CGG GTT TC Reverse - ATC CTG GTG GTT GTC TGG AG
CD44 (v5)	Mouse	Forward - CAG CAC CAG TGC TCA TGG A Reverse - GCT TGT AGC ATG TGG GGT CT
CD44 (v6)	Mouse	Forward - AGC AGA AGC AGC AGC TAC CC Reverse - CCC TTC TGT CAC ATG GGA GT
CD44 (v7)	Mouse	Forward - CCC ACA ACA ACC ATC CAA GT Reverse - TTG ATG ACC TTG TCC CAT TG

Table 3 continued.

CD44 (v8)	Mouse	Forward - ATA CAG ACT CCA GTC ATA GTA CAA CC Reverse - GAG TTG TCA CTG AAA GTG GTC CT
CD44 (v9-10)	Mouse	Forward - TAC ATG GAG AGC CCG GAA GAA Reverse -GTT TTA GCA GGG GTC ACT GG
CD44 (v10)	Mouse	Forward - GGC CGT AAA GAT GCA AGA AG Reverse - CTG GTA AGG AGC CAT CAA CA
Aldh1	Mouse	Forward - ACC CAG TTC TCT TCC ATT TCC Reverse - CAT CAC TGT GTC ATC TGC TCT
Lgr5	Mouse	Forward - GTC AAA GCA TTT CCA GCA AGA Reverse - CTC CAA CCT CAG CGT CTT C
Nanog	Mouse	Forward - CAG AAG GGC TCA GCA CCA G Reverse - AGG CTT CCA GAT GCG TTC A
Lhx9	Mouse	Forward - CAG GCC TGA CCA AAA GAG TT Reverse - TGC CGT CAG CTT TAT CAA CA
Sfrp1	Mouse	Forward - CAG TTG TGG CTT TTG CAT TG Reverse - GAG GGA AGG GAG AGG GTT C
Sca1	Mouse	Forward - GAC CCT GGA GGC ACA CAG CC Reverse - CAT GTG GGA ACA TTG CAG GAC CCC
Brca1	Mouse	Forward - GCT GCA GCT GTG TGG GGG CTT Reverse -CCC GAC ACC GGT AGC TGG AT
SNAIL	Human	Forward - GCT GCA GGA CTC TAA TCC AGA Reverse - ATC TCC GGA GGT GGG ATG
COX2	Human	Forward - CTT CAC GCA TCA GTT TTT CAA G Reverse - TCA CCG TAA ATA TGA TTT AAG TCC AC
TBP	Human	Forward - GAA CAT CAT GGA TCA GAA CAA CA Reverse - ATA GGG ATT CCG GGA GTC AT
CD44	Human	Forward - GGC ATT GAT GAT GAT GAA GAT TT Reverse - GCA GTA GGC TGA AGC GTT GT
BRCA1	Human	Forward - TTG GTT TTT GTG GTA ATG GAA AAG TGT Reverse - CAA AAA ATC TCA ACA AAC TCA CAC CA

2.8: Western blot

Protein was extracted and used for western blot analysis as previously described (McCloskey et al. 2014). Briefly, protein from mOSE cells was extracted using M-PER mammalian protein extraction reagent (GE Healthcare) as per manufacturer's directions and run on NuPAGE 4-12% Bis-Tris gradient gels (Life Technologies). Protein samples were transferred to a polyvinylidene difluoride membrane and were then blocked in 5% non-fat milk or 5% bovine serum albumin prior to antibody incubation. Antibody conditions are described in Table 4. Western blots were developed using Clarity™ Western ECL Substrate (Bio-Rad) and the FluorChem FC2 imaging system (Alpha Innotech).

Table 4: Western blot antibody conditions

Primary Antibody		Secondary Antibody	
Antibody Details	**Incubation Details**	**Antibody Details**	**Incubation Details**
Rabbit anti-Snail (Abcam, ab82846)	1:500 in 5 % non-fat milk overnight, 4 °C	Donkey anti-Rabbit IgG HRP conjugated (GE HEalthcare Life Sciences, NA934)	1:5,000 in 5 % non-fat milk 1 hr, room temperature
Mouse anti-Cdh1 (BD Transduction Laboratories, 610182)	1:5,000 in 5 % non-fat milk overnight, 4 °C	Goat anti-Mouse IgG HRP conjugated (Abcam, ab6728)	1:5,000 in 5 % non-fat milk 1 hr, room temperature
Rabbit anti-PSmad2 (NEB Cell Signalling, 3101S)	1:1,000 in 5 % BSA overnight, 4 °C	Donkey anti-Rabbit IgG HRP conjugated (GE HEalthcare Life Sciences, NA934)	1:2,000 in 5 % non-fat milk 1 hr, room temperature
Rabbit anti-PSmad3 (NEB Cell Signalling, 9520S)	1:500 in 5 % BSA overnight, 4 °C	Donkey anti-Rabbit IgG HRP conjugated (GE HEalthcare Life Sciences, NA934)	1:2,000 in 5 % non-fat milk 1 hr, room temperature
Rabbit anti-Smad2 (Invitrogen, 511300)	1.0 µg/mL in 5 % non-fat milk overnight, 4 °C	Donkey anti-Rabbit IgG HRP conjugated (GE HEalthcare Life Sciences, NA934)	1:5,000 in 5 % non-fat milk 1 hr, room temperature
Rabbit anti-Smad3 (Invitrogen, 511500)	1.25 µg/mL in 5 % non-fat milk overnight, 4 °C	Donkey anti-Rabbit IgG HRP conjugated (GE HEalthcare Life Sciences, NA934)	1:5,000 in 5 % non-fat milk 1 hr, room temperature
Rabbit anti-Cox2 (Abcam, ab15191)	1:1,000 in 5 % non-fat milk overnight, 4 °C	Donkey anti-Rabbit IgG HRP conjugated (GE HEalthcare Life Sciences, NA934)	1:5,000 in 5 % non-fat milk 1 hr, room temperature
Mouse anti-β-Actin (Sigma, A2228)	1:80,000 in 5 % non-fat milk 1 hr, room temperature	Goat anti-Mouse IgG HRP conjugated (Abcam, ab6728)	1:20,000 in 5 % non-fat milk 1 hr, room temperature

Table 4 continued.

Mouse anti-GAPDH (Abcam, ab8245)	1:80,000 in 5 % non-fat milk 1 hr, room temperature	Goat anti-Mouse IgG HRP conjugated (Abcam, ab6728)	1:20,000 in 5 % non-fat milk 1 hr, room temperature
Rabbit anti-CD44 (Abcam, ab41478)	1 µg/mL in 5 % non-fat milk overnight, 4 °C	Donkey anti-Rabbit IgG HRP conjugated (GE HEalthcare Life Sciences, NA934)	1:5,000 in 5 % non-fat milk 1 hr, room temperature
Rabbit anti-BRCA1 (Santa Cruz, c-20)	1:250 in 5 % non-fat milk overnight, 4 °C	Donkey anti-Rabbit IgG HRP conjugated (GE HEalthcare Life Sciences, NA934)	1:10,000 in 5 % non-fat milk 1 hr, room temperature
Rabbit anti-AKT (Cell Signaling, 9272S)	1:1000 in 5 % non-fat milk overnight, 4 °C	Donkey anti-Rabbit IgG HRP conjugated (GE HEalthcare Life Sciences, NA934)	1:10,000 in 5 % non-fat milk 1 hr, room temperature
Rabbit anti-Phospho AKT (Cell Signaling, 9271S)	1:1000 in 5 % BSA overnight, 4 °C	Donkey anti-Rabbit IgG HRP conjugated (GE HEalthcare Life Sciences, NA934)	1:10,000 in 5 % BSA 1 hr, room temperature

2.9: Immunohistochemistry

Tissue sections from superovulated mouse ovaries were used for immunohistochemical analysis as previously described (McCloskey et al. 2014). Briefly, 5 µm sections were deparaffinized in xylenes and rehydrated in an ethanol gradient. Endogenous peroxidase activity was blocked using 3% hydrogen peroxide (H_2O_2) and endogenous avidin and biotin were blocked using an Avidin/Biotin Blocking kit (Dako). Tissue sections were then blocked in a Serum-Free Blocking Reagent (Dako). Sections were incubated overnight at 4 °C in mouse anti-COX2 (Abcam, ab15191) diluted 1:1500 using Antibody Diluent (Dako). Tissue sections were incubated in anti-rabbit horseradish peroxidase-labeled polymer (Dako) for 30 min at room temperature and developed using diaminobenzidine. Sections were counterstained with hematoxylin, dehydrated using an ethanol gradient and mounted using Permount (Fisher Scientific). The Scanscope CS2 (Aperio) was used to acquire images.

2.10: Genotyping by PCR

OSE cells were isolated from *Ptger4*$^{fl/fl}$ mice (Schneider et al. 2004) as described in Section 2.1 and DNA was extracted using the DNeasy Blood and Tissue Kit (Qiagen). DNA was used in PCR analysis using the CloneAmp Hifi PCR Premix (Takara) to detect the unrecombined *Ptger4* gene and the recombined *Ptger4* gene using the following primer pairs: unrecombined: Forward - 5' GGA GTC ACT TTT CCC TTG AGA AG 3' and Reverse - 5'AAC GAG CCA TTT ACC ACT TGC AA 3', recombined: Forward - 5' GGA GTC ACT TTT

CCC TTG AGA AG 3’ and Reverse - 5’CGA GTC CTT AGG CTT TTA AGT GGA 3’. The PCR reaction was run under the following conditions: 94 °C 2 min initial denaturation, 94 °C 10 sec, 62 °C 15 sec, 72 °C 2 min for 35 cycles, 7 °C 5 min.

2.11: Proliferation assay

mOSE cells (5x10^4/well) were seeded into 24-well tissue culture plates (Corning) in mOSE media. Proliferation was assessed by counting viable cells using the Vi-CELL XR cell viability analyzer (Beckman Coulter) for each day of the experiment.

2.12: Migration assay

mOSE cells (7x10^4/well) were plated into 96-well tissue culture plates (Essen ImageLock, Essen Instruments) with or without TGFB1 (10 ng/mL, R&D Systems), 24 hr prior to scratch assay. The scratch assay was performed using the Wound Maker (Essen Instruments) and wound confluence was monitored every 2 hr with the Incucyte Live-Cell Imaging System and software (Essen Instruments).

2.13: Alamar Blue assay

mOSE cells (1x10^4/well) were seeded into 96-well tissue culture plates (Corning) 24 hr prior to administration of treatment. AlamarBlue (Life Technologies) was added to each well and incubated for 8 hr. Fluorescence was measured using excitation and emission values of 530 nm and 590 nm, respectively, using the Fluoroskan Ascent FL (Thermo Scientific).

2.14: Immunofluorescence

Actin

mOSE cells were plated on glass coverslips in mOSE media 24 hr prior to TGFB1 treatment (10 ng/mL, R&D Systems). Cells were fixed with 4% paraformaldehyde for 30 min and permeabilized with 0.2% Triton X-100 (10 min). Cells were probed for ACTIN using ActinRed™ 555 ReadyProbes® Reagent (Life Technologies) following manufacturer's directions and mounted using a DAPI stain (ProLong Gold Antifade Mountant, Thermo Fisher Scientific). Images were acquired with a fluorescence microscope (Zeiss).

Bromodeoxyuridine (BrdU)

Frozen sections (5 µm) were fixed using formalin-vapor fixation (Jockusch, Voigt, and Eberhard 2003) overnight at -20 °C. Samples were then hydrated in PBS and antigen retrieval performed using an antigen unmasking solution (pH 6.0, Vector) in a steam chamber (Hamilton Beach). Slides were then washed in PBS and blocked with 5% goat serum for 1 hr at room temperature. Primary antibodies against BRCA1 (1:200, H-300, rabbit), GFP (1:1000, ab13970, chicken), and BrdU (1:200, ab6326, rat) were added and incubated overnight at 4 °C. Following a PBS wash, species-appropriate secondary antibodies (1:250, Alexafluor 594 nm or 488 nm) were incubated for 1 hr at room temperature. Slides underwent a final PBS wash and were mounted using Prolong Gold with DAPI (ThermoFisher). Positive cells were counted manually.

2.15: Primary sphere forming assay

Free-floating spheres

mOSE cells were cultured in stem cell media (Dulbecco's Modified Eagle's Medium: Nutrient Mixture F-12 (Sigma) supplemented with 1 X B27 supplement [Invitrogen], 0.02 µg/mL EGF [R&D Systems], 0.04 µg/mL fibroblast growth factor (FGF) [R&D Systems], 4 µg/mL heparin [Sigma] and 0.01 mg/mL ITSS [Roche], and 2 µg/mL EGF [R&D Systems]) at $5x10^4$ cells/mL in non-adherent 24-well culture plates (Corning) and incubated at 37 °C, 5% CO_2 for 14 days. Spheres from representative fields of view taken at 20X magnification were quantified using ImageJ with a pixel cutoff of >1000 pixels and a circularity limit of 0.5-1.0 to remove small cell aggregates from the analysis.

Spheres in methylcellulose

mOSE cells were placed in a 1:1 mixture of methylcellulose and stem cell media at $5x10^4$ cells/mL in 24-well culture plates (Corning), and incubated at 37 °C, 5% CO_2 for 28 days. Spheres from representative fields of view taken at 20X magnification were quantified using ImageJ with a pixel cutoff of >500 pixels and a circularity limit of 0.5-1.0 to remove small cell aggregates from the analysis.

2.16: Secondary sphere forming assay

Primary free-floating mOSE spheres were collected and washed in PBS. Spheres were dissociated by first incubating in trypsin/PBS (Invitrogen) at 37 °C for 10 min, then by

passing cells through a 25-gauge needle to obtain a single cell suspension. Single cell suspension was verified using phase contrast microscopy. Cells were washed in PBS, counted using a hemocytometer and plated in stem cell media at $5x10^4$ cells/mL. Cells were incubated in non-adherent 24-well culture plates (Corning) at 37 °C, 5% CO_2 for 14 days. Spheres were quantified using ImageJ using a pixel cutoff of >500 pixels and a circularity limit of 0.5-1.0 to remove small cell aggregates from the analysis.

2.17: *Brca1* deletion in mOSE cells

mOSE cells were isolated from homozygous *Brca1*^{tm1Brn} mice as described in Section 2.1 and then infected with Adenovirus expressing *cre-recombinase* (Ad-*cre*) to achieve *Brca1* knockout (KO). Adenovirus expressing e*GFP* (Ad-*GFP*) was used as a control (WT). Cells were cultured 1 week prior to experimental use.

2.18: BrdU pulse-chase

Brca1^{tm1Brn} mice were bred to *B6.129X1-Gt(ROSA)26Sor*$^{tm1(EYFP)Cos}$*/J* mice to produce *Brca1*^{tm1Brn}*YFP* mice. *Brca1*^{tm1Brn}*YFP* mice were injected intrabursally (IB) with Ad-*cre* ($8x10^7$ PFU) or PBS on day 1 and injected IP with BrdU (0.25 mg daily) on days 7-10. Ovaries were collected on day 40 and frozen in Optimal Cutting Temperature Compound.

2.19: RNA sequencing (RNA-seq)

Sample Preparation

Monolayer conditions

Inducible *Snail*-expressing mOSE cells, *Brca1* knockout mOSE cells and control mOSE cells (1x10^6) were plated 24 hr prior to treatment with TGFB1 (10 ng/mL, R&D Systems) or doxycycline (200 ng/mL, Sigma). RNA was collected 4 days after addition of TGFB1 or doxycycline (RNAeasy Kit, Qiagen).

Sphere forming conditions

mOSE cells (1x10^6) were plated as monolayer cultures 24 hr prior to treatment with TGFB1 (10 ng/mL, R&D Systems). mOSE cells were then plated in free-floating sphere-forming conditions, 4 days after the addition of TGFB1. Cells were maintained in sphere-forming cultures for 2 weeks prior to RNA collection (RNAeasy Kit, Qiagen). TGFB1 was replenished when placing mOSE cells in sphere forming conditions.

Library preparation and sequencing

Total RNA was quantified using a NanoDrop Spectrophotometer ND-1000 (NanoDrop Technologies, Inc.) and its integrity was assessed on a 2100 Bioanalyzer (Agilent Technologies). Libraries were generated from 250 ng of total RNA as following: mRNA enrichment was performed using the NEBNext Poly(A) Magnetic Isolation Module (New England BioLabs). cDNA synthesis was achieved with the NEBNext RNA First Strand

Synthesis and NEBNext Ultra Directional RNA Second Strand Synthesis Modules (New England BioLabs). The remaining steps of library preparation were done using the NEBNext Ultra II DNA Library Prep Kit for Illumina (New England BioLabs). Adapters and PCR primers were purchased from New England BioLabs. Libraries were quantified using the Quant-iT™ PicoGreen® dsDNA Assay Kit (Life Technologies) and the Kapa Illumina GA with Revised Primers-SYBR Fast Universal kit (Kapa Biosystems). Average size fragment was determined using a LabChip GX (PerkinElmer) instrument.

The libraries were normalized, denatured in 0.05 N NaOH and then diluted to 200 pM and neutralized using HT1 buffer. ExAMP was added to the mix and the clustering was done on a Illumina cBot and the flowcell was run on a HiSeq 4000 for 2x100 cycles (paired-end mode) following the manufacturer's instructions. A phiX library was used as a control and mixed with libraries at 1% level. The Illumina control software was HCS HD 3.4.0.38 and the real-time analysis program was RTA v. 2.7.7. The program bcl2fastq2 v2.18 was then used to demultiplex samples and generate fastq reads.

RNA-seq analysis

Transcript quantification for each sample was performed using Kallisto (Bray et al. 2016) with the GRCm38 transcriptome reference and the -b 50 bootstrap option. The R package Sleuth (Pimentel et al. 2017) was then used to construct general linear models for the log-transformed expression of each gene across experimental conditions. For the TGFB1 monolayer, *Snail* overexpression, and *BRCA1* deletion datasets, the model was constructed with only a single variable (ie. condition vs. control). For the sphere forming

analysis, however, the model included the two variables (TGFB1 treatment and culture condition) as well as an interaction term between the two variables to identify expression patterns that are dependent on both conditions. Wald's test was used to test for significant variables for each gene and the resultant p-values were adjusted to q-values using the Benjamini-Hochberg false discovery rate method. Significant changes in gene expression were defined as genes with a q-value < 0.05. Independent effect-size (beta coefficient of the model) cutoffs were also used for each data set, adjusting the stringency based on the distribution of gene expression changes: +/-0.5 for the TGFB1 monolayer data, +/-0.25 for the *Snail* overexpression data, +/-1 for the BRCA1 deletion data, and +/-0.5 for at least one of the three variables in the sphere data.

2.20: CD44 cell sorting

mOSE cells were treated with TGFB1 (10 ng/mL, 2 days) prior to collecting cells for FACS. Cells (1x10^7) were trypsinized and a single-cell suspension was made using a 40 μm cell strainer. Cells were labelled and sorted as previously described (Alwosaibai et al. 2017). Briefly, cells were resuspended in a flow buffer (4% FBS in PBS) and incubated with anti-CD44 conjugated to APC (1:5000; eBioscience, San Diego, CA) for 15 min at 4 °C. Unbound antibody was removed with washing buffer and the fraction of cells with surface protein labeled with CD44 antibody was determined using a MoFlo cell sorter (Dako Cytomation).

2.21: TGFBR1 inhibition

mOSE cells (5x10^6) were plated as monolayer cultures 24 hr prior to treatment with SB431542 (SB; Sigma) or TGFB1 (R&D Systems). mOSE cells were treated with SB (100 µg/mL) 30 min prior to the addition of TGFB1 (10 ng/mL). Cells were isolated for RNA and protein extraction 6 hr after the addition of TGFB1.

2.22: Statistical Analysis

All experiments were conducted a minimum of 3 times and plotted as an average of replicates with error bars showing the standard error of the mean. All statistical analyses were carried out using GraphPad Prism 6 software, unless otherwise stated. An unpaired Student's T-test was used when comparing 2 groups. A one-way ANOVA was used with a Dunnett's post-test to compare 3 or more groups. For comparisons of more than one variable, a two-way ANOVA was used with a Bonferroni post-test. An ANCOVA analysis was used to compare migration, proliferation and survival assays. Significance was determined using a P value of < 0.05.

Chapter 3: Results

3.1: TGFB1 induces an EMT, partially through increased *Snail* expression

TGFB1 is a growth factor found throughout the ovarian environment. It is found in preovulatory follicular fluid (Gamwell et al. 2012), which bathes the surrounding OSE cells after follicular rupture. It is also secreted by immune cells present at the wound site, such as macrophages (Shaw and Martin 2016), and is produced by other ovarian cells (granulosa cells) (Knight and Glister 2006). TGFB1 belongs to a superfamily of genes known to regulate a number of processes including cell proliferation, differentiation and migration (Derynck and Zhang 2003; Xu et al. 2009). In mammals, there are five type II receptors and seven type I receptors that interact upon ligand binding. Once ligands bind to the type II receptor, the type I receptor is activated by phosphorylation to activate a kinase domain (Derynck and Zhang 2003; Xu et al. 2009). There are 29 known ligands in the TGFB family that interact with these receptors, and specific ligand-receptor combinations result in the activation of different signalling pathways, such as the SMAD, MAPK, PP2A/p70S6K, RhoA and TAK1/MEKK1 pathways (Derynck and Zhang 2003).

The canonical SMAD pathway consists of eight proteins and is the most characterized and studied TGFB pathway. Once the TGFB receptors are activated, SMAD2 and SMAD3

are phosphorylated at Ser465/467 and Ser423/425 respectively. The phosphorylated SMADs complex with SMAD4 and are translocated into the nucleus where they act as transcriptional activators (Guo and Wang 2009; Moustakas and Heldin 2005). Inhibitory SMAD6 and SMAD7 proteins are also induced upon SMAD activation and act as a negative feedback loop (Guo and Wang 2009; Moustakas and Heldin 2005). Inhibitory SMADs are exported from the nucleus where they bind to type I receptors and SMAD4 to block SMAD phosphorylation (Moustakas and Heldin 2005). Many factors can interact with SMAD signalling, resulting in context-dependent transcriptional regulation (Derynck and Zhang 2003).

TGFB1 induces an EMT in mouse OSE cells *in vitro*

To study the effects of TGFB1 in OSE cells *in vitro*, mOSE primary cell cultures were exposed to recombinant TGFB1 protein and assessed for classical EMT characteristics. TGFB1 treatment induced actin cytoskeleton rearrangement (Figure 7A) and increased cellular migration (Figure 7B), compared to untreated cells. TGFB1 treatment decreased epithelial gene expression such as *Chd1* and increased mesenchymal gene expression such as *Snail* (Figure 7C-E).

A TGFB1 treatment time course of mOSE cells was used to further validate the loss in epithelial genes and upregulation of mesenchymal genes. It was also used to determine which master regulators of the EMT were upregulated by TGFB1 treatment. TGFB1 increased the mesenchymal gene *Alcam* (3-fold) and decreased the epithelial marker

Krt19 (70% decrease) (Figure 8A-B). *Snail* was the only EMT-associated transcription factor increased by TGFB1 treatment (3.5-fold) (Figure 8C). *Snai2* and *Zeb1* remained unchanged and *Twist1* was decreased by approximately 50% (Figure 8D-F). These data demonstrate that TGFB1 induces a classic EMT in mOSE cultures and suggest this EMT is driven by an upregulation of *Snail*.

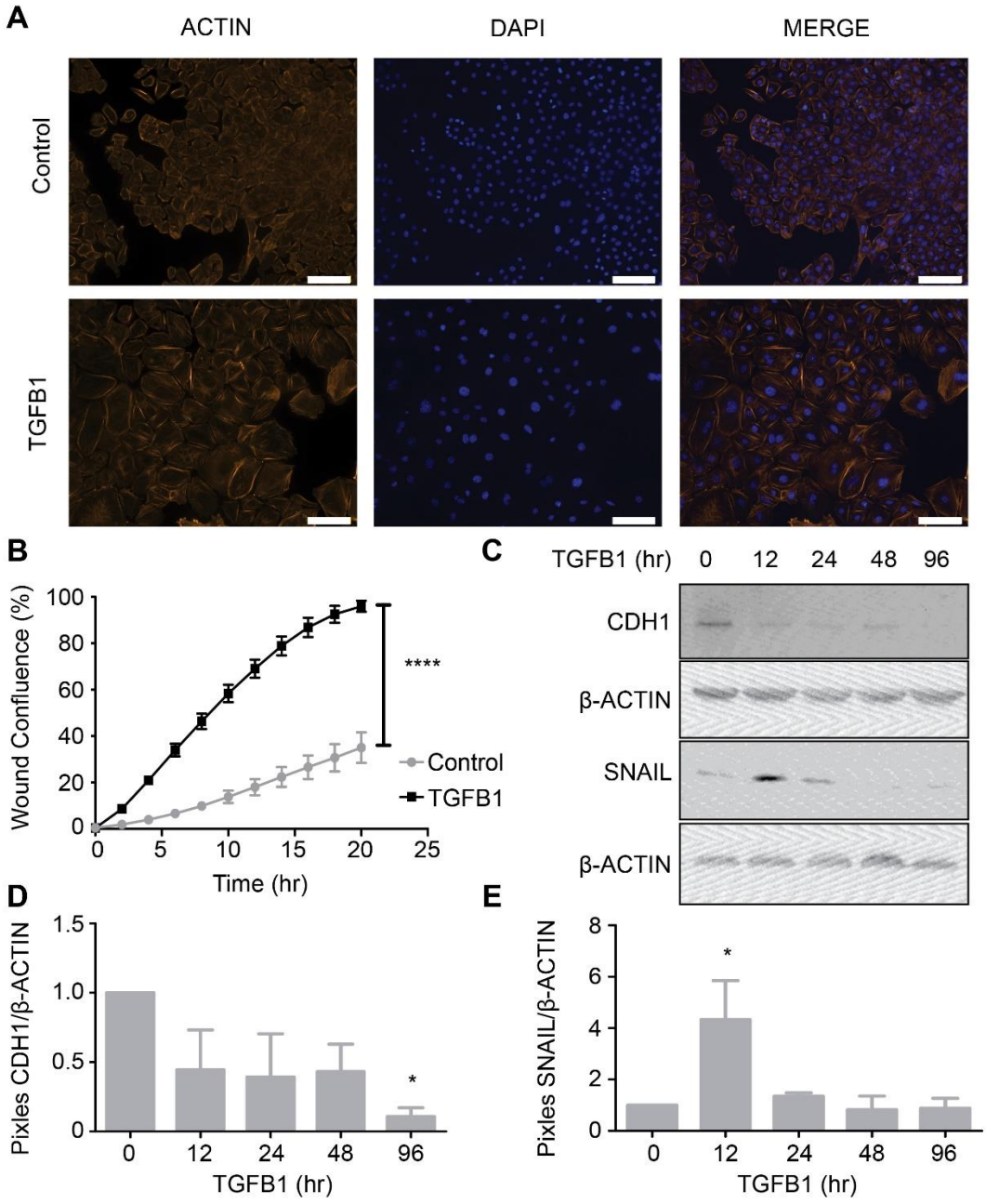

Figure 7. Epithelial-to-mesenchymal transition in mOSE cells treated with TGFB1 (10 ng/mL). **A)** mOSE cells display actin cytoskeletal rearrangement upon TGFB1 treatment (7 days), as determined by ACTIN immunofluorescence (representative image, N=3). **B)** TGFB1 treatment enhances mOSE cell migration compared to untreated controls, as determined using a scratch wound assay (N=3, linear regression ANCOVA). **C-E)** TGFB1 treatment of mOSE cells decreases CDH1 and increases SNAIL compared to untreated controls, as determined by western blot. β-ACTIN was used as a loading control (representative western blot, N=3, One-way ANOVA, Dunnett's post-test). **** indicates a significant difference from the untreated control group, $P < 0.0001$. Scale bar = 100 µm.

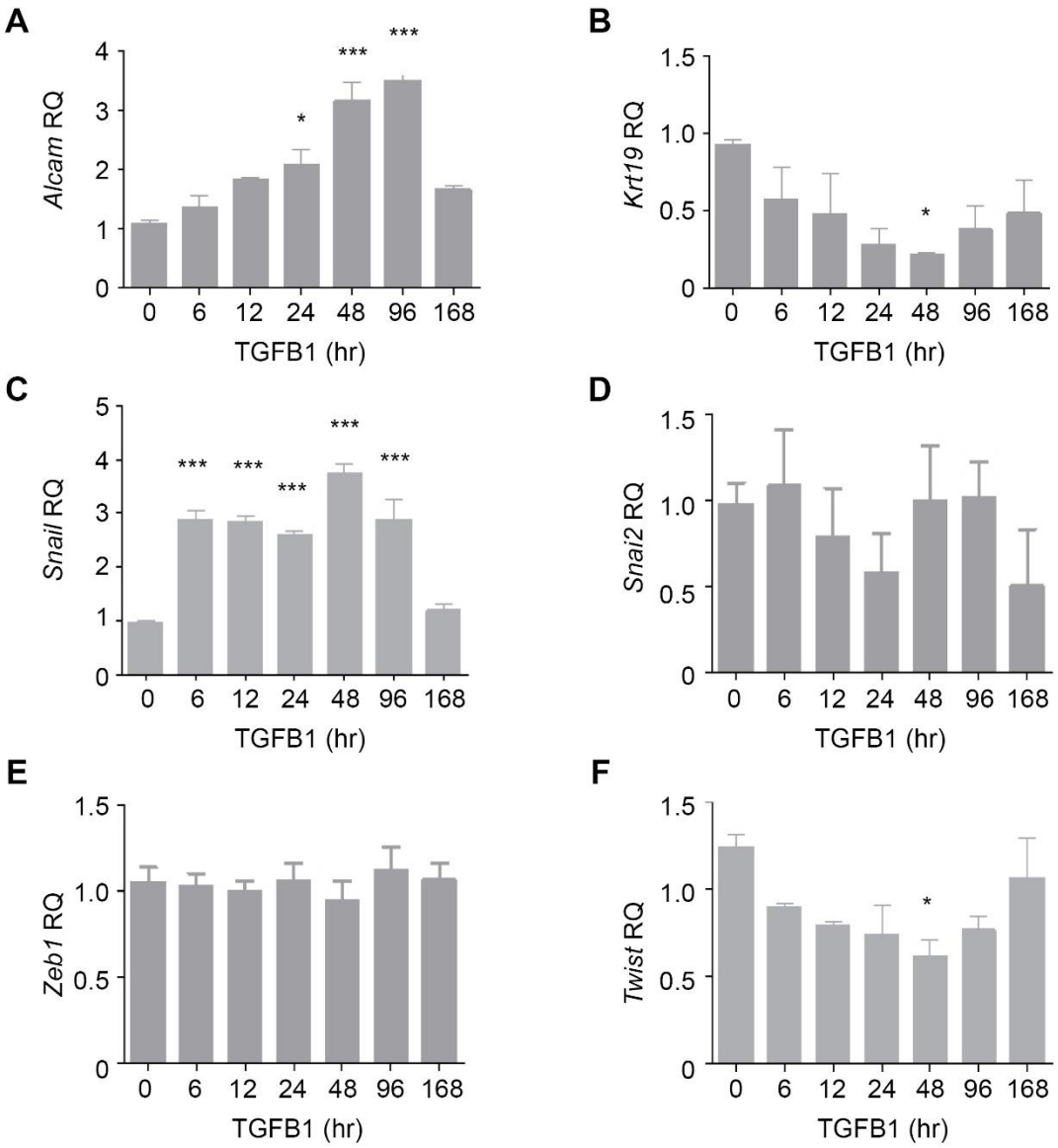

Figure 8. Gene expression analysis of mOSE cells treated with TGFB1 (10 ng/mL). A TGFB1-treatment time course of mOSE cells shows increased *Alcam* and *Snail* expression, decreased *Krt19* and *Twist* expression and unchanged *Zeb1* and *Snai2* expression with TGFB1 treatment, as determined by Q-PCR (N=3, One-way ANOVA, Dunnett's post-test). RQ = relative quantity to untreated control samples. * and *** indicate significant differences from the untreated control group, $P < 0.05$ and 0.001 respectively.

TGFB1 increases *Snail* in a SMAD2/3 dependent manner

We next sought to confirm that the transcriptional targets of TGFB1 treatment in mOSE cells were dependent on the activity of TGFBR1, the receptor that activates the canonical SMAD2/3 pathway. mOSE cells were treated with TGFB1 in the presence of a TGFBR1 inhibitor (SB431542). SB431542 functions as a competitive ATP binding site inhibitor of ALK4, 5, and 7 receptors — the receptors responsible for SMAD2/3 phosphorylation (Inman et al. 2002). In the presence of SB431542, SMAD2/3 phosphorylation were decreased 49% and 47% respectively (Figure 9A). mOSE cells treated with this inhibitor prior to TGFB1 treatment did not show increased *Snail* expression, in comparison to TGFB1 treatment alone (Figure 9B-C). These data suggest that the TGFB1-induction of *Snail* is dependent on the ATP binding site of TGFBR1, the receptor known to activate the Smad2/3 pathway.

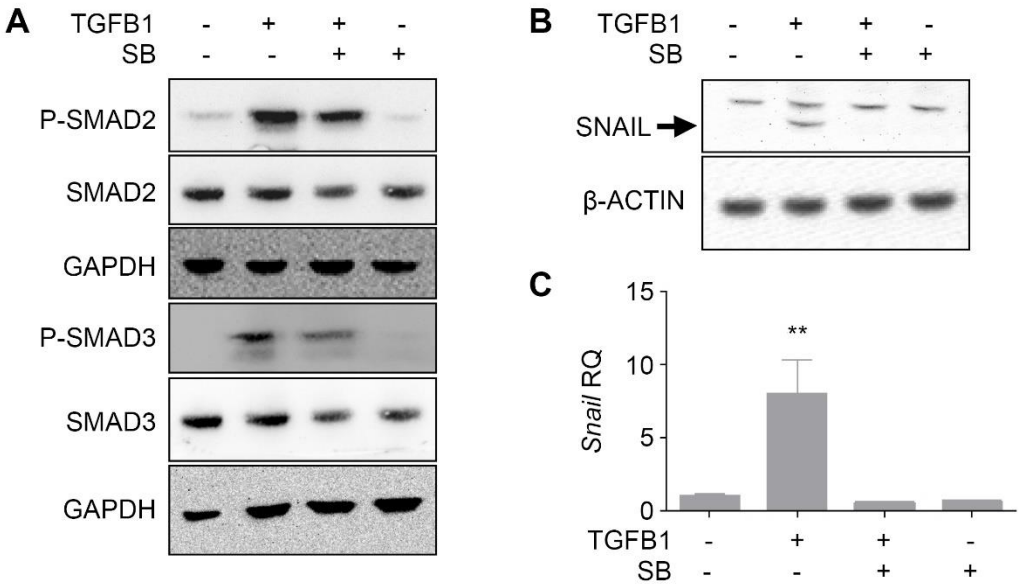

Figure 9. TGFB1-mediated increase in *Snail* expression is dependent on TGFBR1 signalling. **A)** mOSE cells pre-treated with SB431542 (SB) (100 µg/mL, 30 min), have decreased phospho-SMAD2 (P-SMAD2) and phospho-SMAD3 (P-SMAD3) levels compared to TGFB1 treatment alone (10 ng/mL, 6 hr), as determined by western blot. GAPDH was used as a loading control (representative western blot, N=3). **B-C)** mOSE cells treated with TGFB1 have increased *Snail* expression compared to untreated control mOSE. This increase is inhibited in the presence of SB, as determined by western blot (B, representative western blot, N=3) and Q-PCR (C, N=3, One-way ANOVA, Dunnett's post-test). β-ACTIN was used as a loading control for the western blot. RQ = relative quantity to untreated control samples. ** indicates a significant difference among treatment groups, $P < 0.001$.

Forced *Snail* expression induces a partial EMT *in vitro*

To determine the transcriptional targets of SNAIL, its expression was activated using a doxycycline induction system (im*Snail*, Figure 5). In the presence of doxycycline, im*Snail* cells showed increased *Snail* expression (Figure 10A). Actin organization remained unchanged with forced *Snail* expression (Figure 10B), as did traditional EMT associated genes (*Krt19*, *Cdh1*, *Alcam*) (Figure 10A,C). Cellular migration was increased with forced *Snail* expression as assessed using a scratch wound assay (Figure 10D). To ensure the backbone of the construct was not responsible for the partial EMT observed in the im*Snail* cells, mOSE cells were infected with a control construct with doxycycline induced *GFP* expression (i*GFP*) (Figure 6). Forced *GFP* expression did not alter ACTIN organization, EMT associated gene expression or cellular migration (Figure 11A-C respectively), suggesting the partial EMT observed in the im*Snail* cells is due to forced *Snail* expression.

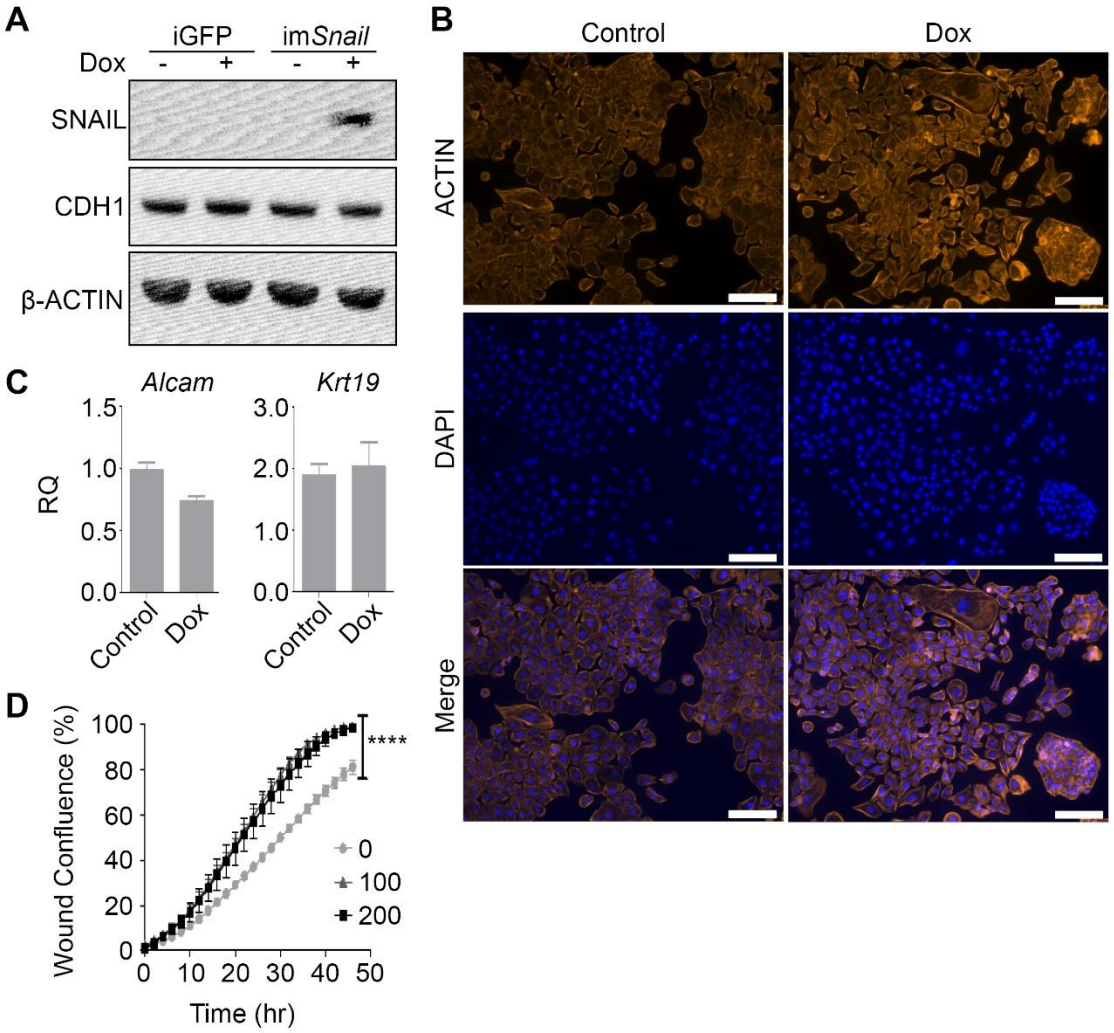

Figure 10. Forced *Snail* expression induces a partial EMT *in vitro*. **A)** Inducible *Snail* (im*Snail*) in mOSE cells show increased SNAIL in the presence of doxycycline (200 ng/mL, 48 hr) compared to the control mOSE cells bearing inducible *GFP* (iGFP), as determined by western blot. CDH1 levels remain unaffected by doxycycline treatment. β-ACTIN was used as a loading control (representative western blot, N=3). **B)** im*Snail* mOSE cells do not alter actin cytoskeletal organization in the presence of doxycycline (200 ng/mL, 48 hr), as determined by ACTIN immunofluorescence (representative image, N=3). Scale bar = 100 µm. **C)** im*Snail* mOSE cells do not alter expression of EMT markers (*Alcam*, *Krt19*) in the presence of doxycycline (200 ng/mL, 48 hr) (N=3, Student T-test). **D)** im*Snail* cells have increased migration in response to doxycycline treatment at two different doses (100 and 200 ng/mL), as determined using a scratch wound assay (N=3, linear regression ANCOVA). RQ = relative quantity to untreated i*GFP* mOSE samples. **** indicates a significant difference from untreated im*Snail* mOSE cells, $P < 0.0001$.

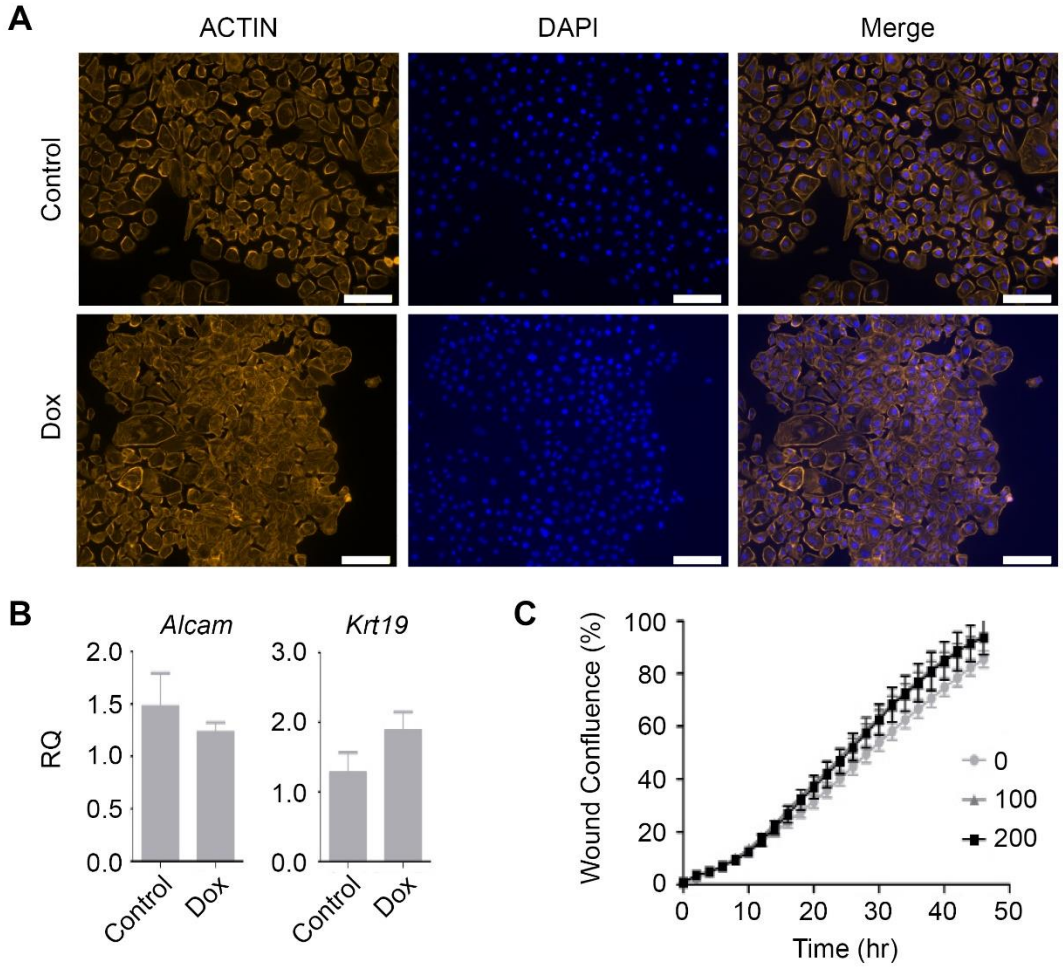

Figure 11. Forced *GFP* expression does not induce an EMT *in vitro*. **A-B)** Inducible *GFP* (i*GFP*) mOSE cells do not alter actin cytoskeletal organization or *Alcam* or *Krt19* mRNA expression in the presence of doxycycline (200 ng/mL, 48 hr) as determined by immunofluorescence for ACTIN expression (A, representative image, N=3) and Q-PCR (B, N=3, Student T-test). **C)** i*GFP* mOSE cells do not have altered migration in the presence of doxycycline (0, 100 or 200 ng/mL), as determined using a scratch wound assay (N=3, linear regression ANCOVA). RQ = relative quantity to untreated i*GFP* mOSE samples. Scale bar = 100 µm.

RNA-seq of mOSE cells treated with TGFB1 reveals an upregulation of ECM deposition

To broaden our understanding of the effects of TGFB1 on OSE cells, RNA-seq was used to assess mOSE cells with and without TGFB1 treatment. RNA-seq revealed 372 significantly upregulated and 220 downregulated genes between control and TGFB1-treated mOSE cells. *Snail* was among the significantly upregulated genes and *Krt19* was downregulated with TGFB1 treatment, in agreement with our Q-PCR and western blot findings (Figure 12A). Gene ontology (GO) term enrichment analysis revealed many significantly enriched terms associated with TGFB1 treatment, including system development, regulation of multicellular organismal process and movement of cell or subcellular component (Figure 12B). The most significant terms enriched in the downregulated genes included cellular response to cytokine stimulus, flavonoid metabolic process and organic hydroxy compound catabolic process (Figure 12B). When examining the entirety of the enriched terms, it is clear that EMT-associated terms are abundant with TGFB1 treatment. Locomotion, cell migration and cell adhesion were all upregulated in TGFB1 treated mOSE cells (Figure 12B). Many collagens, integrins, matrix metalloproteinases and ADAMTS proteins were increased in TGFB1 treated mOSE cells, further characterizing the ECM remodelling that occurs with TGFB1 treatment (Figure 12A). In agreement with our Q-PCR data, the traditional EMT associated TF such as *Twist* and *Zeb1* were unchanged with TGFB1 treatment. However, the RNA-seq data revealed many other transcription factors such as *Lhx4*, *Sox8*/*11* or *Foxs1* that may play a role in inducing the EMT in OSE cells treated with TGFB1. These data give a broad view of the

TGFB1-induced EMT in mOSE cells and highlight the ECM restructuring that occurs with this process. A full list of significantly upregulated and downregulated genes seen with TGFB1 can be found at GSE121936.

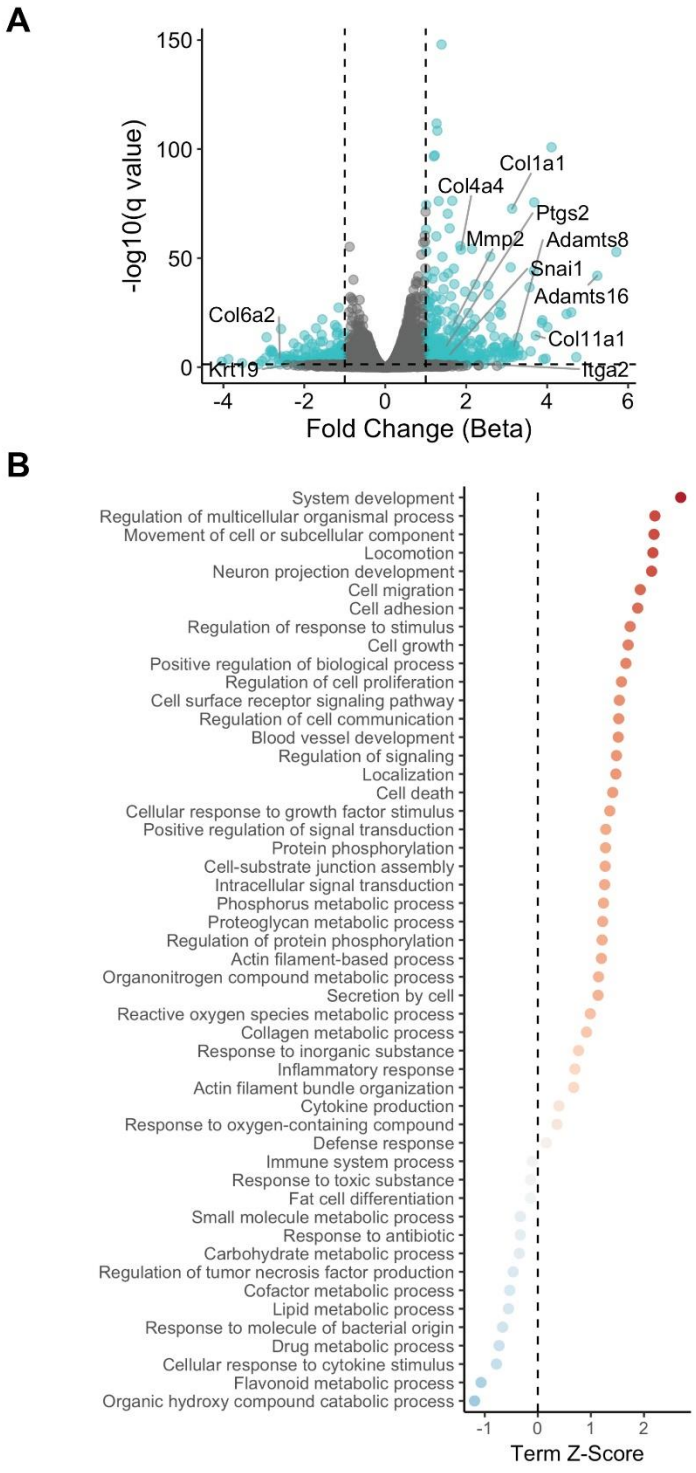

Figure 12. RNA sequencing results of TGFB1-treated mOSE cells (10 ng/mL, 96 hr) shows increased ECM deposition with treatment. **A)** Volcano plot demonstrating increased expression of ECM deposition and remodeling genes observed with TGFB1 treatment. *Snail* is increased with TGFB1 treatment whereas *Krt19* is decreased with treatment. Fold change was determined by assessing the beta coefficient of the general linear models used for differential expression analysis **B)** Plot of significantly enriched terms upregulated and downregulated by TGFB1 treatment.

TGFB1 induces an EMT in human OSE cells

Primary hOSE cells were treated with TGFB1 to assess whether the TGFB1-induced *Snail* expression and induction of an EMT were conserved between the mouse and human. hOSE cells treated with TGFB1 display a mesenchymal morphology and gain a 3-fold increase in *SNAIL* expression (Figure 13A-B, respectively). These data suggest the induction of an EMT and increase in *Snail* expression are conserved in mouse and human OSE cells.

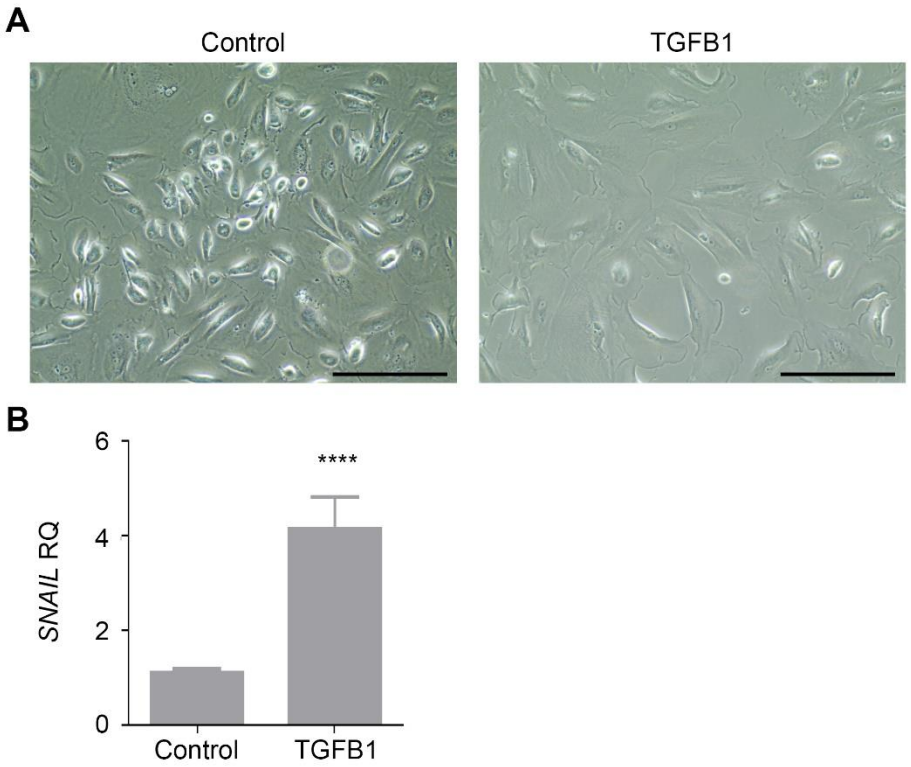

Figure 13. Human OSE cells treated with TGFB1 (10 ng/mL) acquire a mesenchymal phenotype and increased *SNAIL* expression. **A)** Human OSE cells acquire a mesenchymal morphology with TGFB1 treatment (7 days), as determined using phase contrast microscopy (representative image, N=3). **B)** Human OSE cells have increased *SNAIL* mRNA expression when treated with TGFB1 (48 hr), as determined by Q-PCR. (N=3, Student T-test). RQ = relative quantity to untreated samples. **** indicates a significant difference from the untreated control, $P < 0.0001$, Scale bar = 100 µm.

Summary

TGFB1 treatment of mOSE cells induces mesenchymal gene expression such as *Alcam* and *Snail* and decreases epithelial gene expression such as *Cdh1* and *Krt19*. mOSE cells treated with TGFB1 activate the canonical SMAD2/3 pathway, acquire a mesenchymal morphology and display enhanced migration. Together, these results demonstrate that TGFB1 induces an EMT in mOSE cells. *Snail* is the only classic EMT transcription factor increased with TGFB1 treatment and is found downstream of the SMAD2/3 signalling pathway. Forced *Snail* expression induces a partial EMT observed by enhanced migration. RNA-seq in mOSE cells treated with TGFB1 suggests the additional EMT characteristics are downstream of genes related to extracellular matrix remodelling such as collagen and ADAMTS genes. Finally, the TGFB1 induction of an EMT in mouse cells is conserved in human cells as hOSE cells treated with TGFB1 acquire a mesenchymal morphology and have increased *SNAIL* expression.

3.2: TGFB1 increases COX2 expression to promote survival in the OSE

A TGFB1 signalling targets PCR array was used to compare untreated mOSE cells and mOSE cells treated with TGFB1 for 96 hr to elucidate TGFB1 targets in these cells. *Cyclooxygenase 2* (*Cox2*) was the top target in the array showing an 8-fold increase in expression in the TGFB1-treated compared to untreated mOSE cells (Figure 14). The increase in *Cox2* (*Ptgs2*) was also observed in the RNA-seq results in Figure 12.

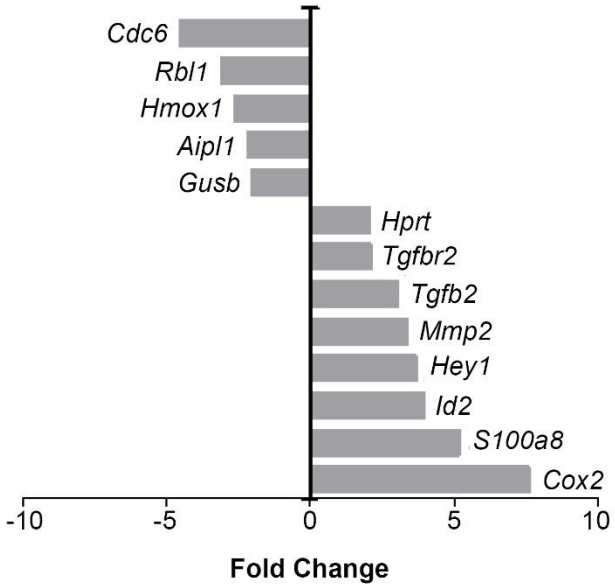

Figure 14. TGFB1 Signalling Targets PCR array of mOSE cells treated with TGFB1 (10ng/mL, 96 hr). mOSE cells treated with TGFB1 have increased *Cox2* expression (N=3, Student T-test).

The COX enzymes (COX1 and COX2) catalyze the conversion of arachidonic acid to prostaglandin H2 intermediates which are then converted into other prostaglandins, prostacyclins and thromboxanes (Kujubu et al. 1991). COX1 is ubiquitously expressed in most tissues including the OSE layer whereas COX2 is induced during inflammatory processes (Hales et al. 2008). During inflammatory events such as wound repair, growth factors and mediators of inflammation such as TNF-alpha or TGFB1 quickly upregulate *Cox2* expression (Smith et al. 2000). Prostaglandin E2 is the most widely produced prostaglandin in the body with the most versatile actions such as inducing angiogenesis and promoting vasodilation (Sugimoto and Narumiya 2007). Prostaglandins are lipid compounds that can act through four receptors, PTGER1-4, preferentially through PTGER2 and 4 (Audoly et al. 1999). This upregulation of *Cox2* and increase in PGE2 is important for successful wound repair, and inhibiting the activity of COX2 or preventing its induction results in delayed wound repair (Goren et al. 2015; Futagami et al. 2002). The role of *Cox2* during ovulatory wound repair is presently unknown. *Cox2* knockout mice do not ovulate because of impaired cumulus expansion, rendering impossible the study of ovulatory wound repair in these mice (Lim et al. 1997; Davis et al. 1999).

The relationship between TGFB1 and PGE2 induction has been shown in other cells types. In prostate cancer cells, Vo et al. (2013) demonstrated that TGFB1 induced PGE2 secretion in a SMAD2/3-dependent manner and increased the cells' migration and invasive potential through the PTGER4 receptor. These findings were supported by studies in normal mammary tissue, where treatment with TGFB1 induced COX2

expression, and stable *Cox2* expression in these cells stimulated their invasive potential (Neil et al. 2008). Based on these studies, as well as others, we hypothesized that in the OSE, TGFB1 induces an EMT by upregulating *Cox2* expression and PGE2 secretion through the SMAD2/3 pathway and the PTGER4 receptor.

TGFB1 increases *Cox2* expression and PGE2 secretion *in vitro*

Using a TGFB1 treatment time course on mOSE cells, *Cox2* expression was confirmed to be increased as early as 12 hr after TGFB1 treatment (Figure 15A-C) and was unchanged by forced *Snail* expression (Figure 15D). A PGE2 ELISA was used to confirm that the increase in COX2 leads to increased prostaglandin production and showed that, after 48 hr of TGFB1 treatment, PGE2 levels were significantly increased compared to the control OSE cells (Figure 15E). Using SB431542, the TGFB1-induced increase in *Cox2* was confirmed to be downstream of TGFBR1 and the Smad2/3 pathway (Figure 16A-B). Furthermore, hOSE cells treated with TGFB1 were also found to have increased *COX2* expression relative to their untreated controls, confirming the increase in *Cox2* from TGFB1 treatment is conserved in mouse and human OSE cells (Figure 17).

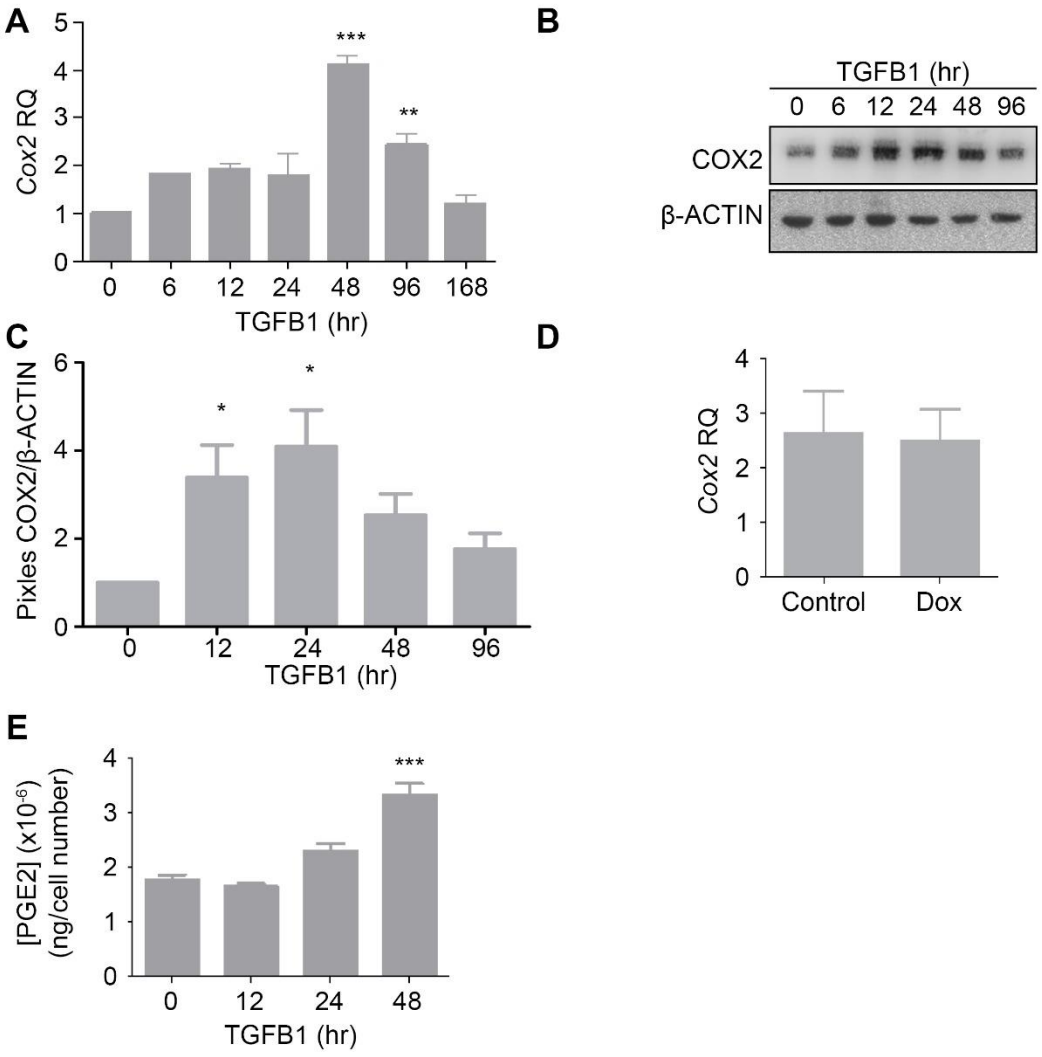

Figure 15. mOSE cells treated with TGFB1 (10 ng/mL) increase *Cox2* expression and PGE2 secretion. **A-C)** mOSE cells treated with TGFB1 have increased *Cox2* mRNA and protein expression as determined by Q-PCR (N=3, One-way ANOVA, Dunnett's post-test) and western blot (representative western blot, N=3, One-way ANOVA, Dunnett's post-test). β-ACTIN was used as a loading control for the western blot. **C)** *Cox2* expression is unaffected in im*Snail* mOSE cells treated with doxycycline (200 ng/mL, 48 hr) as determined by Q-PCR (N=3, Student T-test). **D)** mOSE cells treated with TGFB1 have increased PGE2 production at 48 hr post treatment, compared to untreated mOSE cells, determined by a PGE2-ELISA (N=3, One-way ANOVA, Dunnett's post-test). RQ = relative quantity to untreated samples, or to untreated i*GFP* mOSE samples. ** and *** indicate a significant difference among treatment groups and untreated samples, $P < 0.01$ and 0.001 respectively.

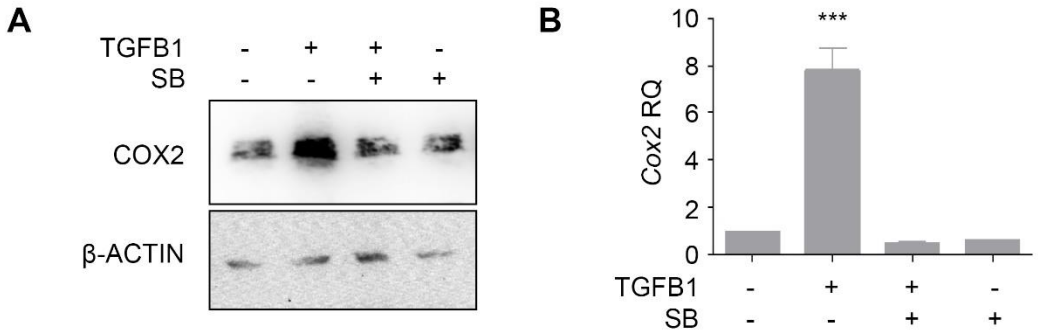

Figure 16. The TGFB1-induced increase in *Cox2* is dependent on TGFBR1 activity. The increase in *Cox2* expression observed in mOSE cells treated with TGFB1 (10 ng/mL, 6 hr) compared to untreated mOSE is inhibited by pre-treatment with SB431542 (SB) (100 µg/mL, 30 min), as determined by western blot (A, representative western blot, N=3) and Q-PCR (B, N=3, One-way ANOVA, Dunnett's post-test). β-ACTIN was used as a loading control for the western blot. RQ = relative quantity to untreated samples. *** indicates a significant difference among treatment groups, $P < 0.001$.

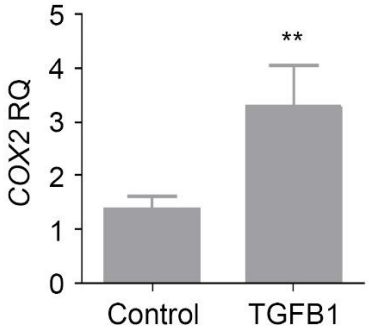

Figure 17. Human OSE cells treated with TGFB1 increase *COX2* expression. Human OSE cells treated with TGFB1 (10 ng/mL, 48 hr) show increased *COX2* expression compared to untreated cells, as determined by Q-PCR (N=3, Student T-test). RQ = relative quantity to untreated samples. ** indicates a significant difference from untreated control cells, $P < 0.01$.

Forced *Cox2* expression induces a partial EMT

To determine if COX2 plays a role in inducing an EMT, we transduced mOSE cells with either a lentiviral *Cox2* overexpression vector, or the empty lentiviral vector (WPI-*Cox2* and WPI respectively, Figures 3-4). Forced *Cox2* expression was validated using Q-PCR and western blot and the levels of expression were found to be similar to that of mOSE cells treated for 12 hr with TGFB1 (Figure 18A). *Cox2* overexpression did modestly, but significantly, increase cell migration (Figure 18B), but did not alter the expression of *Snail* or *Krt19* (Figure 18C), suggesting it plays a role in inducing a partial EMT.

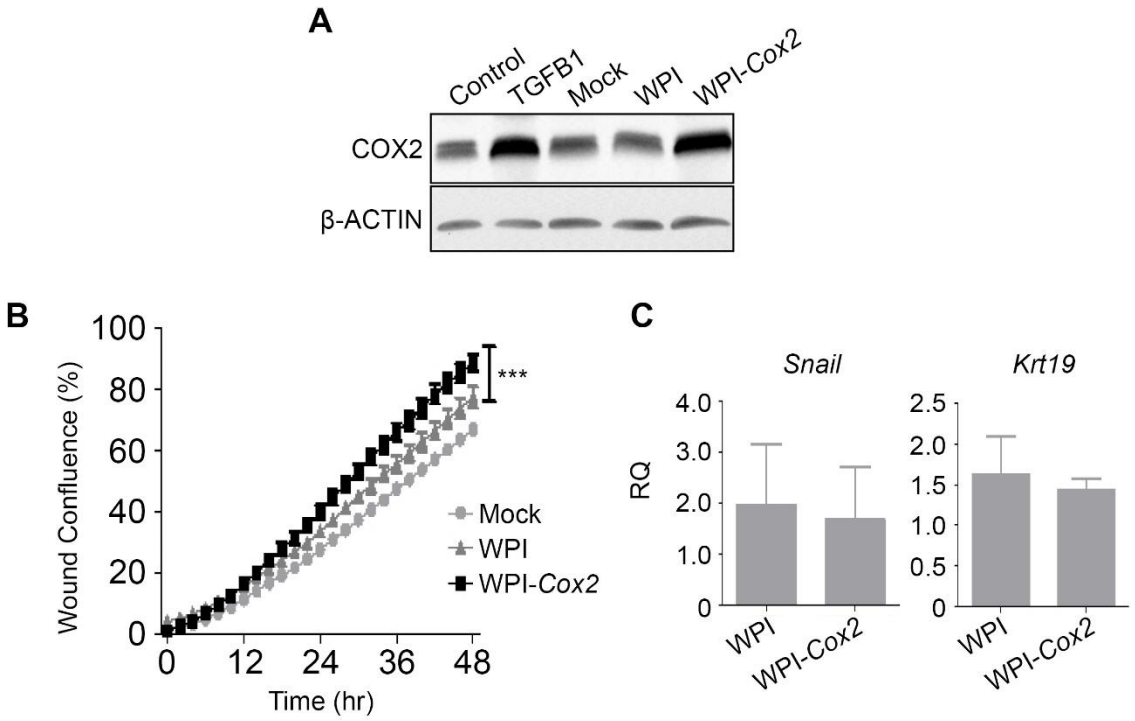

Figure 18. WPI-*Cox2* mOSE cells have a similar amount of COX2 as mOSE cells treated with TGFB1 and exhibit a partial EMT. **A)** mOSE cells overexpressing *Cox2* (WPI-*Cox2*) have increased levels of COX2 compared to mOSE cells infected with the empty vector (WPI), or mock infected cells (mock). WPI-*Cox2* cells express similar levels of COX2 as mOSE cells treated with TGFB1 (10 ng/mL, 12 hr), as determined by western blot (representative western blot, N=3). β-ACTIN was used as a loading control. **B)** WPI-*Cox2* cells show enhanced cell migration compared to WPI mOSE cells, as determined using a scratch wound assay (N=3, linear regression ANCOVA). **C)** WPI-*Cox2* cells do not have altered *Snail* or *Krt19* expression compared to WPI cells, as determined using Q-PCR (N=3, Student T-test). RQ = relative quantity to WPI samples. *** indicates a significant difference from WPI cells, $P < 0.001$.

Forced *Cox2* expression increases OSE cell survival

PGE2 has been shown to activate the AKT signalling pathway to promote cell survival in tissues such as the intestine, bladder and in a variety of cancer cell lines (Tessner et al. 2004; George et al. 2007). Tessner et al. (2004) demonstrated in the intestinal epithelium that PGE2 activates AKT signalling to promote survival in cells challenged with radiation (Tessner et al. 2004). Furthermore, George et al. (2007) showed in Jurkat cells, a model of leukemia, that PGE2 activation of the PTGER4 receptor led to AKT signalling that was responsible for the anti-apoptotic effects of PGE2 treatment on cells challenged with camptothecin (George et al. 2007). Based on these findings, we hypothesized that COX2 plays a role in promoting cell survival in the OSE during ovulatory wound repair, through AKT signalling.

In mOSE cells, both *Cox2* overexpression and PGE2 treatment independently activated AKT signalling, seen with increased levels of phosphorylated AKT (Figure 19). Treating mOSE cells with Celecoxib (a COX2 inhibitor) decreased their viability compared to control cells (Figure 20A). Furthermore, mOSE cells overexpressing *Cox2* had increased resistance to wound repair-related cell stress, showing increased survival in the presence of reactive oxygen species (ROS), induced with H_2O_2 treatment, compared to mOSE cells infected with the vector control (Figure 20B). Using a H_2O_2 dose response, the LD50 of *Cox2*-overexpressing cells was 150 µM, whereas mOSE cells infected with the vector control had a LD50 of 85 µM (Figure 20B). When cultured in hypoxic conditions, vector control-infected mOSE cells showed decreased viability, whereas

Cox2-overexpressing mOSE cells were able to maintain viability under those same conditions (Figure 20C). These findings were supported by the results of a growth curve, where *Cox2*-overexpressing cells maintained their proliferation until day 6 in low oxygen conditions, whereas mOSE cells infected with the vector control showed decreased proliferation by day 4 (Figure 20D-E). Together, these data demonstrate that *Cox2* plays a role in promoting mOSE cell survival when exposed to ovulation-associated stressors.

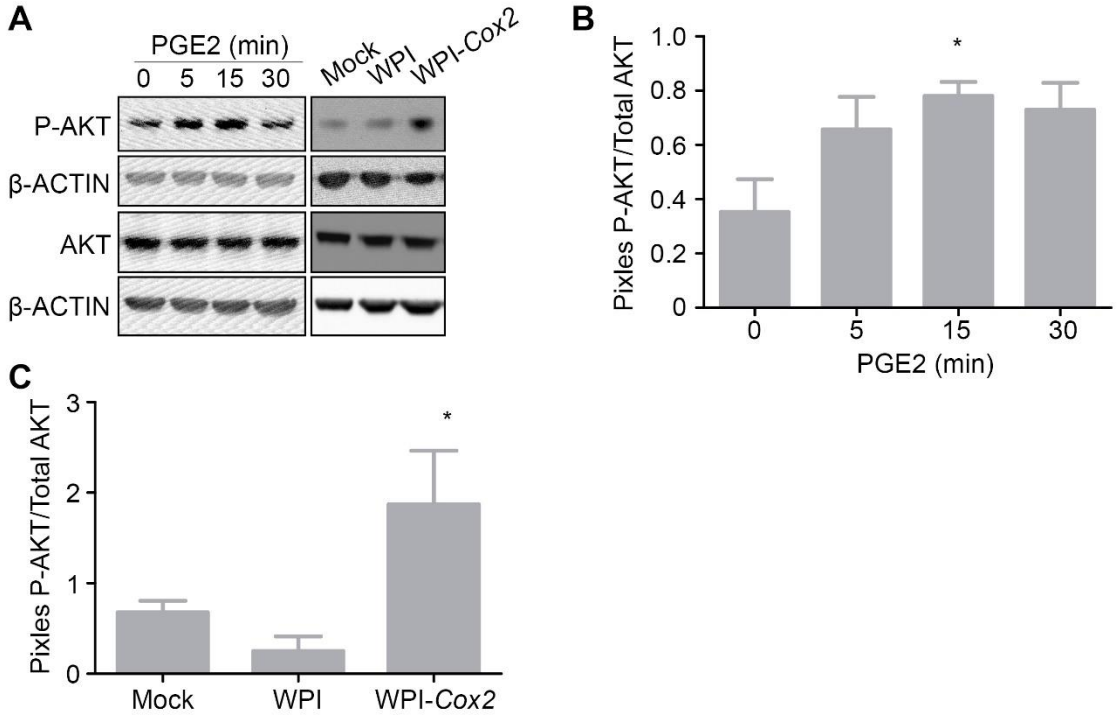

Figure 19. Constitutive *Cox2* overexpression and PGE2 treatment activate AKT signalling in mOSE cells. mOSE cells either treated with PGE2 (8 µg/mL), or overexpressing *Cox2* (WPI-*Cox2*) have increased levels of P-AKT compared to control cells (Mock) or mOSE cells infected with the vector control (WPI) as determined by western blot. β-ACTIN was used as a loading control (representative western blot (A), N=3, Quantified in B-C, One-way ANOVA, Dunnett's post-test).

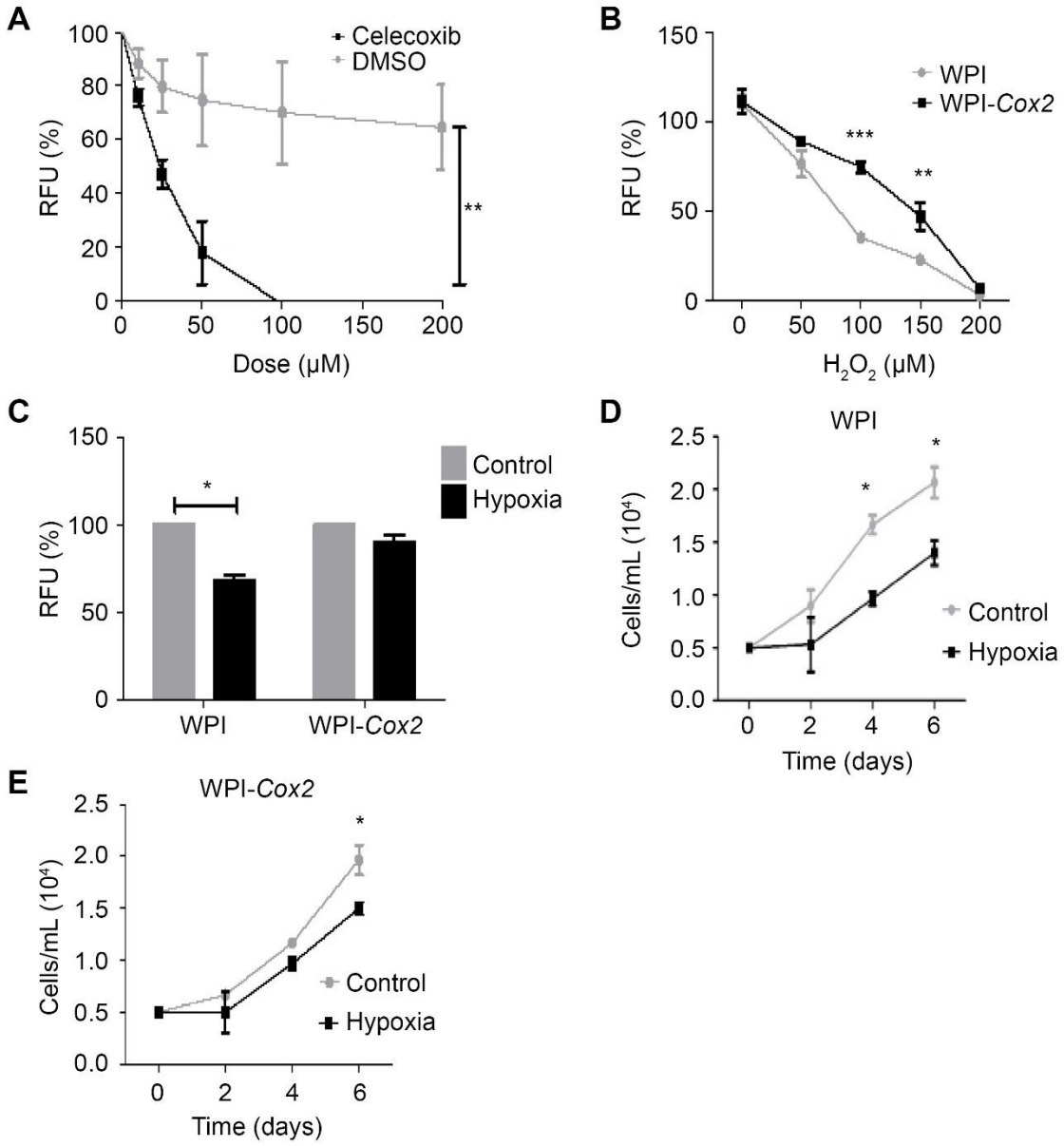

Figure 20. COX2 promotes a cell-survival phenotype in mOSE cells. **A)** mOSE cells treated with celecoxib have reduced viability compared to control treated mOSE cells (DMSO), as determined by an Alamar Blue assay (N=3, Two-way ANOVA, Bonferroni post-test). **B)** mOSE cells overexpressing *Cox2* (WPI-*Cox2*) are more resistant to H_2O_2 treatment than mOSE cells infected with the control vector (WPI), as determined using an Alamar Blue assay (N=3, Two-way ANOVA, Bonferroni post-test). **C)** WPI mOSE cells cultured in low oxygen (5% O_2, 6 days) have reduced viability compared to WPI-*Cox2* mOSE cells which maintain their viability, as determined using an Alamar Blue assay (N=3, Student T-test). **D-E)** WPI mOSE cells cultured under low oxygen have decreased proliferation at 4 days in culture whereas WPI-*Cox2* mOSE cells maintain their proliferation rate at least until 6 days in culture (N=3, Two-way ANOVA, Bonferroni post-test). RFU = relative fluorescence units compared to untreated control cells. *, **, *** indicate a significant difference from the control treated or WPI group, $P < 0.05$, 0.01 and 0.001 respectively.

In many epithelial cells, PGE2 binds to the PTGER4 receptor to activate the AKT pathway (George et al. 2007). To determine if PTGER4 is the prostaglandin receptor that is required for maintaining cell proliferation and survival, mOSE cells were isolated from *Ptger4*-floxed mice (Schneider et al. 2004) and infected with Ad-*cre* to achieve *Ptger4* deletion (Figure 21A). Following *Ptger4* deletion, mOSE cells did not proliferate and had reduced viability compared to *Ptger4* wildtype cells (Figure 21B-C). These data suggest PTGER4 is important to maintain mOSE cell survival and proliferation. Treating the *Ptger4* knockout cells with TGFB1 still enhanced migration, suggesting PTGER4 is not required for TGFB1-induced migration (Figure 21D).

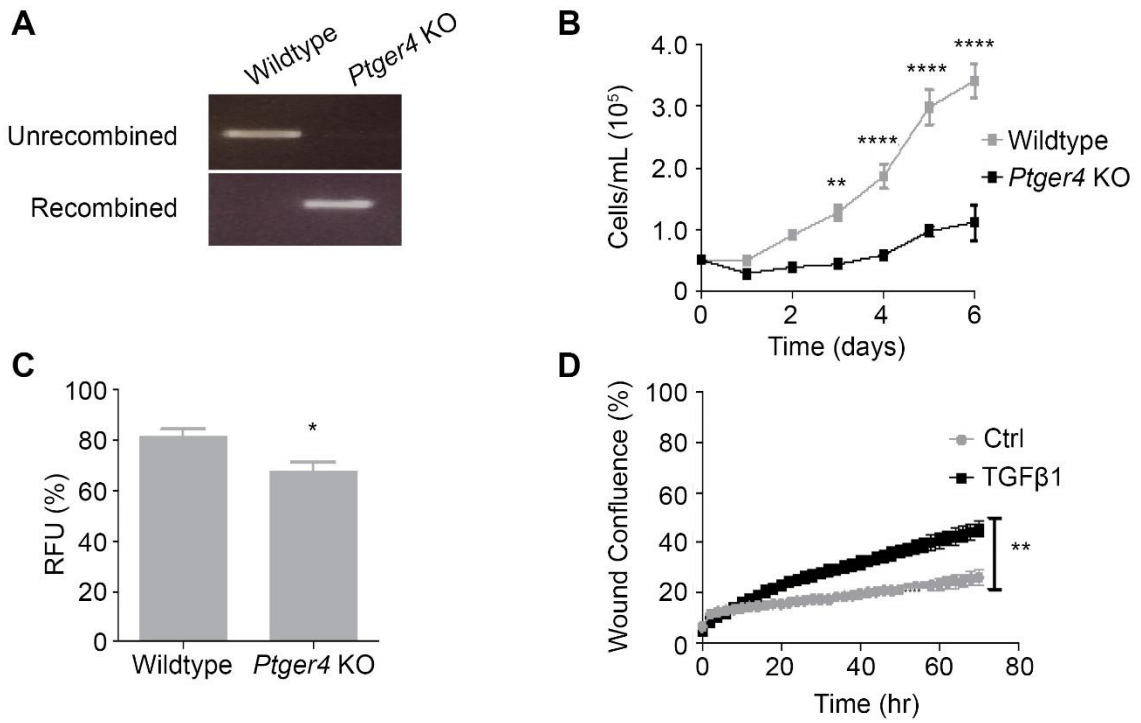

Figure 21. PTGER4 is necessary to maintain mOSE cell viability. **A)** PCR efficiency of *Ptger4* deletion in *Ptger4*-floxed mOSE cells. Wildtype *Ptger4*-floxed mOSE cells (Wildtype) have only unrecombined *Ptger4*, and the *Ptger4*-floxed knockout mOSE cells (*Ptger4* KO) have only the recombined form of the *Ptger4* gene (representative PCR, N=3). **B-C)** *Ptger4* KO mOSE cells have reduced proliferation and viability compared to wildtype mOSE, as determined using a growth curve (B, N=3, Two-way ANOVA, Bonferroni post-test) and trypan blue exclusion (C, N=3, Student T-test). RFU = relative fluorescence units to untreated mOSE cells. **D)** TGFB1 treatment (10 ng/mL) increases migration in *Ptger4* KO mOSE cells, as determined using a scratch wound assay (N=3, linear regression ANCOVA). *, **, **** indicate a significant difference from the untreated control or wildtype group, $P < 0.05, 0.01, 0.0001$ respectively.

COX2 is expressed during ovulatory wound repair in mouse ovaries

The involvement of COX2 in ovulatory wound repair is not known; however, its promotion of cell survival may contribute to efficient repair. Given COX2 expression increases as cells undergo an EMT, we predicted that its expression would increase during ovulatory wound repair. To explore this *in vivo*, we collected ovaries from superovulated mice and assessed COX2 expression. In preovulatory follicles examined 6 hours after treatment with hCG to induce ovulation, COX2 was expressed in the granulosa cells, as expected, but in the OSE cells surrounding the antral follicle, COX2 remained undetectable (Figure 22A). However, after ovulation occurred, the OSE cells surrounding the ovulatory wound sites expressed COX2 (Figure 22B), but not surrounding non-ovulating sites (Figure 22C). These data suggest that COX2 is induced after ovulation to maintain cell viability during wound repair.

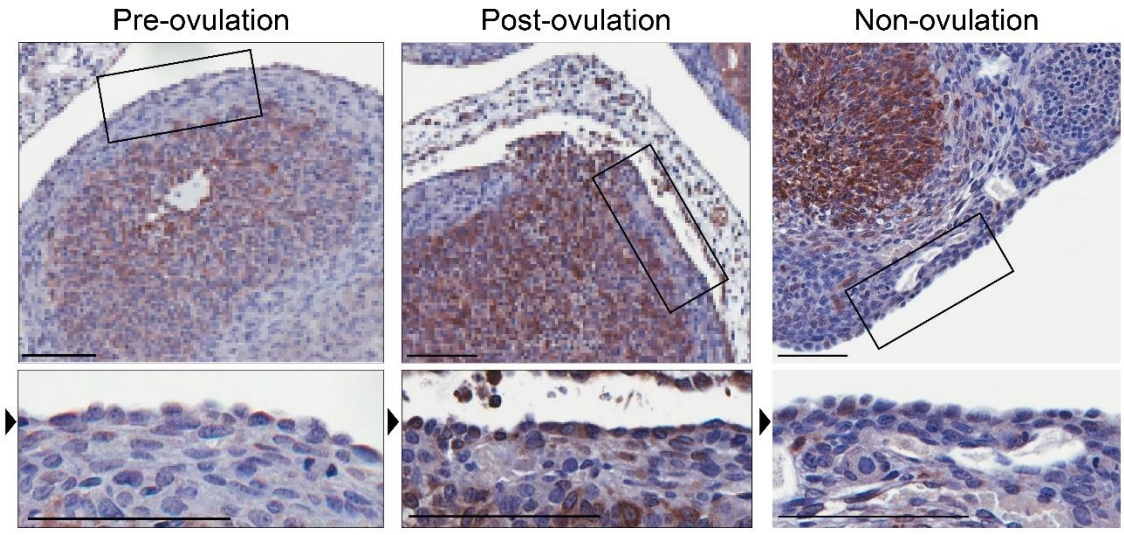

Figure 22. Immunohistochemistry detecting COX2 during ovulatory wound repair. OSE in the ovary sections collected prior to ovulation (6 hr post-hCG; Pre-ovulation) do not express COX2 whereas the OSE in ovary sections collected after ovulation (14 hr post-hCG) do express COX2, as indicated by the box and arrowhead. OSE surrounding non-ovulatory sites in ovary sections collected after ovulation (14 hr post hCG) do not express COX2, as indicated by the box and arrowhead. Granulose cells express COX2 and act as a positive control. Representative sections, N=5. Scale bar = 100 µm.

Summary

TGFB1 treatment of mOSE cells increases the expression of *Cox2* and secretion of PGE2. mOSE cells overexpressing *Cox2* have modestly increased cell migration but do not have altered *Snail* or *Krt19* expression. *Cox2* overexpression and PGE2 treatment independently activate the AKT pathway and promote cell survival in cells undergoing ovulation-associated stress. Cell viability is decreased in the presence of a COX2 inhibitor and by deletion of the PGE2 receptor *Ptger4*. These data suggest the TGFB1-mediated increase in COX2 promotes a survival phenotype in mOSE cells through PGE2 production and signalling through the PTGER4 receptor to activate the AKT signalling pathway.

3.3: TGFB1 promotes stemness partially through *Snail* upregulation and *Brca1* downregulation

Over the past 10 years, 7 studies have reported that the OSE cell layer contains a population of stem/progenitor cells (summarized in Figure 2). It has been hypothesized that these cells contribute to maintaining homeostasis in the OSE. What is clear from these studies, and recently reviewed by Ng and Barker (2015), is that there are many markers of OSE stemness that have been found including *Aldh1*, *Lgr5* and *Ly6a* (*Sca1)*. Isolating OSE cells expressing these markers independently enriches for cells with stem cell characteristics (Gamwell et al. 2012; Flesken-Nikitin et al. 2013; Ng et al. 2014). However, what remains unclear from these studies is if this population of cells can be

purified by enriching for a combination of these markers. Furthermore, there is currently no knowledge of how this population of cells is regulated.

TGFB1 promotes stemness in the OSE

As mentioned in the introduction, stemness may be best represented as a cell state rather than a defined population of cells. In the context of ovulatory wound repair, we can speculate that this stemness state would allow the OSE to assume a less differentiated state to help maintain homeostasis. After wound repair is completed, the OSE cells would then convert back to a more differentiated state to maintain the epithelial barrier. Our lab previously reported the ability of mOSE cells to acquire *Sca1* expression when cultured with TGFB1, demonstrating their plasticity (Gamwell et al. 2012). Furthermore, we demonstrated that mOSE cells have approximately 0.17% sphere forming efficiency which is roughly six times greater in the presence of TGFB1 (Gamwell et al. 2012). To validate the findings that OSE cells treated with TGFB1 assume a stem-like state, mOSE cells were cultured with TGFB1 for 2 weeks in free-floating sphere forming conditions. mOSE cells treated with TGFB1 have enhanced primary and secondary sphere formation, in agreement with the previous studies from our lab (Figure 23A-B) (Gamwell et al. 2012). Morphologically, mOSE spheres appeared uniform is size and shape (large and compact), regardless of TGFB1 treatment (Figure 23C). To validate this capacity in human cells, hOSE cells were cultured with TGFB1 in methylcellulose sphere forming conditions. As observed with the mOSE cells, hOSE cells treated with TGFB1 also displayed enhanced sphere formation compared to untreated

hOSE cells (Figure 24A). Morphologically, TGFB1-treated hOSE spheres appear uniform, as small and compact spheres (Figure 24B). hOSE sphere forming assays were performed in methylcellulose as primary spheres to prevent cell aggregation, and because of the limited proliferative capacity of these cells.

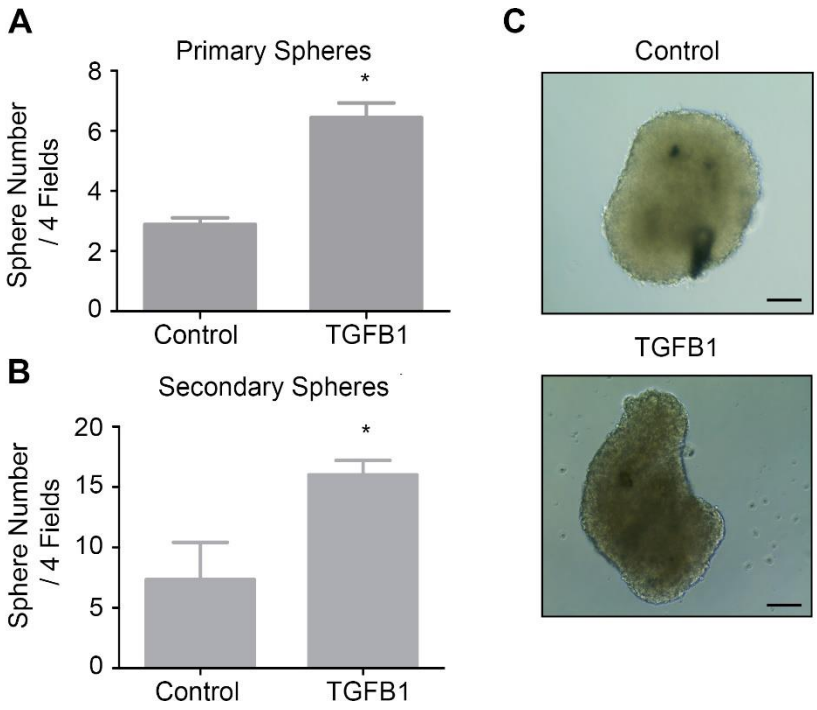

Figure 23. TGFB1 increases sphere formation in mOSE cells. **A-B)** mOSE cells treated with TGFB1 (10 ng/mL) have enhanced primary (A) and secondary (B) sphere formation compared to untreated cells, as determined using a free-floating sphere assay (N=3, Student T-test). **C)** Morphologically, control and TGFB1-treated spheres appear large and compact, as determined using phase contrast microscopy (representative image, N=3 sphere forming assays, 3 wells/N and 4 fields/well). * indicates a significant difference from the untreated control group, $P < 0.05$. Scale bar = 100 µm.

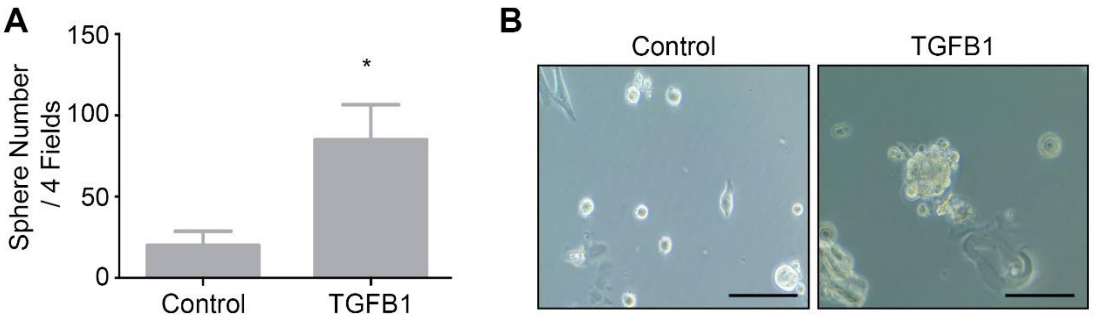

Figure 24. TGFB1 increases sphere formation in hOSE cells. **A)** hOSE cells treated with TGFB1 (10 ng/mL) have enhanced primary sphere formation compared to untreated cells, as determined using a methylcellulose sphere forming assay (N=3, Student T-test). **B)** TGFB1-treated spheres appear uniform in structure, as small and compact spheres, as determined using phase contrast microscopy (representative image, N=3 sphere forming assays, 3 wells/N and 4 fields/well). * indicates a significant difference from the untreated control group, $P < 0.05$. Scale bar = 100 µm.

TGFB1-treated mOSE cells were used to assess whether the increase in sphere formation coincided with an increase in the expression of previously reported OSE stemness markers. mOSE cells treated with TGFB1 did not increase the expression of *Aldh1*, *Lgr5*, *Nanog*, *Lhx9* or *SFRP1* (Figure 25). These data suggest the stemness characteristics induced with TGFB1 treatment are not due to increased expression of previously reported mOSE stem cell markers.

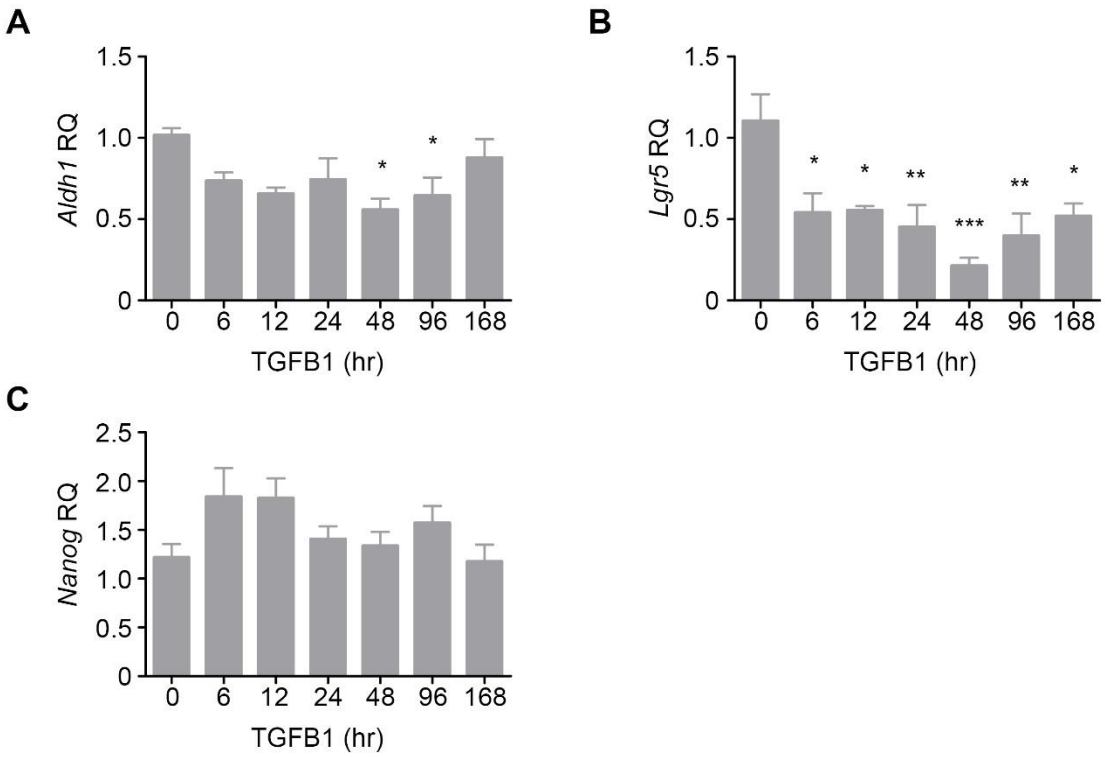

Figure 25. TGFB1 does not induce the expression of previously reported markers of OSE stemness in mOSE cells. mOSE cells cultured with TGFB1 (10 ng/mL) decrease the expression of *Aldh1* and *Lgr5* (A-B) and do not alter the expression of *Nanog* (C), as determined by Q-PCR (N=3, One-way ANOVA, Dunnett's post-test). *Lhx9* and *SFRP1* were not detectable in these samples (data not shown). RQ = relative quantity to untreated samples. *, **, *** indicate a significant difference from the untreated control group, $P < 0.05$, 0.01 and 0.001 respectively.

A stem cell PCR array was used to further characterize OSE stemness induced by TGFB1 treatment. The stem cell array identified increased expression of *Ncam1* (14-fold), *CD44* (13-fold) and *Ascl2* (6-fold) as the top 3 TGFB1-induced genes in mOSE cells (Figure 26). *CD44* has previously been reported as a marker of stemness in the fallopian tube and was recently found to be expressed in mOSE cells (Paik et al. 2012; Alwosaibai et al. 2017). The increase in *CD44* expression in mOSE cells was validated using a time course of TGFB1 treatment (Figure 27). To validate *CD44* expression as a stemness marker, CD44-positive mOSE cells were isolated from mOSE cells by FACS and placed in methylcellulose sphere-forming conditions. The FACS sorting enriched for mOSE cells expressing CD44 variant exons 3, 4, 7 and 8 (Figure 28A) and, when placed in sphere-forming conditions, CD44-positive mOSE cells had a higher sphere-forming capacity than CD44-negative mOSE cells (Figure 28B). Morphologically, CD44-positive spheres appeared small and compact (Figure 28C). These data suggest *CD44* expression is a marker of TGFB1-induced mOSE stemness.

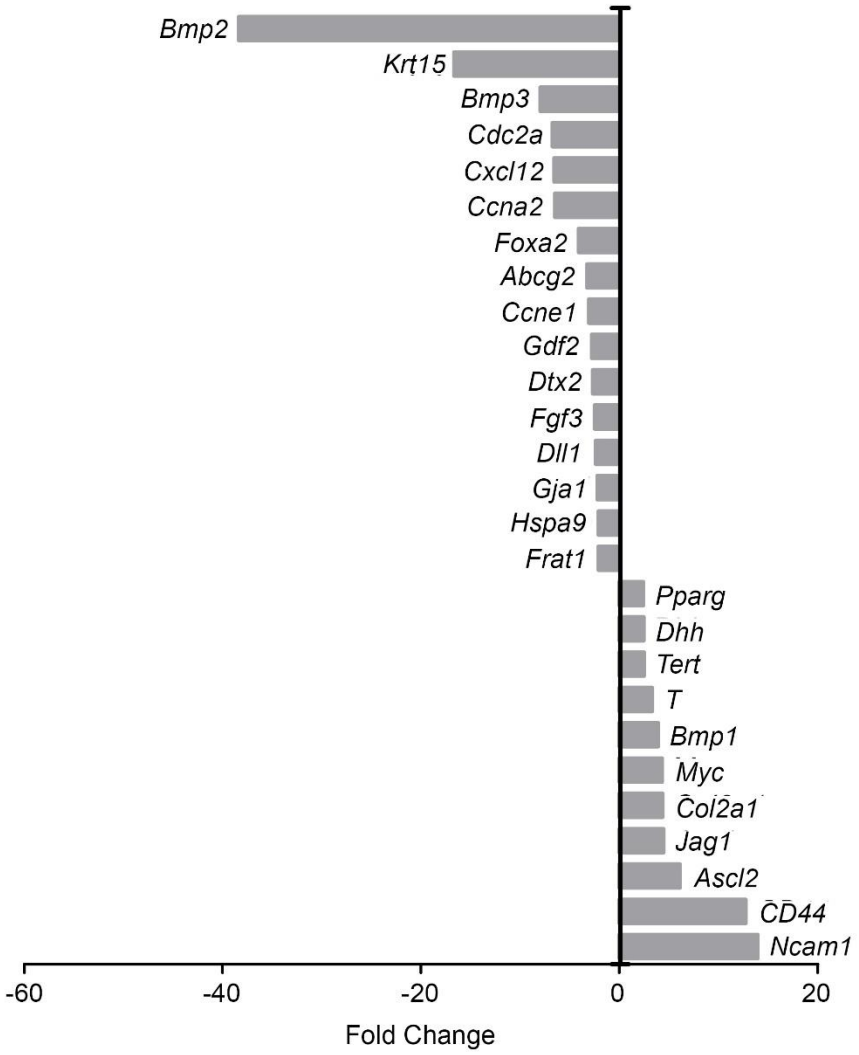

Figure 26. Stem cell PCR array of RNA extracted from mOSE cells treated with TGFB1 (10 ng/mL, 7 days). Genes presented are significantly upregulated and downregulated by TGFB1 treatment (N=3, Student T-test).

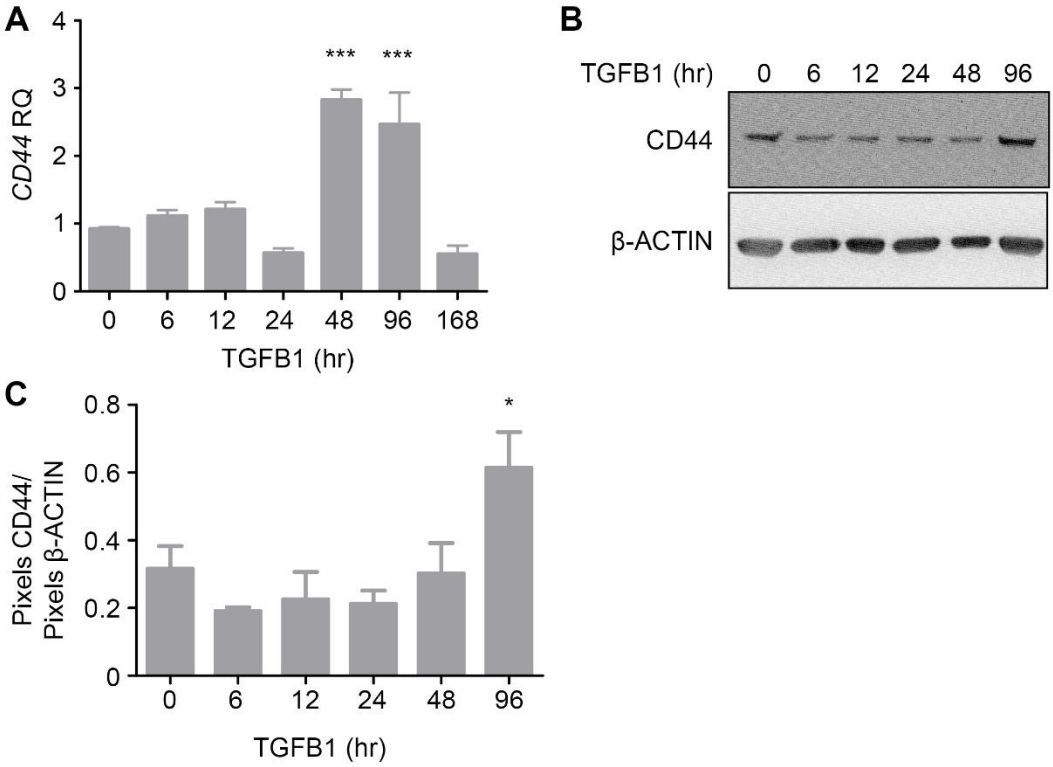

Figure 27. mOSE cells treated with TGFB1 increase *CD44* expression. mOSE cells treated with TGFB1 (10 ng/mL) have increased *CD44* expression, as determined by Q-PCR (A, N=3, One-way ANOVA, Dunnett's post-test) and western blot (B, quantified in C). β-ACTIN was used as a loading control for the western blot (representative western blot, N=3, One-way ANOVA, Dunnett's post-test). RQ = relative quantity to untreated mOSE cells. *, *** indicate a significant difference from the untreated control group, $P<0.05$ and 0.001 respectively.

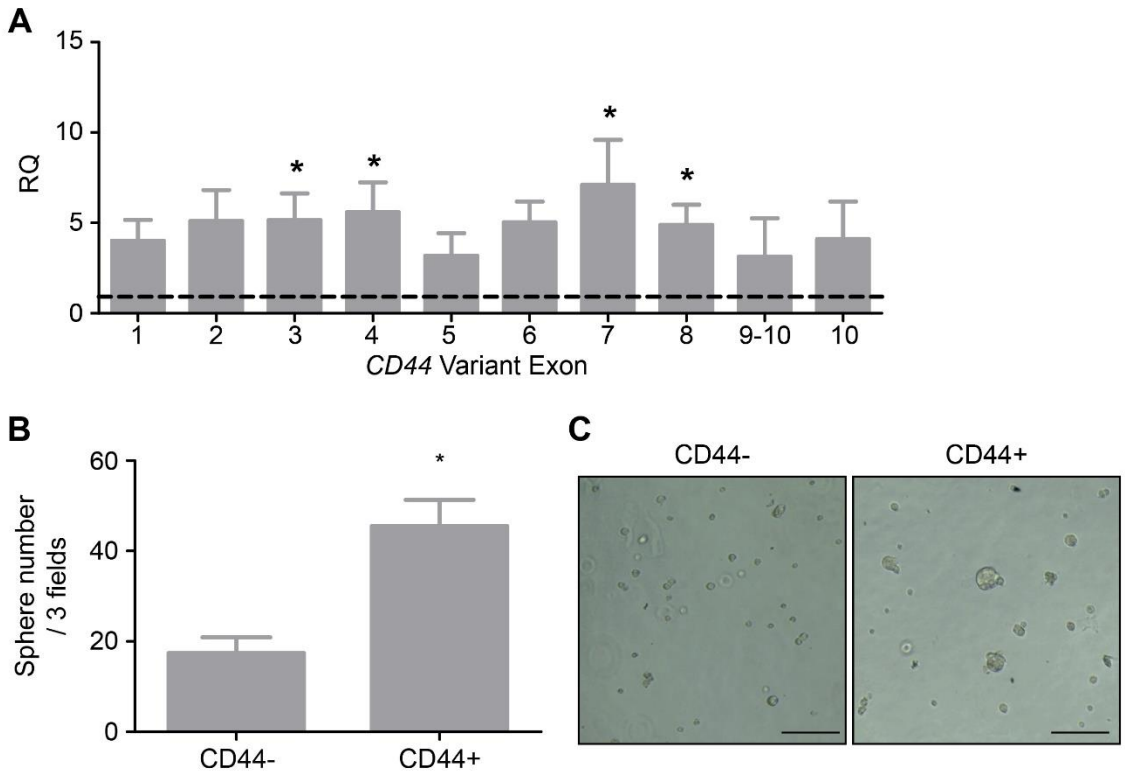

Figure 28. mOSE cells enriched for *CD44* expression have enhanced sphere formation. **A)** CD44-positive mOSE cells are enriched for variant exons 3, 4, 7 and 8, as determined by Q-PCR (N=3, Paired T-test). The dotted line represents the expression levels in unsorted mOSE cells. **B)** CD44-positive mOSE cells have enhanced sphere formation compared to CD44-negative mOSE cells, as determined using a methylcellulose sphere forming assay (N=3, Student T-test). **C)** The spheres formed from CD44-positive mOSE cells appear small and compact, as determined using phase contrast microscopy (representative image, N=3 sphere forming assays, 3 wells/N and 3 fields/well). RQ = relative quantity to unsorted mOSE cells. * indicates a significant difference from the CD44-negative group, $P < 0.05$. Scale bar = 100 µm.

To better characterize mOSE stemness and to help define the regulators of this phenotype, mRNA from mOSE cells cultured as monolayers and as spheres, with or without TGFB1 treatment were used for RNA-seq. Sequencing results identified 5682 differentially expressed genes among treatment groups. Hierarchical clustering revealed 7 clusters of gene expression patterns corresponding to TGFB1 treatment and culture conditions (Figure 29A). GO Term analysis of the genes found within each cluster revealed enriched terms that are unique to each cluster (Figure 29B). Sample genes found within each cluster are depicted in Figure 29C.

Cluster 1 was comprised of 1471 genes that enriched for the terms developmental process and regulation of response to stimulus. Cluster 1 genes were induced by TGFB1 only in monolayer culture conditions. *Tgfbr2* was a notable gene found within this cluster. Cluster 2 was comprised of 1733 genes, and primarily enriched for cell cycle and proliferation genes, such as *Cdk1/4*. Cluster 2 genes were found to be decreased in sphere forming culture conditions and include *Brca1* and *Col1a1*. Cluster 3 was comprised of 306 genes and enriched for terms such as cellular response to chemical stimulus. Cluster 3 genes were primarily decreased by TGFB1 treatment in both monolayer and sphere forming conditions and include genes such as *Krt19*. Cluster 4 was comprised of 795 genes that enriched for the GO term response to interferon-beta. Cluster 4 genes were decreased in sphere forming culture conditions and were unaffected by TGFB1 treatment. *Lats2* is an example of a gene found within cluster 4. Cluster 5 was comprised of 406 genes and enriched for terms including positive

regulation of developmental process and response to chemical. Sample genes found within this cluster include *Zeb1/2*, *Sox9*, *Greb1*, *Aldh1a7*, *Esr1*, *Twist1* and *Pax8*. This cluster represents genes that were primarily induced by sphere-forming culture conditions. Cluster 6 was comprised of 818 genes and enriched for system development and cell adhesion. Sample genes found within this cluster include *Mmp2* and were found to be increased by TGFB1, primarily in sphere-forming culture conditions. Cluster 7 was comprised of 153 genes and enriched for system development and inactivation of MAPK activity. Sample genes found within this cluster include *Snail* (*Snai1*), *Cox2* (*Ptgs2*), *Tgfb1* and *CD44*. These genes were increased by TGFB1, and more so by sphere-forming culture conditions. A complete list of genes in each cluster can be found at can be found at GSE121936.

Cluster 5 is of particular interest because it highlights the genes increased by culturing mOSE cells in sphere forming conditions and presumably, the genes promoting this phenotype. The EMT TFs found in this cluster (*Zeb1/2*, and *Twist1*) were not increased by TGFB1 treatment. Furthermore, the expression of the stem cell markers *Aldh1a7* and *Sox9* found in this cluster were not enhanced by TGFB1 treatment. This data suggests that although TGFB1 enhances sphere formation in mOSE cells, other EMT associated pathways are involved in the regulation of mOSE stemness. Additional EMT associated genes and stem cell markers were elevated in sphere forming conditions with the addition of TGFB1 (Cluster 7 genes, ex: *Snail*, *Cox2*, *CD44*), and are presumably the genes associated with TGFB1-enhanced stemness. These data highlight the different genes

associated with monolayer vs spheroid cultures and control vs TGFB1-treated OSE in these cultures.

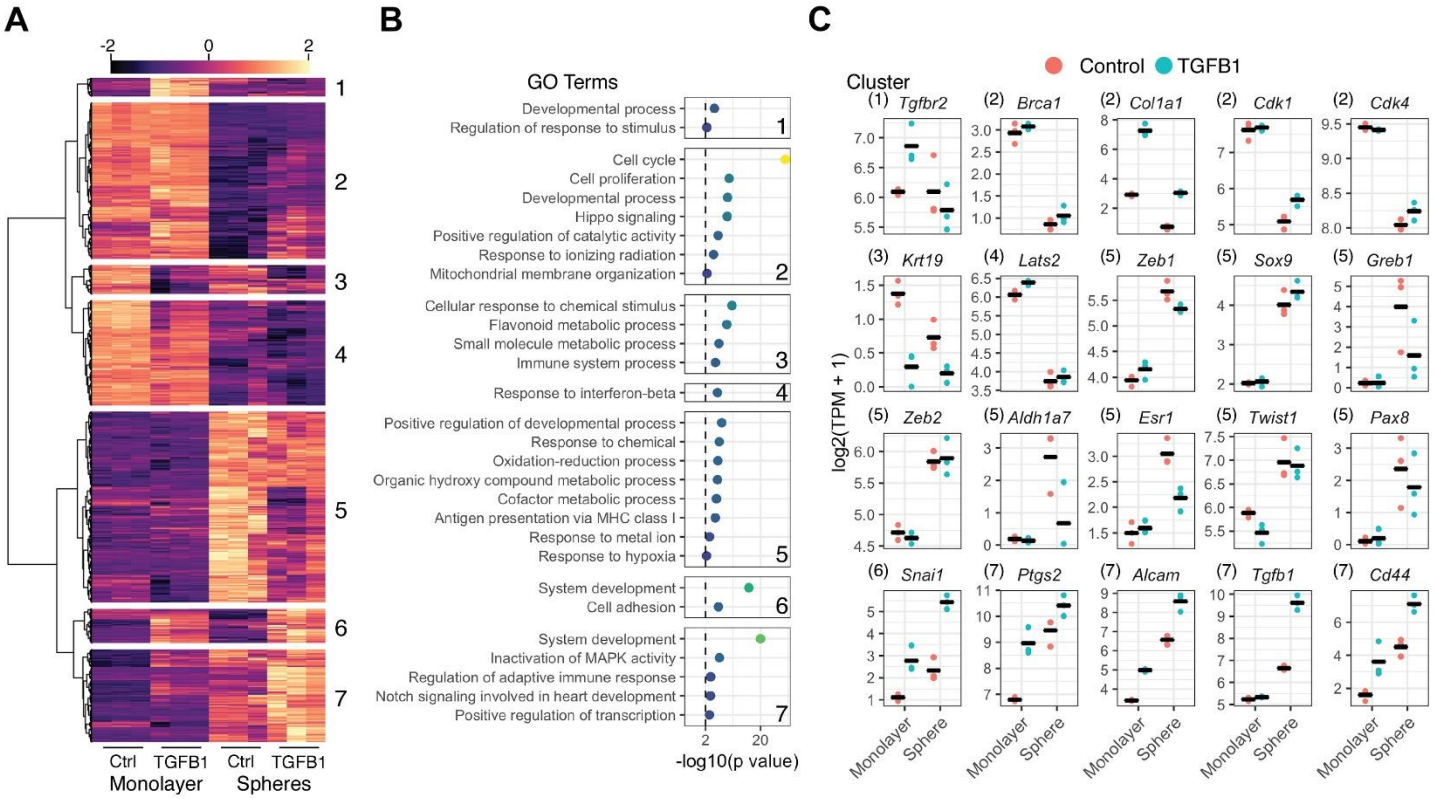

Figure 29. Transcriptional profiling of mOSE cells cultured as monolayer or in spheroid conditions, with or without TGFB1 (10 ng/mL). **A)** Heat-map representation of RNA sequencing results demonstrating 7 clusters of gene expression patterns between treatment groups. **B)** GO terms corresponding to the 7 gene expression clusters identified in A. **C)** Sample genes from each of the 7 gene expression clusters identified in A.

Snail expression promotes sphere formation in mOSE cells

Many of the genes found within cluster 7 are components of the TGFB1 response in OSE cells described in chapters 3.1 and 3.2. These genes are found to be increased by sphere-forming culture conditions, and further increased by TGFB1 treatment. We hypothesized that the increase in expression of cluster 7 genes, such as *Snail*, drives some of the increased stemness observed with TGFB1 treatment. To address this hypothesis, we first assessed stemness characteristics in mOSE cells with doxycycline induced *Snail* overexpression or *GFP* expression (im*Snail* and i*GFP* cells), as described in Chapter 3.1. Neither the induction of *Snail* or *GFP* significantly altered the expression of *Sca1* or *CD44* in mOSE cells (Figure 30). However, when cultured as spheres, *Snail* induction increased both primary and secondary sphere formation (Figure 31A). Sphere formation was not affected in the control cells with induced *GFP* expression (Figure 31A). The spheres formed by inducible *Snail* expression were consistent in size and shape, regardless of doxycycline treatment (large and compact) whereas the spheres formed with induced *GFP* expression were compact and decreased in size with increasing doxycycline dose (Figure 31B).

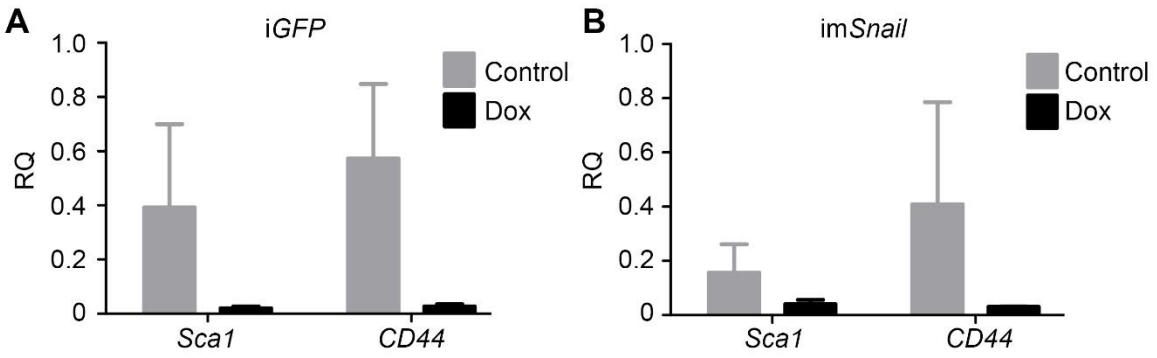

Figure 30. Inducible expression of *Snail* or *GFP* does not alter *Sca1* or *CD44* expression in mOSE cells. i*GFP* (A) and im*Snail* (B) treated with doxycycline (Dox) (200 ng/mL, 2 days) do not have altered *Sca1* or *CD44* expression, as determined by Q-PCR (N=3, Student T-test). RQ = relative quantity to untreated mOSE cells.

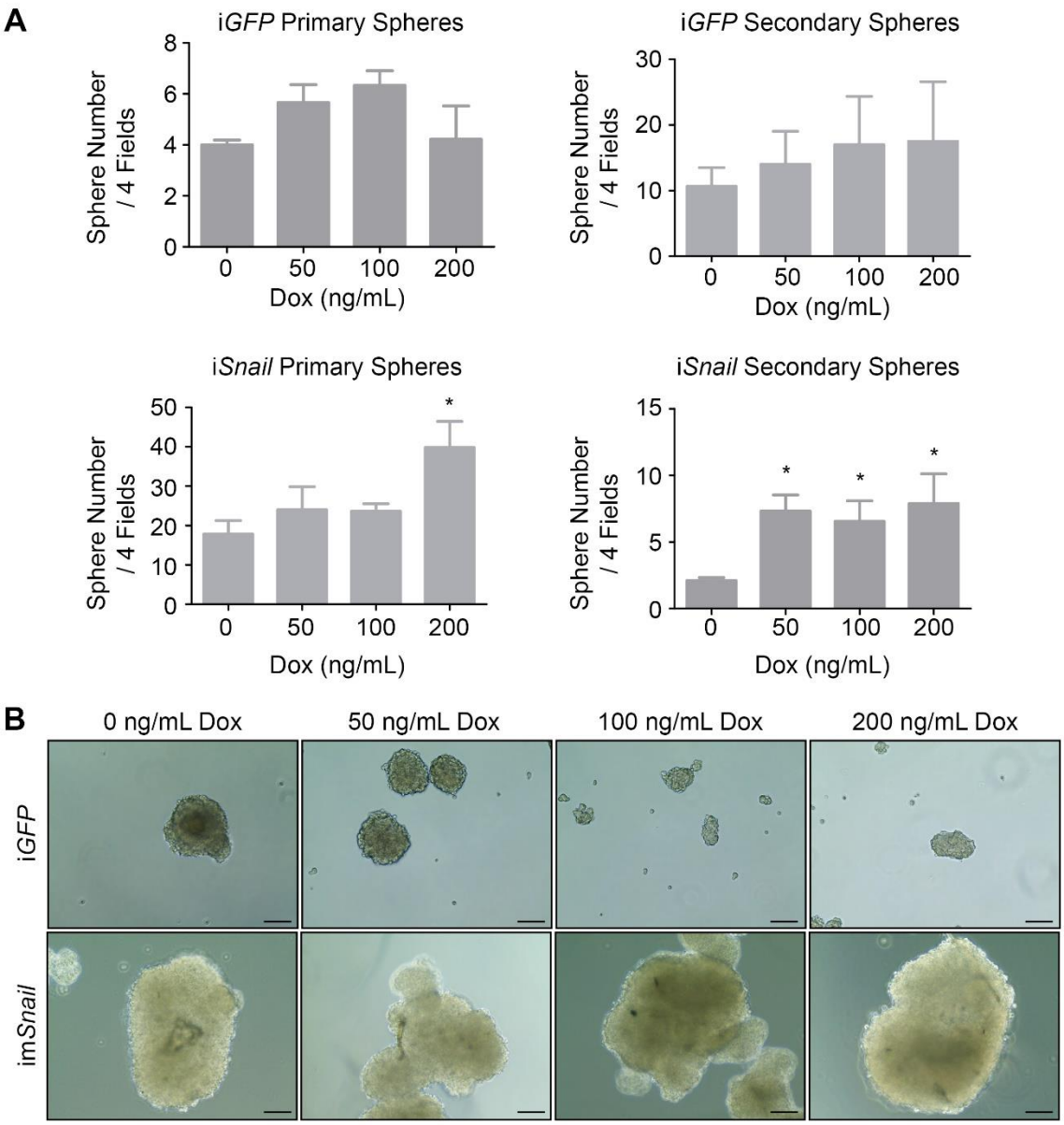

Figure 31. Inducible *Snail* expression promotes sphere formation in mOSE cells. **A)** mOSE cells with doxycycline (Dox) induced *Snail* expression (im*Snail*) have increased primary and secondary sphere formation compared to untreated im*Snail* mOSE cells. Sphere formation in mOSE cells with dox-induced *GFP* (i*GFP*) is unaffected, as determined using free-floating sphere assays (N=3, One-way ANOVA, Dunnett's post-test). **B)** i*GFP* spheres appear increasingly smaller and more compact with Dox treatment, whereas im*Snail* cell spheres appear consistently large and compact with Dox treatment, as determined by phase contrast microscopy (representative image, N=3 sphere forming assays, 3 wells/N and 4 fields/well). * indicates a significant difference from the untreated group, $P < 0.05$. Scale bar = 100 µm.

To determine which actions of TGFB1 are associated with the actions of SNAIL, we used RNA-Seq to examine the effects of *Snail* expression on the transcriptional profile in im*Snail* mOSE cells, cultured in monolayer conditions and treated with doxycycline to induce *Snail* expression, compared to untreated im*Snail* mOSE cells. There were 358 genes upregulated by *Snail* overexpression and 556 genes downregulated. GO term analysis revealed EMT terms enriched by *Snail* expression including ECM-receptor interaction and locomotion (Figure 32A). Many of the genes found to be upregulated by *Snail* induction were collagens (ex: *Col1a1*, *Col6a1*, *Col18a1*), as demonstrated in a volcano plot (Figure 32B). Other genes found to be increased by *Snail* overexpression include ADAMTS genes such as *Adamts4*. Genes found to be decreased by *Snail* overexpression include keratins such as *Krt18*, and interestingly, some mesenchymal genes such as *Itga7* and *Alcam* (Figure 32B). Much of the gene expression induced by TGFB1 was not associated with *Snail* induction and enriched for EMT associated GO terms such as cell adhesion and cell migration (gene list available at GSE121936. Although many EMT characteristics are induced by *Snail* overexpression, much of the TGFB1-induced EMT response is independent of *Snail*, and helps to explain why *Snail* overexpression induced only a partial EMT in mOSE cells (Chapter 3.1). This data also suggests that the genes in common between TGFB1 treatment and *Snail* overexpression, such as collagens, may promote the enhanced stemness phenotype observed with TGFB1 treatment.

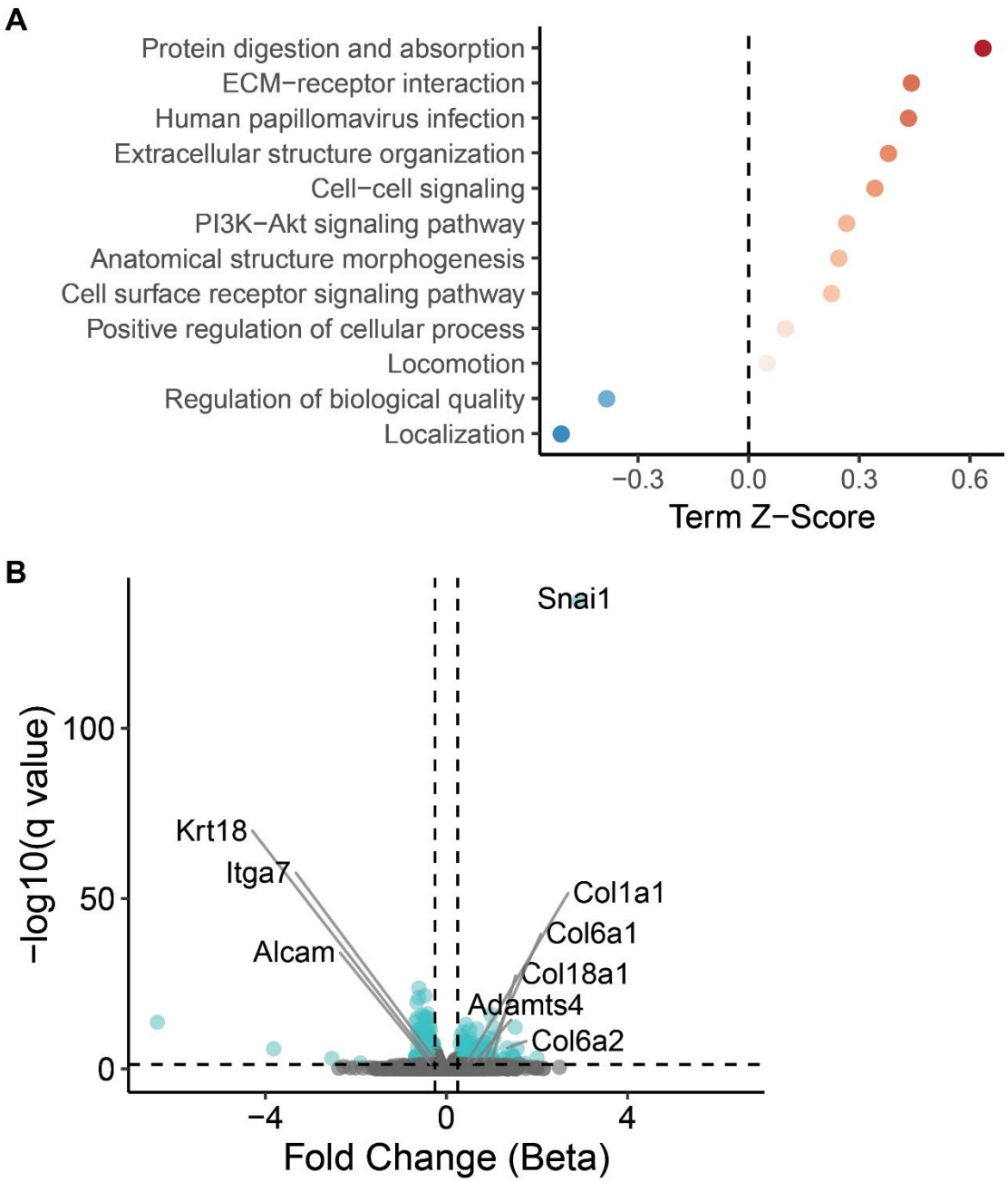

Figure 32. Transcriptional profile of induced *Snail* expression in mOSE cells. **A)** Plot of GO terms enriched with doxycycline induced *Snail* overexpression (200 ng/mL, 96 hr) in im*Snail* mOSE cells. **B)** A volcano plot showing examples of upregulated and downregulated genes associated with *Snail* overexpression. Data were generated using RNA-seq (N=3).

COX2 expression promotes sphere formation in mOSE cells

We next sought to determine whether *Cox2*, another gene found within cluster 7, is also able to promote sphere formation in mOSE cells. To address this objective, COX2 overexpressing mOSE cells (WPI-*Cox2*, described in Chapter 3.2) were cultured in free-floating sphere conditions. WPI-*Cox2* mOSE cells produced the same number of primary spheres as mOSE cells infected with the empty vector (WPI) (Figure 33A). However, when these spheres were dissociated, WPI-*Cox2* mOSE cells formed significantly more secondary spheres than WPI mOSE cells (Figure 33A). Morphologically, the spheres in all conditions appeared large and compact, similar to those seen with induced SNAIL overexpression and TGFB1 treatment (Figure 33B). RNA was assessed for the TGFB1-enhanced stem cell markers *CD44* and *Sca1*, which were not found to be different between WPI-*Cox2* and WPI mOSE cells, nor was *Snail* expression (Figure 34). These data suggest that genes found within cluster 7 promote the enhanced sphere formation present in TGFB1 treated mOSE cells, and that COX2 overexpression does not promote *Snail* expression.

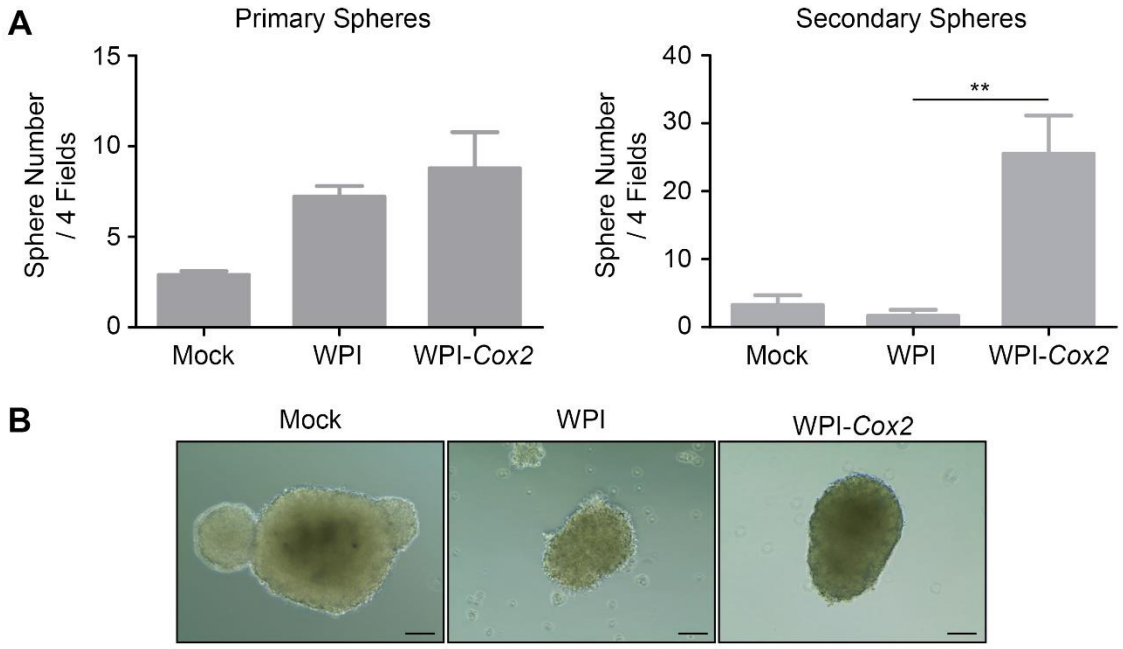

Figure 33. mOSE cells overexpressing COX2 have enhanced secondary sphere formation. **A)** mOSE cells overexpressing COX2 (WPI-*Cox2*) do not have altered primary sphere formation but have enhanced secondary sphere formation, compared to mOSE cells infected with the empty vector (WPI), as determined using a free-floating sphere assay (N=3, One-way ANOVA, Dunnett's post-test). **B)** Sphere morphology is large and compact regardless of COX2 expression, as determined using phase contrast microscopy (representative image, N=3 sphere forming assays, 3 wells/N and 4 fields/well). ** indicates a significant difference from the WPI control group, $P < 0.01$. Scale bar = 100 µm.

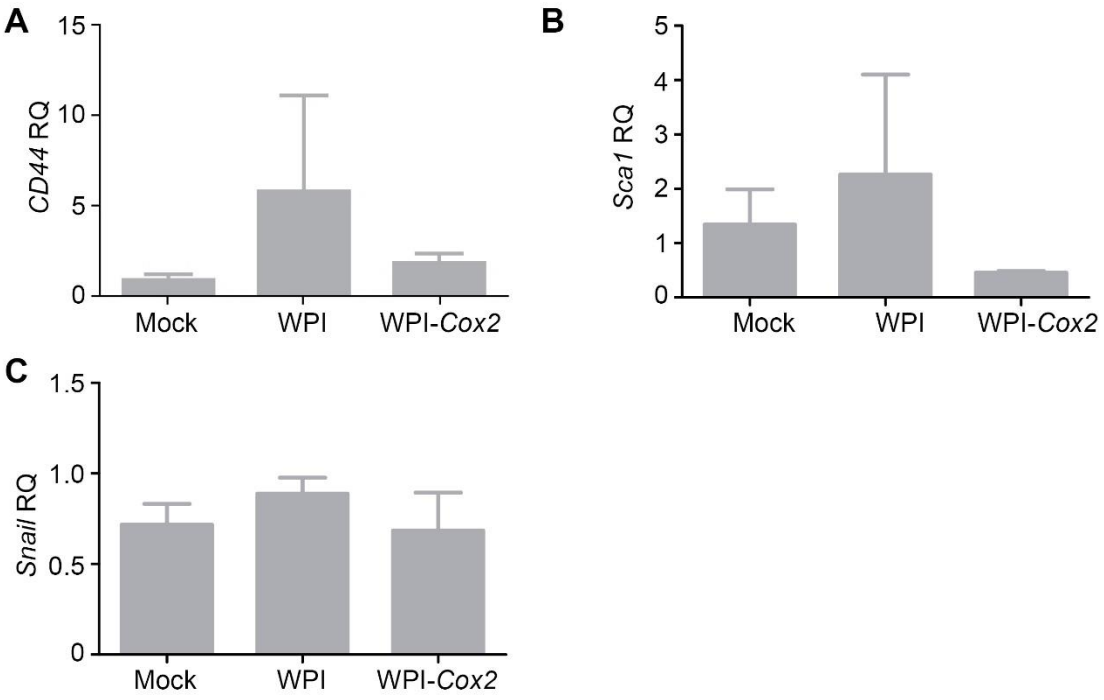

Figure 34. mOSE cells overexpressing COX2 do not have altered *CD44*, *Sca1* or *Snail* expression. mOSE cells overexpressing COX2 (WPI-*Cox2*) do not have altered *CD44* (A), *Sca1* (B) or *Snail* (C) expression levels compared to uninfected mOSE cells (Mock) or mOSE cells infected with the vector control (WPI), as determined using Q-PCR (N=3, One-way ANOVA, Dunnett's post-test). RQ = relative quantity.

Loss of BRCA1 promotes stemness in the OSE

The genes found within cluster 2 represent those whose expression is decreased primarily by culturing OSE cells in sphere forming conditions compared to monolayer conditions and are less influenced by TGFB1 treatment alone (Figure 29). *Brca1* is a notable gene found within cluster 2 and has been shown to regulate stemness and EMT induction in mammary epithelium (Bai et al. 2014). The RNA-seq data were obtained from mOSE monolayers after 96 hr of TGFB1 treatment. To better define if a relationship exists between TGFB1 treatment and *Brca1* expression, a TGFB1 time course in mOSE cells was used to assess *Brca1* expression at earlier time points. *Brca1* was shown to be decreased as early as 6 hr after TGFB1 treatment of mOSE cells and was not significantly different at 96 hr, in agreement with the RNA-seq results (Figure 35A). The decrease in *BRCA1* was confirmed in hOSE cells treated with TGFB1 for 2 days (Figure 35B). Furthermore, *Brca1* expression was unaffected by induced SNAIL or constitutive COX2 overexpression in mOSE cells, suggesting the *Brca1* repression by TGFB1 is transient, and independent of the TGFB1-induction of SNAIL and COX2 (Figure 35C-D).

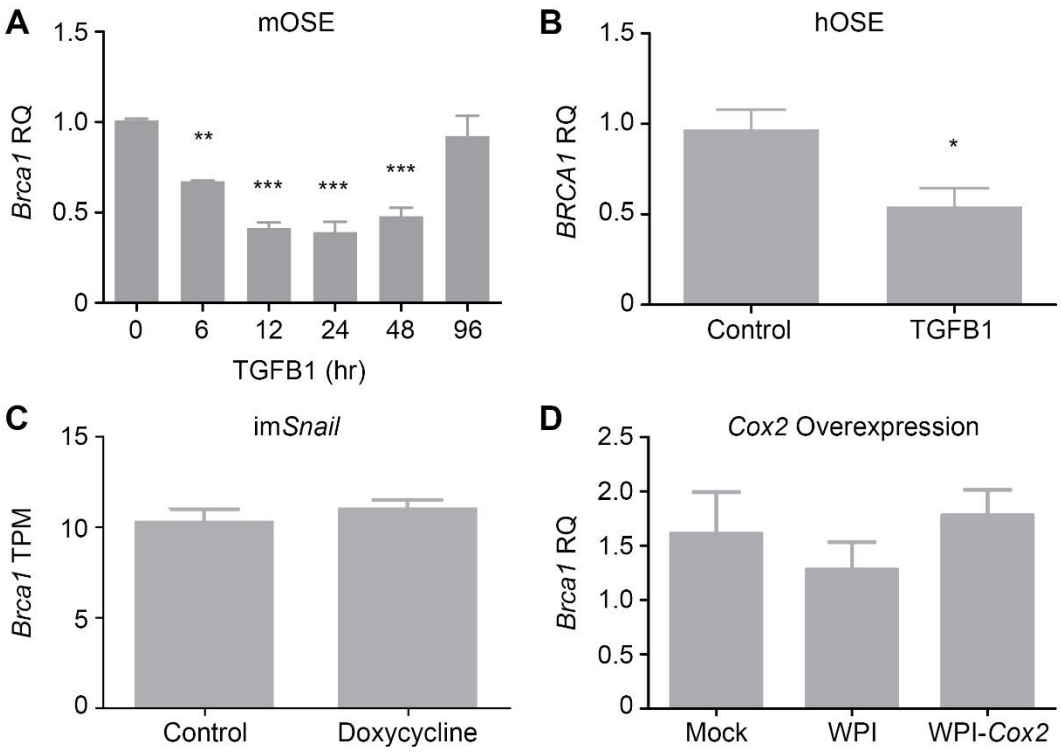

Figure 35. *Brca1* expression is decreased transiently by TGFB1 treatment, independent of *Snail* and *Cox2* overexpression. **A)** mOSE cells treated with TGFB1 (10 ng/mL) have decreased *Brca1* expression compared to untreated cells, as determined by Q-PCR (N=3, One-way ANOVA, Dunnett's post-test). **B)** hOSE cells treated with TGFB1 (10 ng/mL, 2 days) have decreased *BRCA1* expression compared to untreated cells, as determined by Q-PCR (N=3, Student T-test). **C)** *Brca1* expression is unaffected by induced *Snail* overexpression (Doxycycline, 200 ng/mL, 4 days) in im*Snail* mOSE cells compared to untreated cells, as determined by RNA-seq (N=3). TPM = transcripts per million. **D)** *Brca1* expression is unaffected by *Cox2* overexpression in WPI-*Cox2* mOSE cells compared to uninfected mOSE cells (Mock), or mOSE cells infected with the control vector (WPI), as determined by Q-PCR (N=3, One-way ANOVA, Dunnett's post-test). RQ = relative quantity to mock infected or untreated OSE cells. *, **, *** indicate a significant difference from the WPI control or untreated control group, $P < 0.05$, 0.01, 0.001 respectively.

To determine whether a loss of *Brca1* expression promotes OSE stemness, similar to that seen in mammary epithelium, mOSE cells were isolated from homozygous *Brca1*^{tm1Brn} mice and infected with Ad-*cre* to facilitate *Brca1* deletion (KO). Ad-*GFP* was used as a control (WT). *Brca1* deletion was verified by Q-PCR and western blot (Figure 36A-B). *Brca1* deletion increased *Sca1* expression and decreased *CD44* expression (Figure 36B-D). When culturing these cells in sphere-forming conditions *in vitro*, *Brca1* deletion promoted both primary and secondary sphere formation (Figure 36E-F). These spheres appeared more loosely aggregated than the TGFB1-treated spheres (Figure 36G). When examining the expression of *Cox2* and *Snail* for potential feedback into these components of the TGFB1-induced EMT, *Brca1* deletion decreased *Snail* and had no effect on *Cox2* expression (Figure 37). These data suggest that the loss of *Brca1* expression promotes the *Sca1*-associated stemness phenotype and promotes the formation of loosely aggregated spheres. Furthermore, these data suggest *Brca1* deletion negatively regulates the TGFB1-induction of *Snail* and *CD44* expression.

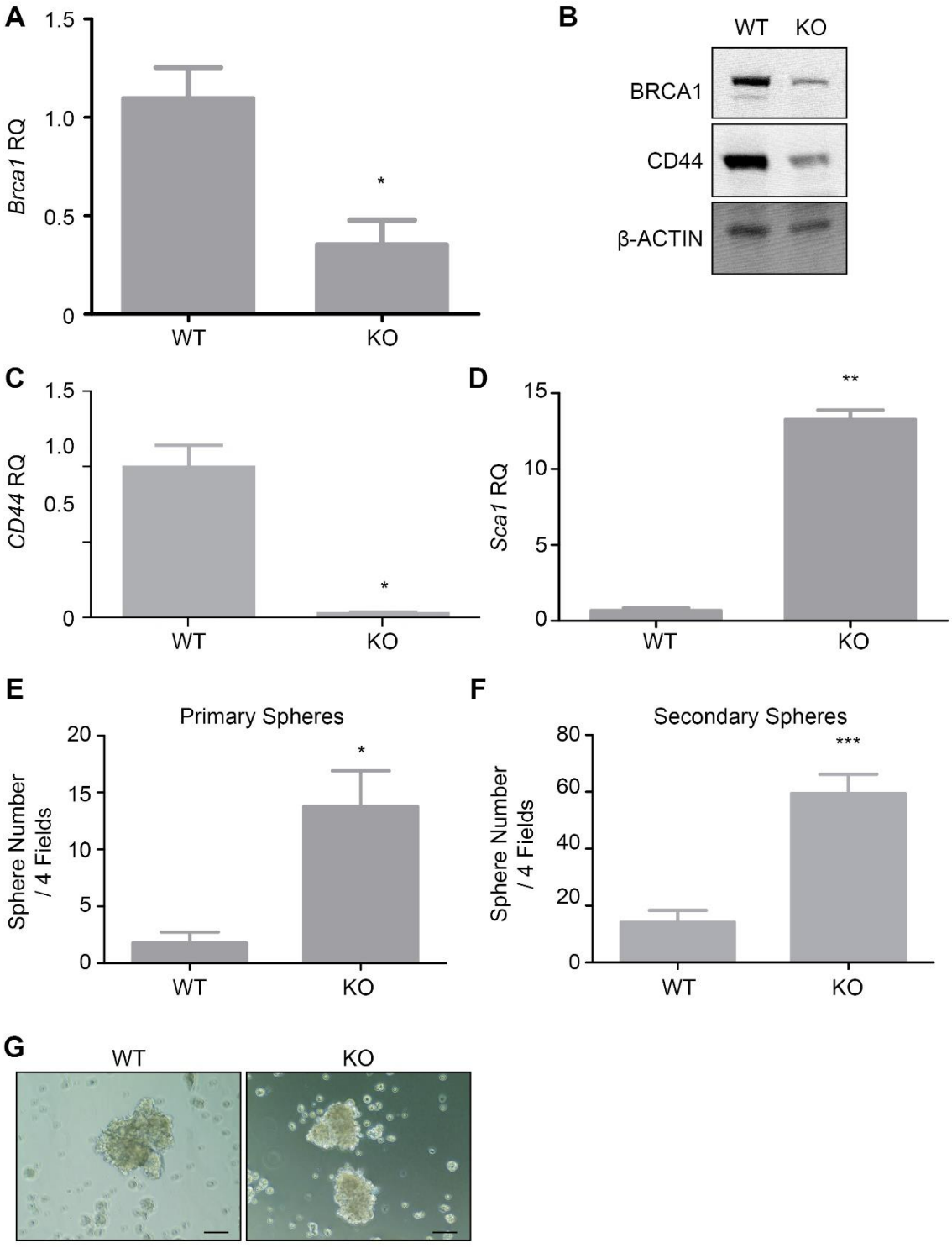
A
1.5
1.0
0.5
0
Brca1 RQ
*
WT
KO
B
WT
KO
BRCA1
CD44
β-ACTIN
C
1.5
1.0
0.5
0
CD44 RQ
*
WT
KO
D
15
10
5
0
Sca1 RQ
**
WT
KO
E
Primary Spheres
20
15
10
5
0
Sphere Number / 4 Fields
*
WT
KO
F
Secondary Spheres
80
60
40
20
0
Sphere Number / 4 Fields
***
WT
KO
G
WT
KO

Figure 36. *Brca1* knockout promotes *Sca1* expression and sphere formation in mOSE cells. **A)** mOSE cells isolated from *Brca1*^{tm1Brn} mice, infected with Ad-*cre* (KO) have decreased *Brca1* expression compared to *Brca1*^{tm1Brn} mOSE cells infected with Ad-*GFP* (WT), as determined by Q-PCR (N=3, Student T-test). **B)** KO mOSE cells show decreased BRCA1 and CD44 expression compared to WT mOSE, as determined by western blot. β-ACTIN was used as a loading control (representative western blot, N=3). **C-D)** KO mOSE cells have decreased abundance of *CD44* transcripts and increased *Sca1* transcripts compared to WT mOSE cells, as determined using Q-PCR (N=3, Student T-test). **E-F)** KO mOSE cells have increased primary (E) and secondary (F) sphere formation compared to WT mOSE cells as determined by a free-floating sphere assay (N=3, Student T-test). **G)** Morphologically, WT and KO spheres are large and loosely associated, as determined using phase contrast microscopy (representative image, N=3 sphere-forming assays, 3 wells/N and 4 fields/well). RQ = relative quantity to WT mOSE cells. *, **, and *** indicate a significant difference from the WT control group, $P < 0.05$, 0.01 and 0.001 respectively. Scale bar = 100 µm.

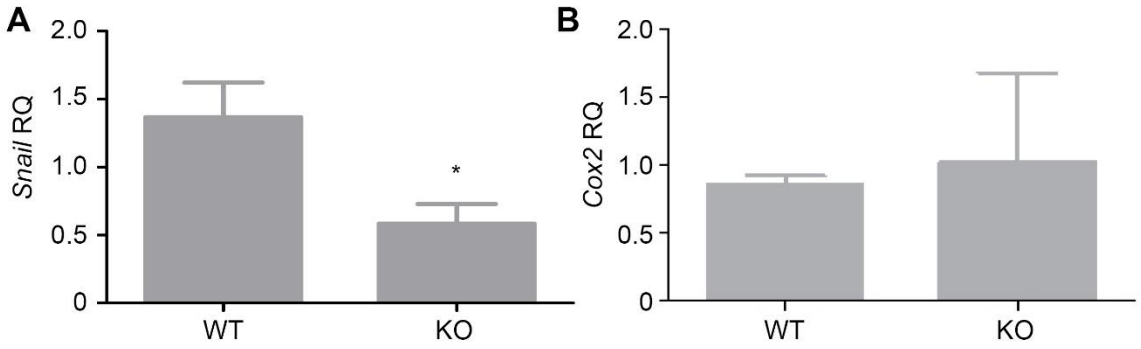

Figure 37. *Brca1* knockout decreases *Snail* expression in mOSE cells. **A)** mOSE cells isolated from *Brca1*^{tm1Brn} mice, infected with Ad-*cre* (KO) have decreased *Snail* expression compared to *Brca1*^{tm1Brn} mOSE cells infected with Ad-*GFP* (WT), as determined by Q-PCR (N=3, Student T-test). **B)** *Cox2* expression remains unchanged in WT and KO mOSE cells, as determined using Q-PCR (N=3, Student T-test). RQ = relative quantity to WT mOSE cells. * indicates a significant difference from the WT control group, $P < 0.05$.

Stozek et al. (2008) were the first to demonstrate a label retaining population of OSE cells in the mouse ovary. We therefore next sought to determine whether *Brca1* loss increased BrdU label retention in the OSE cells of *Brca1*^{tm1Brn} mice. First, we crossed the *Brca1*^{tm1Brn} mice with *B6.129X1-Gt(ROSA)26Sor*$^{tm1(EYFP)Cos}$*/J* mice to produce *Brca1*^{tm1Brn}*YFP* mice. *Brca1*^{tm1Brn}*YFP* mice were injected intrabursally (IB) with Ad-*cre* or PBS, and injected IP with BrdU. Ovaries were collected after a 30-day chase period and assessed for retention of the BrdU label and activation of the YFP reporter (as a indicator of *Brca1* deletion). Ad-*cre* injection IB in *Brca1*^{tm1Brn}*YFP* mice showed successful activation of the YFP reporter, compared to the PBS injection (Figure 38A). When combining the IB injections with an IP BrdU injection, Ad-*cre* treatment increased the number of label retaining OSE cells, without activation of the YFP reporter, but the label retention was significantly enhanced with activation of the YFP reporter (Figure 38B-C). These data suggest that *Brca1* deletion increases label retention as an indicator of stemness in the OSE *in vivo*.

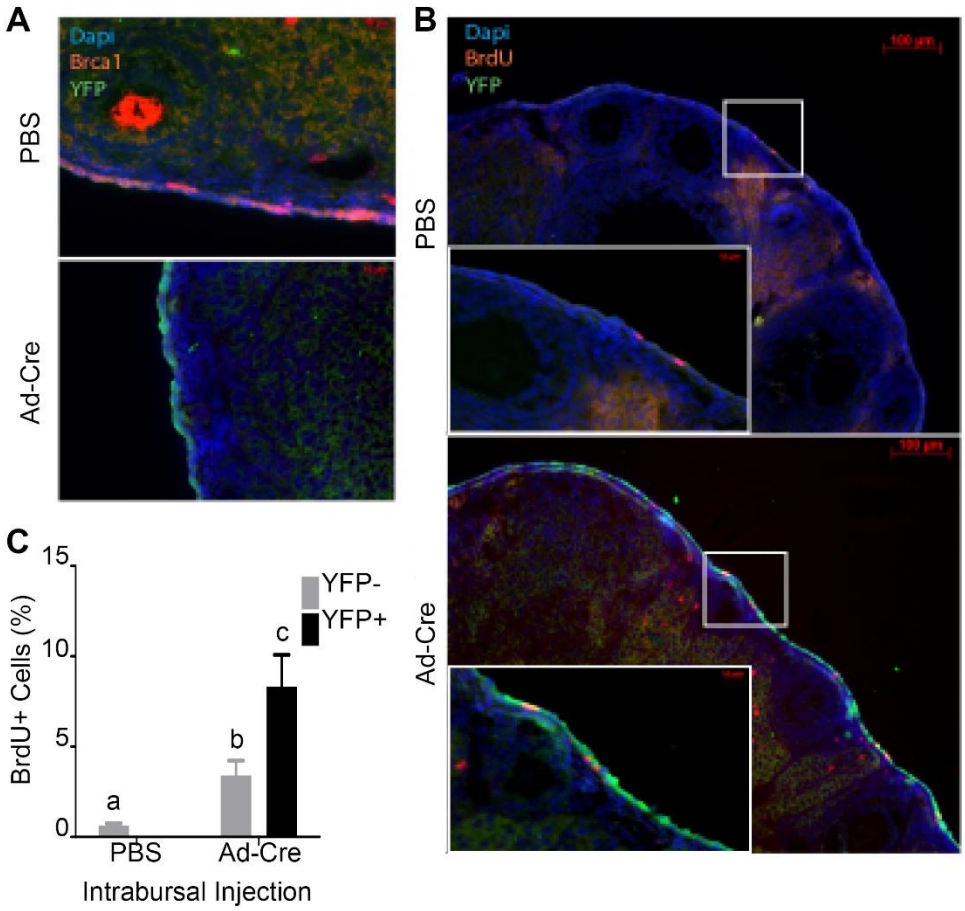

Figure 38. *Brca1* deletion increases label retention in mOSE cells *in vivo*. **A)** OSE layer of *Brca1*^{tm1Brn}*YFP* mice injected intrabursally (IB) with PBS or Ad-*cre* showing efficiency of *Brca1* deletion and activation of *YFP* expression (day 40 post injection). **B)** OSE layer of *Brca1*^{tm1Brn}*YFP* mice injected IB with PBS or Ad-*cre* and injected intraperitoneally with BrdU, identifying label retaining cells expressing *YFP* as a reporter for *Brca1* deletion (30-day post BrdU injection). **C)** Quantification of OSE cells retaining the BrdU label and expressing *YFP* as a reporter of *Brca1* deletion from panel B (N=4). a, b and c indicate a significant difference between treatment groups ($P < 0.05$). (Two-way ANOVA, Bonferroni post-test).

To further characterize the increased mOSE stemness seen with *Brca1* deletion, RNA was isolated from *Brca1*^{tm1Brn}*YFP* mOSE cells infected with Ad-*GFP* or Ad-*cre* and assessed using RNA-seq. There were 1028 significantly increased genes and 1101 significantly decrease genes with *Brca1* deletion. GO term analysis of these genes revealed transmembrane transport, ion transport and carboxylic acid transport as the top significantly enriched terms with *Brca1* loss whereas cell cycle, cellular response to DNA damage stimulus and cellular component organization or biogenesis were among the significantly downregulated terms (Figure 39A). There were also many pro-cancerous terms enriched in mOSE cells with *Brca1* deletion including gastric cancer, breast cancer and pathways in cancer (Figure 39A). Figure 37B highlights specific genes altered with *Brca1* deletion including the validation of increased *Sca1* (*Ly6a*) and decreased *CD44* expression. *Lgr5* is also significantly increased with *Brca1* deletion along with *Greb1* and *Esr1*. *Acta2, Twist* and cadherins such as *Cdh26* were decreased with *Brca1* deletion (Figure 39B). Among the significantly increased and decreased genes, there was no clear indication that these cells underwent an EMT with *Brca1* deletion, suggesting EMT is not associated with stemness under these conditions. A complete list of significantly altered genes can be found at GSE121936. These data suggest that the loss of *Brca1* expression promotes stemness and a pro-cancerous phenotype in mOSE cells.

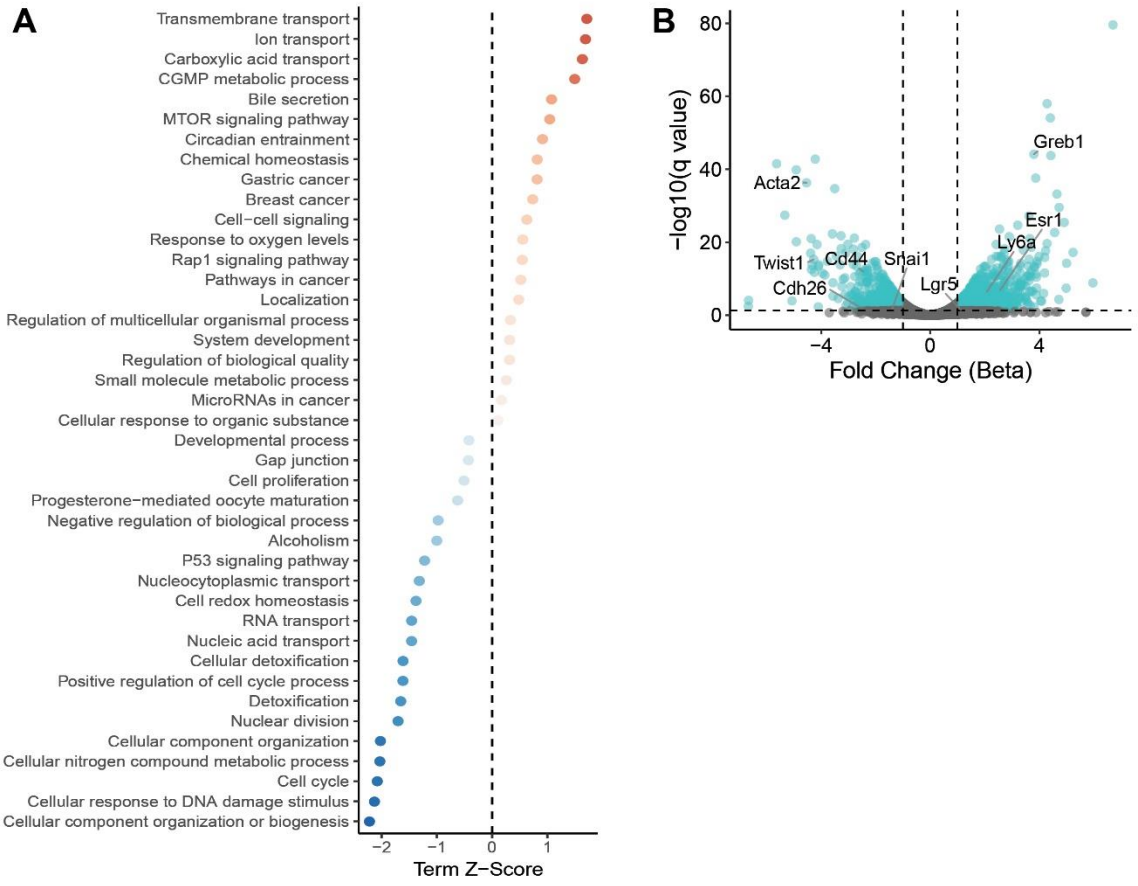

Figure 39. Transcriptional profile of *Brca1* deletion in mOSE cells. **A)** Plot of GO terms enriched with *Brca1* deletion in *Brca1*^{tm1Brn}*YFP* mOSE cells. **B)** A volcano plot showing examples of upregulated and downregulated genes associated with *Brca1* deletion in *Brca1*^{tm1Brn}*YFP* mOSE cells. Data were generated using RNA-seq (N=3).

Summary

TGFB1 treatment of OSE cells increased their sphere formation and the expression of the stem cell marker *CD44*. Isolating CD44-expressing mOSE cells enriched for those with sphere forming capacity as CD44-positive mOSE cells formed more spheres than CD44-negative mOSE cells. RNA-seq data showed stemness to be associated with mesenchymal gene expression. This was validated by *Snail* overexpression, which induced a partial EMT and was shown to promote sphere formation in mOSE cells. The expression of ovarian cancer associated genes including *Pax8*, *Greb1* and decreased *Brca1* expression was also associated with stemness and *Brca1* deletion was shown to promote stemness both *in vitro* and *in vivo*. The TGFB1 target *Cox2*, when overexpressed, also increased stemness in the mOSE. Comparing the transcriptional profile of mOSE cultured as monolayers, or as spheres, with or without TGFB1 showed stemness is not always associated with a mesenchymal gene expression, but that TGFB1 may promote stemness by promoting the mesenchymal state. These data characterize the transcriptional profile of inherent mOSE stemness vs TGFB1-induced stemness.

Chapter 4: Discussion

4.1: Wound Repair and re-epithelialization

Wound repair in the ovary is a process that is not well defined, in contrast to wound repair in other tissues such as the skin or intestine, which have been studied extensively. Reviewed in many papers, the early stages of wound repair in the skin include the formation of a fibrin-clot to mechanically plug the wound. Inflammation is then induced by the secretion of inflammatory cytokines such as Interleukin-1 and TNF-alpha from epithelial cells surrounding the wound and the fibrin clot. These cytokines induce an influx of immune cells to help clear the debris. The next phase of repair is re-epithelialization, which occurs within hours of tissue injury. Epithelial cells proliferate to replace the tissue lost during wounding. These new cells migrate into the wounded area to help close the wound. During this phase of repair, new matrix is deposited for the cells to migrate over and fibroblasts proliferate and differentiate into myofibers to aid in tissue contraction that helps to force the wound closed. Lastly, the fibrin clot is replaced by a collagen-rich tissue and keratinocytes differentiate and undergo stratification to restore the epithelial barrier (Kondo and Ishida 2010; Leoni et al. 2015; Eming et al. 2014).

TGFB1 promotes re-epithelialization in the OSE by inducing an EMT, partially through *Snail* expression, and by promoting ECM remodelling

In this work, we sought to better understand the mechanism of re-epithelialization that occurs during ovulatory wound repair. TGFB1 is a known to be a classical inducer of an EMT, and is a prevalent cytokine in wound repair (Kondo and Ishida 2010; Leoni et al. 2015; Eming et al. 2014). During a previous assessment of cytokine levels in preovulatory follicular fluid, we identified an abundance of TGFB1 (Gamwell et al. 2012). At ovulation, TGFB1 is released in the follicular fluid and bathes the surrounding OSE cells after follicular rupture. It is also secreted by immune cells present at the wound site, such as macrophages (Shaw and Martin 2016), and is produced by other ovarian cells (granulosa cells) (Knight and Glister 2006). When combined with results of the experiments described in this thesis, it becomes apparent that TGFB1 induces an EMT in OSE cells and requires the activity of the ATP domain of TGFBRI. The sole traditional EMT transcription factor induced by TGFB1 treatment of the mOSE was *Snail*, but interestingly, and contrary to the mammary epithelium (Mani et al. 2008), *Snail* induction alone only induced a partial EMT. This finding has not been previously reported in the ovary, however a partial EMT following *Snail* expression has been observed in renal epithelial cells (Grande et al. 2015). These results suggest the additional characteristics driven by TGFB1 are mediated by other genes either alone, or in conjunction with *Snail*. This concept supports the theory proposed by Jolly et al. (2017) that EMT characteristics are best observed as separate vectors on the EMT continuum and are controlled by different factors.

In the OSE cells, we have found that SNAIL mediates their migratory capacity and COX2 promotes their survival, but other factors downstream of TGFB1 are required for altered morphology or loss of additional epithelial characteristics. The TGFB Signalling Targets array identified genes such as *Hey1* and *Mmp2* as being significantly increased by TGFB1 treatment. In addition, RNA-seq of TGFB1-treated mOSE cells identified a large number of collagens and ADAMTS genes increased with treatment. These genes are known to be associated with an EMT in other tissues (Thiery and Sleeman 2006; Kalluri and Weinberg 2009; Ruff et al. 2015; Shintani et al. 2008), although none have yet been reported to play a role in the ovulatory wound repair process in mammals. In the *Snail* overexpressing mOSE cells, many ADAMTS genes were modestly increased, as well as the expression of *Mmp9*, and many collagens. These differences were modest, and many genes that were increased by TGFB1-treatment were not found to be increased by SNAIL overexpression. Perhaps these genes contribute to the additional EMT characteristics seen with TGFB1 treatment and help explain why *Snail* overexpression promotes only a partial EMT. The RNA-seq data also revealed many TFs such as *Lhx4*, *Sox8*/*11* or *Foxs1* to be increased by TGFB1 treatment. Although these TF are not the traditional EMT TF, they may play a role in inducing the TGFB1-induced EMT in OSE cells. Furthermore, both the TGFB Signalling Targets array and RNA-seq were used to determine the effects of TGFB1 treatment after 96 hours, when OSE cells have morphologically undergone an EMT. A more thorough investigation of the

transcriptional targets of short term TGFB1 treatment might shed light on additional TGFB1 targets that would lead to these mesenchymal characteristics.

Remodeling of the ECM is essential for wound repair, but in case of dysregulation or repetitive wounding and repairing, it can result in fibrosis or scarring. Fibrosis, which is a feature of aged mouse ovaries (Briley et al. 2016), occurs when the amount of ECM deposited is greater than the amount being degraded, and induces a chronically inflamed environment which can lead to transformation (Nieto et al. 2016). Our RNA-seq data revealed a large number of ECM proteins upregulated by TGFB1 treatment, many of which were collagens. Dysregulation of ovulatory wound repair, or repetitive wounding and repairing of the OSE layer could lead to excessive collagen deposition and formation of a fibrotic lesion. Furthermore, ovulation in mice creates 8-10 wound sites every 4 days, which might not allow for complete repair between ovulation cycles. Interestingly, wound healing in the fetus is scarless, whereas wound healing in adult tissue is not (Rolfe and Grobbelaar 2012). This is suggested to be due to a decreased inflammatory response to wounding in the fetus, leading to a lack of COX2 induction and PGE2 secretion (Rolfe and Grobbelaar 2012). Introducing exogenous PGE2 to a fetal model of wound repair induces scar formation (Wilgus et al. 2004) and blocking COX2 using Celecoxib in adult wound repair reduces scarring (Wilgus et al. 2003). This suggests that in the adult ovary, the increase in COX2 at ovulation, while necessary for ovulation to occur, will also promote scarring and may lead to the accumulation of fibrotic lesions.

COX2 promotes cell survival during re-epithelialization

Cell survival is another important component of wound repair, as OSE cells mediating this repair are surrounded by harsh environmental conditions. In the hours preceding ovulation, vasoconstriction at the apex of the ovulating follicle occurs, which decreases blood flow to the follicle and its surrounding ovarian tissue (Migone et al. 2016). Additionally, ovulatory wound sites are in contact with the immune cells that populate the forming corpus luteum after ovulation to promote repair (Brannstrom et al. 1994; Cohen et al. 1997). Due to the increase in OSE proliferation around the wound site, the influx of immune cells, and transient loss of local vasculature, the ovulating environment is transiently hypoxic (Brannstrom et al. 1994; Cohen et al. 1997). There is an elevation of ROS in the OSE at the time of ovulation, which also contributes to this harsh environment that the OSE must survive for efficient wound repair to occur (Murdoch and Martinchick 2004). We found that *Cox2* induction was associated with enhanced survival when mOSE cells were exposed to these stressors *in vitro*. *In vivo*, COX2 expression in the OSE follows ovulation, and is therefore only present during ovulatory wound repair. Therefore, the induction of *Cox2* by TGFB1 may facilitate wound repair by improving OSE cell survival after ovulation. Additional experiments are required to directly assess the importance of COX2 expression and wound repair *in vivo*. In the skin, COX2 inhibition by topical application of Celecoxib increases the time for complete wound repair to occur (Futagami et al. 2002). We hypothesize that mice lacking *Cox2* or *Ptger4* in the OSE layer would also severely delay ovulatory wound repair.

Potential consequences of *Cox2* induction

Ovulation is the primary non-hereditary risk factor for ovarian cancer, with ovarian cancer risk increasing with the number of lifetime ovulation cycles (Jayson et al. 2014). The incessant ovulation hypothesis suggests that the high rate of cell turnover during ovulation, in conditions with high ROS, can lead to DNA damage and mutations in the OSE (Fathalla 1971). Murdoch and Martinchick (2004) showed an accumulation of mutagenic 8-oxoguanine modifications in the surviving OSE cells after ovulation. The induction of *Cox2* may promote cell survival and the potential transformation of these cells that exhibit DNA damage. Furthermore, COX2 may promote the formation of fibrotic lesions over time. These data are supported by a recent review showing the benefits of aspirin, a nonsteroidal anti-inflammatory drug (NSAID) that acts as a COX inhibitor, as a preventative agent for ovarian cancer (Verdoodt et al. 2017). The authors state a more thorough study of non-aspirin NSAIDs, selective for COX2 inhibition is warranted due to the present lack of comprehensive data available for these NSAIDs and ovarian cancer risk (Verdoodt et al. 2017). This decrease in ovarian cancer risk was not observed in the ovarian cancer hen model fed flaxseed to inhibit COX activity (Ansenberger et al 2010). Flaxseed in the hen model decreased ovarian cancer progression, but not ovarian cancer incidence (Ansenberger et al 2010). Further studies are required to assess whether this discrepancy is species specific, or perhaps due to the strength of COX inhibition.

4.2: Stemness and ovarian homeostasis

As recently reviewed by Ng and Barker (2015), there have been several reports over the past 10 years identifying populations of stem cells in the OSE. Although many studies have shown the existence of these cells, there have not been any studies showing enrichment for this cell type when sorting for a combination of OSE stem cell markers. Furthermore, there has not been a consensus on the location of this cell type within the OSE. Flesken-Nikitin et al. (2013) suggest this population is found predominantly in the hilum region of the OSE, whereas Ng et al. (2014) show this population to be dispersed throughout the OSE layer and enriched in areas surrounding ovulatory wound sites. Gamwell et al. (2012) did not see an enrichment for *Sca1* expression associated with any particular ovarian structure. This suggests that the OSE population of stem cells is different from that found in other tissues that have defined hierarchical stem cell populations such as in the intestine or the hematopoietic system.

As discussed in the Introduction, the OSE stem cell population may be best represented as a state rather than a defined population of cells, where OSE cells have the capacity to interchange between a “less differentiated state” exhibiting stem cell characteristics and a “more differentiated” cell state exhibiting committed epithelial cell characteristics. Previously, Gamwell et al. (2012) showed that TGFB1 enhances the stem cell properties in mOSE cells. These findings suggest the OSE displays plasticity along a spectrum of differentiation, similar to the plasticity observed with the EMT continuum. The increase in stem cell characteristics has been previously associated with an induction of an EMT

in other tissues including the FTE, but this has never been directly studied in the OSE (Mani et al. 2008; Guo et al. 2012; Morel et al. 2008; Schmidt et al. 2015; Alwosaibai et al. 2017).

TGFB1 promotes OSE stemness *in vitro*

Sphere formation assays were used to validate the TGFB1-induced increase in OSE stemness *in vitro* in both human and mouse OSE cells. The expression levels of previously reported OSE stem cell markers were assessed in TGFB1-treated mOSE cells to determine if the TGFB1-induced sphere formation was due to an expansion of these populations of cells. None of these markers was significantly increased by TGFB1 treatment. In contrast, *Lgr5* and *Aldh1* expression were both significantly decreased by TGFB1 treatment. This suggests the TGFB1-increased sphere formation in mOSE cells was not due to expansion of a previously published mOSE stem cell population.

A stem cell PCR array was therefore used to assess TGFB1-treated mOSE cells for a panel of stem cell markers, and genes known to regulate stem cell properties. Examining the top upregulated targets of this array, it became clear that the stemness-associated genes increased by TGFB1 treatment are also associated with an EMT. *CD44*, *Jag1*, *Ncam1* and *Myc* expression are all upregulated by TGFB1 treatment and have all been shown to either promote or be induced by EMT (Tian et al. 2014; Brown et al. 2011; Zavadil et al. 2004; Ma et al. 2010). *Col2a1* has not specifically been studied as a driver or as a consequence of an EMT, but culturing MCF7 cells on a collagen scaffold induces

mesenchymal gene expression (Chen et al. 2012). These data suggest the TGFB1-induced stemness is in part driven by the EMT-associated genes *CD44*, *Jag1*, *Ncam1*, *Myc* and *Col2a1.*

The downregulated genes found in the stem cell PCR array included *Bmp2* and *Bmp3,* both members of the TGFB1 superfamily. It is not surprising to see a downregulation of these genes, because BMP2/3 proteins signal through the alternative SMAD pathway (SMAD1/5/8), as opposed to the SMAD2/3 pathway that is activated by TGFB1, and activation of TGFB1 signalling has been shown to inhibit BMP signalling (Guo and Wang 2009; Kawahara et al. 2015). *Cdc2a* and *Ccna2* are cell cycle genes and decreased by TGFB1 treatment. This data is in agreement with previous work from our lab showing decreased mOSE proliferation with TGFB1 treatment and also in support of the stem cell property of slowly proliferating cells (Gamwell et al. 2012). *Cxcl12* expression was decreased in TGFB1-treated cells. In colorectal cancer cells, decreased *Cxcl12* expression is associated with differentiation, further supporting the TGFB1-induced stem cell phenotype (Brand et al. 2005). Finally, expression of the epithelial gene *Krt15* is decreased by TGFB1 treatment, supporting the characterization of stem cells as having a more mesenchymal phenotype. Taken together, these data suggest the TGFB1-induced stemness phenotype coincides with a loss of epithelial characteristics and decreased cell proliferation.

CD44 is a marker of TGFB1-induced mOSE stemness

We hypothesized that isolating mOSE cells for the expression of the genes found to be upregulated in the stem cell PCR array would enrich for the TGFB1-induced stem cell phenotype. *NCAM1* expression is a marker of stemness in many cell types including malignant renal cells, mesenchymal stem cells, liver and pancreatic stem cells (Pode-Shakked et al. 2009; Klonisch et al. 2008). Recently, NCAM has been identified as a marker of metastatic high grade ovarian cancer, but its expression has not been reported in normal OSE cells (Davidson et al. 2015). CD44 is a widely studied stem cell marker in many cancers, including gastric, breast and head and neck cancers (Takaishi et al. 2009; Joshua et al. 2012; Morel et al. 2008; Al-Hajj and Clarke 2004). Recently, Alwosaibai *et al.* (2017) showed *CD44* expression enriches for a stem cell population in the normal FTE, and that *CD44* is also expressed in normal mOSE cells. Based on these findings, we chose to isolate *CD44* expressing mOSE cells to assess their stem cell characteristics.

CD44 is a transmembrane glycoprotein with 3 distinct domains: the extracellular domain, the transmembrane domain and the intracellular domain (Iczkowski 2010). As reviewed by Senbanjo and Chellaiah (2017), the extracellular domain interacts with the cellular microenvironment to sense external stimuli, the transmembrane domain interacts with cofactors and adaptor proteins and the intracellular domain has functions including nuclear localization and transcription mediation. *CD44* has multiple alternative splice sites within the extracellular domain (Cichy and Puré 2003). Antibodies used to

isolate CD44 expressing cells have not been designed for specific for CD44 variants and therefore understanding which variants are associated with stem cell properties can be difficult to determine. Todaro *et al.* (2014) suggested that CD44v6 enriches for stem cell properties in colorectal cancer, but this variant of *CD44* has not been implicated in stemness in other cell types.

CD44-positive and -negative mOSE cells were isolated by FACS. CD44 expression was validated using Q-PCR and showed enrichment for *CD44* variants 3, 4, 7 and 8 in the CD44-positive population of cells. These variants generate alternative exons in the membrane-proximal portion of the extracellular domain (Cichy and Puré 2003). It is speculated that variants allow for different interactions within the extracellular domain of the CD44 protein, however this has yet to be confirmed. When placed in methylcellulose sphere cultures, the CD44-positive mOSE cells showed increased primary sphere formation compared to the CD44-negative mOSE cells, suggesting CD44 is a marker of TGFB1-induced mOSE stemness. The spheres formed were small and tightly compact, similar to the morphology of previously reported TGFB1-treated mOSE spheres in methylcellulose cultures (Gamwell et al. 2012). The size limitation of these spheres is likely due to the harsh experimental conditions of FACS, however further studies are required to assess this phenotype in more detail. Whether these CD44-positive and negative mOSE cells maintain their expression status long term is also of interest for future evaluation. Stable expression of *CD44* is unlikely because of previous studies showing the reversibility of *Sca1* expression in the mOSE (Gamwell et al. 2012), however additional experiments are required to address this question. If CD44 positivity

or negativity was maintained long term, secondary sphere formation could be assessed to confirm that CD44 expression enriches for a mOSE stem cell population. Furthermore, whether CD44 expression enriches for cells expressing additional stem cell markers such as *Sca1* is of interest for further studies. As the mOSE represents a heterogeneous cell population, using techniques such as single cell RNA-seq would allow for better resolution of individual cell gene expression to elucidate whether cells acquire the expression of multiple stem cell markers simultaneously, or if these are separate cell populations.

Additional experiments are required to determine whether CD44 functionally acts to promote stemness, or whether its expression simply correlates with the phenotype. Many studies have shown that CD44 expression is associated with EMT and stem cell characteristics, but the only function of CD44 that has been studied in relation to these characteristics is the function of CD44 as a hyaluronic acid receptor. Neutralizing antibodies and molecular inhibitors of CD44 receptor activity have been used to implicate this protein in regulating the EMT characteristics migration and invasion (Chen et al. 2018). In ovarian cancer specifically, Strobel et al (1997), show that inhibition of CD44 receptor activity decreased ovarian cancer intra-abdominal spread. There are many ligands for CD44, all of which are components of the ECM and secreted by mesenchymal cells (ex: hyaluronic acid, osteopontin, chondroitin, collagen, fibronectin and serglycin/sulfated proteoglycan) (Chen et al. 2018). As the mesenchymal phenotype

is associated with stemness, perhaps this is why CD44 is highly regarded as a stem cell marker.

Transcriptional profile of mOSE spheres

mOSE cells treated with TGFB1 for 7 days were used to assess TGFB1-induced stemness by PCR array. Our results suggest *CD44* as a marker of TGFB1-induced stemness, and further analysis of its expression showed CD44 is significantly increased by 4 days of TGFB1 treatment. To obtain a more thorough analysis of TGFB1-induced mOSE stemness, as well as a characterization of mOSE cells that have inherent stemness features (without TGFB1 treatment), RNA-seq was utilized to compare mOSE cells cultured as monolayers and as spheres, with and without TGFB1 treatment. mOSE cells were cultured in the absence or presence of TGFB1, in monolayer conditions for 4 days prior to RNA isolation or plating in free-floating sphere conditions, maintaining the absence or presence of TGFB1 in the sphere cultures. Analysis of the RNA-seq data revealed 7 clusters of gene expression patterns across culture conditions.

Inherent stemness in mOSE cells

Cluster 2 genes were decreased simply by culturing mOSE cells in sphere-forming conditions. The primary GO terms associated with this cluster include cell cycle and cell proliferation, which validate the cell cycle genes found to be decreased in the stem cell PCR array. Other genes found within cluster 2 include *Brca1* and collagens such as *Col1a1*, *Col5a2*, *Col4a4* and *Col4a3*. *Brca1* loss has been shown to promote stemness in the mammary epithelium (Bai et al. 2014). Its expression has also been shown to

decrease cell proliferation in ES cells (Hakem et al. 1996), so it is unsurprising to see it cluster with cell cycle genes. In contrast, decreased collagens in sphere cultures was surprising as the literature would suggest increased collagen deposition is a characteristic of mesenchymal cells, which are associated with increased stem cell characteristics. However, decreased collagen could be indicative of the culture conditions. Under free-floating sphere conditions, cells do not attach to the culture plate and have no need to migrate along the plate surface. As collagens promote cell migration, perhaps a decrease in collagen expression in sphere cultures is reflective of these conditions. These data suggest that sphere-forming culture conditions reduce cell growth.

Cluster 4 genes were also decreased by sphere forming culture conditions. The GO term associated with this gene cluster is response to Interferon-beta. This is in agreement with a recent study done by Doherty et al. (2017) showing treatment of breast cancer cells with Interferon-beta decreases stem cell characteristics. Interestingly, *Lats2* and *Crb2*, genes belonging to the Hippo signalling pathway, are also found within this cluster. Decreased *Lats2* and *Crb2* suggest increased YAP nuclear localization and active transcription of downstream targets that are known to promote stemness in many cell types (Mo et al. 2014). This may, however, also be due to the presence of EGF in the stem cell media, a factor known to inhibit Hippo pathway signalling (Gumbiner and Kim 2014). Interestingly, disruption of the CRB complex has been shown to enhance the cellular response to TGFB1 and predispose cells to an EMT (Varelas et al. 2010). Future

work should address the relationship of Interferon-beta and the immune response and the involvement of Hippo signalling in the regulation of OSE stem cell characteristics.

Cluster 5 genes were increased by sphere-forming culture conditions. The GO terms associated with these genes include positive regulation of developmental process and response to chemical. Rather surprisingly, many of the genes found within this cluster are transcription factors well associated with an EMT including *Zeb1*, *Zeb2* and *Twist1* (Lamouille et al. 2014; Savagner 2015). This suggests that sphere formation is sufficient to shift the cells to a more mesenchymal state. The stem cell associated gene *Sox9* was also found in cluster 5. Guo et al. (2012) show in mammary epithelium that *Sox9* works synergistically with *Slug*, anther classical EMT transcription factor, to promote stem cell properties. Although *Slug* was not significantly different among treatment groups in this study, future experiments to determine whether *Sox9* works cooperatively with *Zeb1*, *Zeb2* or *Twist1* expression would shed light onto this potential relationship. *Aldh1a7* was also found in cluster 5. *Aldh1a7 h*as not directly been associated with OSE stemness, but more broadly, ALDH1 expression and its family member *Aldh1a2* have been identified as OSE stem cell markers (Flesken-Nikitin et al. 2013; Ng et al. 2014). These data suggest that stem cell activity by OSE cells involves an increase in mesenchymal transcription factors and the stem cell markers *Aldh1a7* and *Sox9*. Whether OSE stemness is dependent on any of those factors remains to be determined.

Several genes associated with ovarian cancer were present in cluster 5, including *Greb1* and *Pax8*. *Greb1* has previously been studied in the context of ovarian cancer and found to promote proliferation and to be downstream of ESR1, but it has not been studied in the context of stem cell maintenance (Hodgkinson et al. 2018). Progesterone is a component of the B27 supplement found in the stem cell media and has been shown to increase *Greb1* expression in endometrial cells (Camden et al. 2017). Interestingly, others in this lab have recently found that *Greb1* is induced specifically in areas of dysplasias when mOSE cells are cultured for prolonged periods in the presence of estradiol (Vuong et al. 2018), drawing another association between loss of epithelial status with gain of GREB1. Future studies are warranted to determine whether *Greb1* and *Esr1* expression are important for mOSE sphere formation, or whether these are artifacts from the culture conditions. These findings could shed light on the function of *Greb1* in normal and transformed ovarian cells.

Pax8 is a transcription factor known to be expressed by the secretory cells of the FTE. Its expression was originally thought to be devoid in the adult OSE, however a recent report suggests *Pax8* is expressed in 44-71% of human OSE cells (Adler et al. 2015). Rodgers et al. (2016) reported that OSE cells acquire *Pax8* expression upon malignant transformation. The STOSE ovarian cancer model is another example of mOSE cells acquiring *Pax8* expression upon transformation (McCloskey et al. 2014). *Pax8* expression has not been assessed in the context of stem cell maintenance in the OSE, however ectopic *Pax8* expression in mOSE cells was shown to promote their mesenchymal

characteristics such as a mesenchymal morphology and increased migration (Rodgers et al. 2016). These data suggest that mOSE cell stemness is associated not only with increased mesenchymal gene expression, but also increased expression of factors associated with ovarian cancer It is tempting to speculate that any combination of these pro-cancer genes may provide mechanisms to explain the increased ovarian cancer risk associated with incessant ovulation.

TGFB1-induced mOSE stemness

Cluster 6 and 7 genes were increased by sphere-forming cultures, and more so by TGFB1 treatment. We therefore hypothesize these genes are responsible for the increased stemness characteristics observed with TGFB1 treatment. Cluster 6 genes are associated with the GO terms system development and cell adhesion. Many genes found within this cluster were ECM remodelling genes such as the matrix metalloproteinases *Mmp2* and *Mmp9*, and ADAMTS genes including *Adamts10* and *Adamts16*. Integrins including *Itgb1* and *Itgb5* were also found in this cluster. These genes have all been associated with the induction of an EMT (Radisky and Radisky 2010; Wang et al. 2003; Lamouille et al. 2014). Sodek et al. (2009) showed these EMT-associated genes can promote the compact sphere morphology observed in control and TGFB1-treated mOSE spheres. In a panel of ovarian cancer cell lines, compact sphere morphology was associated with mesenchymal gene expression and mesenchymal properties such as invasion. These data suggest ECM formation and remodeling proteins are induced by sphere forming culture, more so by TGFB1 treatment, and may promote the compact morphology present in mOSE spheres.

Cluster 7 genes enriched for the GO terms system development and inactivation of MAPK activity. In a recent study of non-small cell lung cancer cells, inactivation of the MAPK pathway was also shown to promote stem cell characteristics (Fang et al. 2017). Many of the genes found within cluster 7 were those commonly found to be induced by TGFB1 treatment, and included genes such as *Snail*, *Cox2*, *Alcam* and *CD44*, discussed in Chapters 3.1 and 3.2. *CD44* was also identified as a top target in the stem cell PCR array. As described above, these genes have all been associated with an EMT. Interestingly, *Tgfb1* was also found in cluster 7 and further promotes the hypothesis that an EMT is associated with a stem cell phenotype and shows that mOSE spheres have an increased ability to maintain a mesenchymal status.

In summary, sphere-forming culture conditions promoted expression profiles associated with stemness and interestingly, also promoted the expression of the pro-cancer genes *Pax8* and *Greb1*. These conditions also promoted the expression of EMT-associated genes, many of which were further enhanced by TGFB1 treatment. The TGFB1-induced mesenchymal genes were not identical to those induced by sphere-forming culture conditions alone (ex: *Twist*, *Zeb1/2*), and suggest that additional studies are warranted to better understand the regulation of these genes. These data support the hypothesis that a mesenchymal phenotype is associated with stem cell characteristics (Mani et al. 2008; Guo et al. 2012; Morel et al. 2008; Schmidt et al. 2015; Alwosaibai et al. 2017).

SNAIL overexpression and mOSE stemness

To further characterize the EMT-associated stem cell phenotype observed with TGFB1 treatment, im*Snail* mOSE cells were examined for stem cell characteristics. SNAIL overexpression did not promote *Sca1* expression (a previously reported mOSE stem cell marker), or the expression of *CD44* (a mOSE stem cell marker found within cluster 7), however it did increase both primary and secondary sphere formation. From Chapter 3.1, it is clear that SNAIL overexpression induces only a partial EMT, displaying enhanced migration as a mesenchymal characteristic. RNA-seq was used to assess the transcriptional profile of *Snail* overexpressing mOSE cells to determine how SNAIL promotes this partial EMT, and how this is different from TGFB1 treatment that was shown to induce *Snail* expression, but also promotes a full EMT.

One of the top GO terms associated with the genes upregulated by SNAIL overexpression was ECM−receptor interaction. Many of the genes increased by SNAIL were collagens including *Col1a1*, *Col6a1*, *Col18a1* and *Col6a2*. These genes support the migration phenotype associated with SNAIL overexpression because culturing cells on a collagen matrix is known to enhance migration (Chen et al. 2012). *Krt18* was decreased by SNAIL overexpression which suggests the cells are more mesenchymal, however *Alcam* was also suppressed, as well as *Itgs7*, both mesenchymal-associated genes, shedding light onto the partial EMT observed in these cells.

Morphologically, the im*Snail* spheres appeared compact, but less so than TGFB1-treated spheres. This may be representative of the difference in ECM genes expressed under these conditions. im*Snail* mOSE cells have primarily increased collagen gene expression whereas TGFB1 treated spheres have primarily MMPs and ADAMTS, genes associated with stemess. As described by Sodek et al. (2009), MMPs are essential for compact sphere morphology. These results taken together suggest the partial EMT induced by SNAIL overexpression is sufficient to promote mOSE stemness, in agreement with work done by Guo et al. (2012) on mammary epithelium stemness. im*Snail* spheres are also larger than their respective controls (i*GFP* spheres). GO term analysis of the RNA-seq data from *Snail* overexpressing mOSE cells shows increased PI3K-Akt signalling, a pathway known to promote cell survival and proliferation, and may be responsible for the larger sphere size. It is interesting that the RNA-seq data did not show enhanced gene expression of any known stem cell markers with *Snail* overexpression. Future studies to identify novel stem cell markers regulated by SNAIL are warranted.

COX2 overexpression and mOSE stemness

COX2 overexpression did not increase *Sca1* or *CD44* expression, or primary sphere formation, but did increase secondary sphere formation in mOSE cells. In the stem cell field, it is readily accepted that serial passaging of spheres enriches for self-renewing stem cells/progenitor cells and depletes the culture of more committed progenitor cells. TGFB1 treatment and SNAIL overexpression both independently increased primary and secondary spheres, however COX2 overexpression only increased secondary spheres.

One major difference between these conditions is that TGFB1 treatment and SNAIL overexpression induced mesenchymal-associated gene expression whereas COX2 overexpression did not. This suggests that EMT-associated factors can promote enhanced stemness characteristics, but other genes such as COX2 can also promote stemness without an associated EMT shift. How COX2 enhances secondary sphere formation is unknown but may be associated with the pro-survival phenotype described in Chapter 3.2. As increased cell survival is a stem cell trait, it has perhaps enhanced their capacity to survive the sphere dissociation that is required for this assay. Further characterization of the transcriptional profile of these cells would allow for a better understanding of the genes associated with COX2-induced mOSE stemness and their morphology.

BRCA1 loss promotes mOSE stemness

One of the most interesting observations in this project was that mOSE cells cultured in sphere-forming conditions had decreased *Brca1* expression. In the mammary epithelium, decreased *Brca1* expression has been associated with an induction of an EMT through *Twist* activation, and increased stem cell characteristics (Bai et al. 2014). In mOSE cells, *Brca1* knockout promoted primary and secondary sphere formation *in vitro*, similar to that seen with SNAIL overexpression and TGFB1 treatment. Furthermore, *Brca1* knockout *in vivo* promoted label retention in mOSE cells, another characteristic of stem cells. Furthermore, *Sca1* and *Lgr5* expression were increased by *Brca1* deletion and *CD44* expression was decreased. This discrepancy may be because TGFB1 treatment

induces a transient loss in *Brca1* expression, whereas in these cell cultures, *Brca1* loss is sustained.

To better understand the contribution of decreased *Brca1* expression to mOSE stemness, RNA-seq was used to examine the transcriptional profile of these cells. Similar to cluster 2 showing decreased *Brca1* expression and cell cycle genes associated with OSE stemness, one of the top GO terms enriched for the genes associated with *Brca1* deletion was reduced cell cycle and nuclear division. GO terms associated with the genes that are upregulated following *Brca1* deletion include many cancer-associated pathways such as gastric, breast and pathways in cancer. This is also supported by the GO term cellular response to DNA damage stimulus that was decreased with *Brca1* deletion. These gene associations agree with the known functions of BRCA1, as BRCA1 is known to play a role in cell cycle, DNA repair, and in transcriptional regulation (Clark et al. 2012). These data suggest that the loss of BRCA1 not only causes the slowing of cell growth and increased *Sca1* and *Lgr5* expression associated with stem cells, but the activation of pathways linked to cancers hints at changes that may link a transient decrease in BRCA1 at each ovulation to an increased risk of cancer initiation.

Examining specific genes associated with *Brca1* deletion, *Lgr5*, previously identified as an OSE stemness marker (Ng et al. 2014), was increased with *Brca1* deletion. Interestingly, *Greb1* and *Esr1* were increased by *Brca1* deletion as well. *Greb1* and *Esr1* were also associated with sphere-forming cultures as described above and hypothesized

to be a result of stem cell media components. These data would suggest that media components do not provide a full explanation, as the *Brca1*-deleted mOSE cells were cultured in monolayer conditions but still increased the expression of these genes. These data suggest *Greb1*, associated with decreased *Brca1* expression, may function to promote stem cell characteristics in mOSE cells.

A common theme throughout this study is that EMT characteristics are usually associated with stemness, but stemness is not dependent on EMT. Examining the EMT-associated genes that are differentially expressed with *Brca1* deletion, it is not evident that *Brca1* loss promotes an EMT in these cells. In contrast, based on the expression patterns, the data suggest mOSE cells with *Brca1* deletion maintain their epithelial phenotype. *Twist* expression is repressed, in contrast to the mammary epithelium (Bai et al. 2014), as well as *Snail* and *CD44* expression. However, these cells do not have a more epithelial phenotype either, as they have decreased cadherins such as *Cdh26* and cytoskeletal genes including *Acta2*. Perhaps the loosely adherent morphology of *Brca1* knockout spheres is representative of the lack of ECM-related gene expression patterns. Like the overexpression of COX2, these data indicate that a loss in *Brca1* expression does not promote an EMT yet is still able to increase many stem cell characteristics.

The OSE stemness continuum

Taken together, our results clearly show that mOSE stemness is not associated with a specific epithelial or mesenchymal cell state. Furthermore, while we attempted to

identify the pathways that promote OSE stemness, it is clear that there are multiple genes that can enhance stemness, but no consistent gene expression patterns to identify that state. As mentioned in the Introduction, perhaps this confusion is a consequence of a transient stem cell population in the OSE, and not a static one, like a hierarchical stem cell population. As a result, OSE stemness is perhaps best represented as a continuum, similar to how we observe the EMT. This may explain why clonal expansion in the OSE to reconstitute the OSE layer has never been shown. Ng et al. (2014) showed that *Lgr5*-expressing OSE stem cells can clonally divide in the OSE layer; however, the clonal expansion of LGR5-positive cells was inconsistent. Larger expansion of this population occurred next to ovulating sites and surrounding non-ovulating areas the clonal expansion was limited (Ng et al. 2014). This suggests that the OSE stem cell population is dynamic and expands and restricts depending on its location on the ovarian surface and likely the microenvironment near the OSE in each region.

There are many factors known to induce an EMT, and in a similar fashion, there are many factors that can promote stemness. Figure 40 depicts this stem cell continuum, how it intersects with the EMT continuum and how our results fit within this model. Using this representation of OSE stemness, it is possible to have cells exhibiting epithelial characteristics and stemness characteristics simultaneously as evident in the *Brca1* knockout mOSE and COX2-overexpressing mOSE. It is also possible to have cells exhibiting mesenchymal characteristics and stemness characteristics simultaneously as observed in the im*Snail* mOSE and TGFB1-treated mOSE. This model is in agreement

with the hypothesis proposed by Jolly et al. (2015) who discussed the “window of stemness” within the EMT continuum, and how this window is positioned differently for each cell type, and how different gene expression patterns can alter where this window lies.

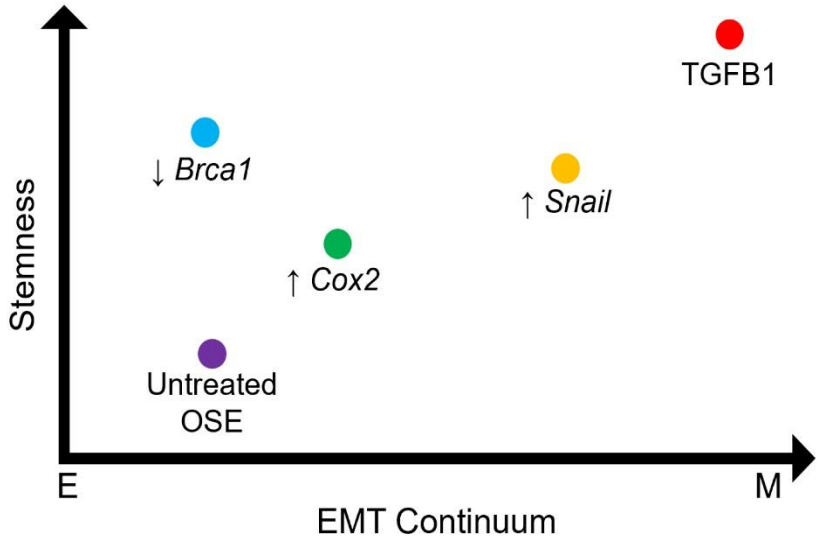

Figure 40. Combining the EMT and stemness continuums in mOSE cells. Genetic manipulations, and treatment of mOSE cells display varying levels of stem cell characteristics (stemness). These same conditions also influence the EMT state of these cells. Deletion of *Brca1* and COX2 overexpression independently increase stemness, but do not induce an EMT. SNAIL overexpression induces a partial EMT and also stemness. TGFB1 treatment induces a full EMT in mOSE cells and also increases stemness. This model shows that stem cell characteristics are not always correlated to mesenchymal gene expression. E = epithelial and M = mesenchymal.

Over the past 10 years, there have been several demonstrations of OSE stemness. Some studies have even shown OSE stem cells to be capable of differentiating into oocytes, granulosa cells and FTE (Johnson et al. 2004; Zou et al. 2009; Virant-Klun et al. 2008, 2009; Pacchiarotti et al. 2010; White et al. 2012). These studies all have one aspect in common: OSE cells can be treated with a variety of cytokines or growth factors that promote stem cell properties and which can then be exploited to promote differentiation of these cells into different ovarian structures. These data all support that OSE stemness can be induced and regulated by a variety of factors, similar to that observed in induced pluripotent stem cells (iPSCs). iPSCs exhibit pluripotency when cultured under the right conditions and when these conditions are suboptimal, the degree of pluripotency is reduced (Hirano et al. 2012). This concept is supported by this study showing that OSE, when cultured under the right conditions, can acquire expression of stem cell markers and form spheres, a process that is enhanced in the presence of TGFB1.

OSE stemness, ovarian homeostasis and potential consequences

OSE cells displaying stem cell characteristics would enable the maintenance of OSE homeostasis. However, promotion of stem cell characteristics or persistent stemness in the OSE could have negative consequences. TGFB1 treatment transiently decreased *Brca1* expression and increased *Cox2* and *Snail* expression in OSE cells, all contributing the increased stemness phenotype. After ovulation *in vivo*, these expression differences would be expected to be transient and thus would promote a short-lived increase in

stem cell characteristics, perhaps to maintain OSE homeostasis. However, under constant TGFB1 signalling, like that present in age-associated ovarian fibrosis (Border and Noble 1994) or perhaps in a *Brca1* mutation carrier with permanent *Brca1* loss, this stemness state would be maintained. As discussed above, *Brca1* deletion is associated with active cancer signalling pathways and induces the expression of ovarian cancer associated genes such as *Greb1*. Previously, studies from our lab have demonstrated that *Brca1* deletion on its own in OSE cells is not sufficient to induce tumor formation (Clark-Knowles et al. 2007). Perhaps in the presence of age-associated ovarian fibrosis with persistent TGFB1 signalling, *Brca1* loss would be combined with a pro-survival phenotype in an inflammatory environment. These cells, exhibiting stem cell characteristics, a pro-survival phenotype and decreased DNA repair capacity in an inflammatory environment, may be prone to DNA damage and transformation.

The expression of EMT associated transcription factors such as *Snail*, *Twist* and *Zeb1* have been shown to allow cells to overcome oncogene-induced senescence, as reviewed in Puisieux (2014). In the context of ovarian cancer initiation, *Snail* expression induced by TGFB1 may allow cells who have acquired a *TP53* mutation (the most common mutation in high grade serous ovarian cancer) to promote tumour initiation. Normal *TP53* expression has been shown to maintain cells in an epithelial state by inhibiting EMT transcription factors such as *Twist* and *Zeb1* (Kim et al 2011). In the presence of a *TP53* mutation, this inhibition would be abolished, allowing the cell to assume a mesenchymal phenotype and allow this pathway to proceed in a cell with a

mutated tumour suppressor. Taken together, these data suggest a mechanism for OSE homeostasis, and propose a mechanism for the increased risk for OSE transformation with incessant ovulation.

Chapter 5: Conclusion

These studies are the first to characterize an OSE signalling pathway, summarized in Figure 41, that drives EMT-mediated re-epithelialization, a component of wound repair. The EMT is widely accepted as a mediator for re-epithelialization and can be induced by many cytokines found in the ovarian environment or follicular fluid. Here, we assessed TGFB1 signalling and found that it acts through the canonical SMAD2/3 pathway to induce the expression of *Snail* and *Cox2*. SNAIL acts to increase the migratory capacity of OSE cells along with COX2, however COX2 primarily induces PGE2 secretion which activates the AKT pathway to maintain cell proliferation and survival. The induction of an EMT and maintenance of cell survival likely facilitates ovulatory wound repair but may also render cells more susceptible to transformation. Future studies examining how other cytokines present at the wound site, such as IGF1 or DKK3 (Zamah et al. 2015), act independently, or in conjunction with TGFB1, are warranted.

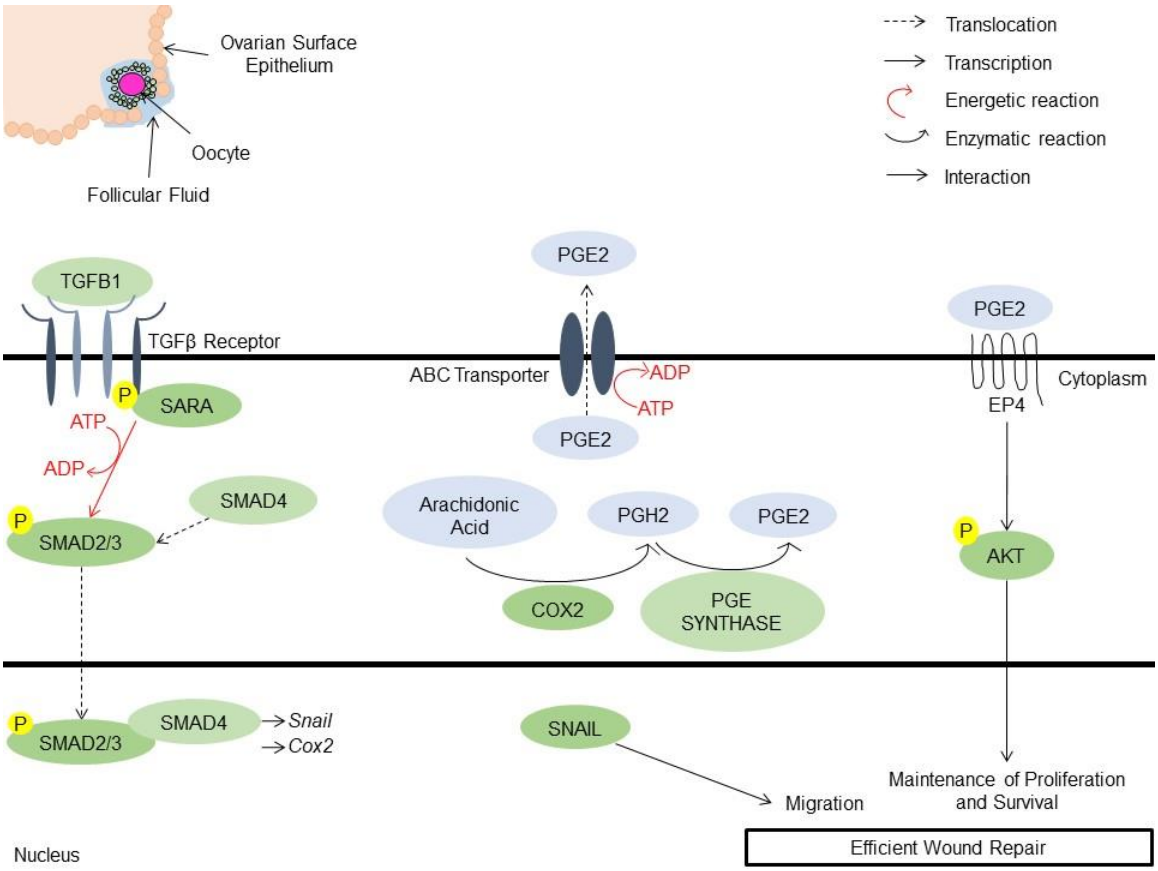

Figure 41. Mechanism by which TGFB1 promotes ovulatory wound repair. TGFB1 signals through TGFBRI to activate the SMAD2/3 signalling pathway and induce an EMT. The SMAD complex induces the expression of *Snail* which promotes a partial EMT seen by enhanced cell migration. The SMAD complex also induces *Cox2* expression which promotes cell survival through the PTGER4 receptor and increased AKT activity. Together, by the induced EMT and pro-survival phenotype, TGFB1 contributes to ovulatory wound repair.

These studies are the first to characterize the pathways that may regulate the OSE stem cell phenotype. We propose OSE stemness is best described as a continuum, rather than a defined cell state, where environmental cues either promote differentiation or stem cell characteristics to maintain OSE homeostasis. RNA-seq showed mOSE spheres acquire a mesenchymal gene expression pattern, that is further enhanced with TGFB1 treatment, suggesting the increase in mOSE stemness by TGFB1 is through activation of EMT-related genes. Independently, factors downstream of TGFB1 (*Snail* and *Cox2*) also increase stem cell characteristics, however do not affect the expression of each other. *Brca1* deletion also promotes stemness in the OSE but did not induce an EMT. These data suggest that stemness does not always correlate with an EMT and that, although each of these TGFB1-induced factors promote the stemness state, they regulate this phenotype independently and differently. This is similar to how EMT seems to occur, where different factors are able to promote the same EMT phenotype.

Understanding re-epithelialization and mechanisms of OSE homeostasis are essential to understanding ovulatory wound repair. As conditions in the ovary such as fibrosis and ovarian cancer increase with age and ovulation number, it is important to understand the mechanisms underlying ovulatory wound repair. Here we showed that TGFB1 induces an EMT and COX2 expression in the OSE. COX2 activates a pro-survival phenotype in mOSE cells to assist in ovulatory wound repair. TGFB1 also increases mOSE stemness, through its downstream targets including decreased *Brca1* expression. A decrease in *Brca1* expression in OSE cells also experiencing a survival phenotype, under

inflammatory conditions such as ovulation or fibrosis, may lead to the accumulation of DNA damage and a transformation event. Understanding these mechanisms are necessary to develop reliable early detection methods for ovarian disease and better prevention strategies.

References

Adler E, Mhawech-Fauceglia P, Gayther SA, and Lawrenson K. 2015. “PAX8 Expression in Ovarian Surface Epithelial Cells.” *Human Pathology* 46 (7): 948–56.

Ahmed N, Maines-Bandiera S, Quinn MA, Unger WG, Dedhar S, and Auersperg N. 2006. “Molecular Pathways Regulating EGF-Induced Epithelio-Mesenchymal Transition in Human Ovarian Surface Epithelium.” *American Journal of Physiology-Cell Physiology* 290 (6): C1532–42.

Ahmed N, Thompson EW, Quinn MA. 2007. “Epithelial–mesenchymal Interconversions in Normal Ovarian Surface Epithelium and Ovarian Carcinomas: An Exception to the Norm.” *Journal of Cellular Physiology* 213 (3): 581–88.

Al-Hajj M, and Clarke MF. 2004. “Self-Renewal and Solid Tumor Stem Cells.” *Oncogene* 23 (43): 7274–82.

Alwosaibai K, Abedini A, Al-Hujaily EM, Tang Y, Garson K, Collins O, and Vanderhyden BC. 2017. “PAX2 Maintains the Differentiation of Mouse Oviductal Epithelium and Inhibits the Transition to a Stem Cell-like State.” *Oncotarget* 8 (44): 76881–97.

Ansenberger K, Richards C, Zhuge Y, Barua A, Bahr JM, Luborsky JL, Hales DB. 2010. “Decreased severity of ovarian cancer and increased survival in hens fed a flaxseed enriched diet for 1 year.” *Gynecol. Oncol* 117, 341–347.

Aoudjit L, Potapov A, and Takano T. 2006. “Prostaglandin E2 Promotes Cell Survival of Glomerular Epithelial Cells via the EP4 Receptor.” *American Journal of Physiology. Renal Physiology* 290 (6): F1534–42.

Audoly LP, Tilley SL, Goulet J, Key M, Nguyen M, Stock JL, McNeish JD, Koller BH, and Coffman TM. 1999. “Identification of Specific EP Receptors Responsible for the Hemodynamic Effects of PGE2.” *The American Journal of Physiology* 277 (3 Pt 2): H924–30.

Auersperg N. 2013. “The Stem-Cell Profile of Ovarian Surface Epithelium Is Reproduced in the Oviductal Fimbriae, with Increased Stem-Cell Marker Density in Distal Parts of the Fimbriae.” *International Journal of Gynecological Pathology: Official Journal of the International Society of Gynecological Pathologists* 32 (5): 444–53.

Auersperg N, Pan J, Grove DB, Peterson T, Fisher J, Maines-Bandiera S, Somasiri A, and Roskelley CD. 1999. “E-Cadherin Induces Mesenchymal-to-Epithelial Transition in Human Ovarian Surface Epithelium.” *Proceedings of the National Academy of Sciences of the United States of America* 96 (11): 6249–54.

Auersperg N, Wong AST, Choi KC, Kang SK, and Leung PCK. 2001. “Ovarian Surface Epithelium: Biology, Endocrinology, and Pathology.” *Endocrine Reviews* 22 (2): 255–88.

Bai F, Chan HL, Scott A, Smith CF, Herschkowitz JI, Perou CM. 2014. “BRCA1 Suppresses Epithelial-to-Mesenchymal Transition and Stem Cell Dedifferentiation during Mammary and Tumor Development.” *Cancer Research* 74 (21): 6161–72.

Bai F, Smith MD, Chan HL, Pei XH. 2013. “Germline Mutation of Brca1 Alters the Fate of Mammary Luminal Cells and Causes Luminal-to-Basal Mammary Tumor Transformation.” *Oncogene* 32 (22): 2715–25.

Border WA and Noble NA. 1994. “Transforming Growth Factor β in Tissue Fibrosis.” *The New England Journal of Medicine* 331 (19): 1286–92.

Bowen NJ, Walker LD, Matyunina LV, Logani S, Totten KA, Benigno BB, and McDonald JF. 2009. “Gene Expression Profiling Supports the Hypothesis That Human Ovarian Surface Epithelia Are Multipotent and Capable of Serving as Ovarian Cancer Initiating Cells.” *BMC Medical Genomics* 2: 71.

Brand S, Dambacher J, Beigel F, Olszak T, Diebold J, Otte JM, Göke B, and Eichhorst ST. 2005. "CXCR4 and CXCL12 Are Inversely Expressed in Colorectal Cancer Cells and Modulate Cancer Cell Migration, Invasion and MMP-9 Activation." *Experimental Cell Research* 310 (1): 117–30.

Brannstrom M, Giesecke L, Moore IC, and Van Den Heuvel CJ. 1994. "Leukocyte Subpopulations in the Rat Corpus Luteum during Pregnancy and Pseudopregnancy'." *Biology of Reproduction* 50: 1161–67.

Brannstrom M, Pascoe V, Norman RJ, and McClure N. 1994. "Localization of Leukocyte Subsets in the Follicle Wall and in the Corpus Luteum throughout the Human Menstrual Cycle." *Fertility and Sterility* 61 (3): 488–95.

Bray NL, Pimentel H, Melsted P, and Pachter L. 2016. "Near-Optimal Probabilistic RNA-Seq Quantification." *Nature Biotechnology* 34 (5): 525–27.

Briley SM, Jasti S, McCracken JM, Hornick JE, Fegley B, Pritchard MT, and Duncan FE. 2016. "Reproductive Age-Associated Fibrosis in the Stroma of the Mammalian Ovary." *Reproduction* 152 (3): 245–60.

Brown RL, Reinke LM, Damerow MS, Perez D, Chodosh LA, Yang J, and Cheng C. 2011. "CD44 Splice Isoform Switching in Human and Mouse Epithelium Is Essential for Epithelial-Mesenchymal Transition and Breast Cancer Progression." *The Journal of Clinical Investigation* 121 (3): 1064–74.

Burdette JE, Kurley SJ, Kilen SM, Mayo KE, and Woodruff TK. 2006. "Gonadotropin-Induced Superovulation Drives Ovarian Surface Epithelia Proliferation in CD1 Mice." *Endocrinology* 147 (5): 2338–45.

Camden AJ, Szwarc MM, Chadchan SB, DeMayo FJ, O'Malley BW, Lydon JP, and Kommagani R. 2017. "Growth Regulation by Estrogen in Breast Cancer 1 (GREB1) Is a Novel Progesterone-Responsive Gene Required for Human Endometrial Stromal Decidualization." *Molecular Human Reproduction* 23 (9): 646–53.

Chen C, Zhao S, Karnad A, Freeman JW. 2018. "The Biology and Role of CD44 in Cancer Progression: Therapeutic Implications." *Journal of Hematology & Oncology* 11 (1): 64.

Chen L, Xiao Z, Meng Y, Zhao Y, Han J, Su G, Chen B, and Dai J. 2012. "The Enhancement of Cancer Stem Cell Properties of MCF-7 Cells in 3D Collagen Scaffolds for Modeling of Cancer and Anti-Cancer Drugs." *Biomaterials* 33 (5): 1437–44.

Cichy J, and Puré E. 2003. "The Liberation of CD44." *The Journal of Cell Biology* 161 (5): 839–43.

Clark-Knowles KV, Garson K, Jonkers J and Vanderhyden BC. 2007. "Conditional Inactivation of Brca1 in the Mouse Ovarian Surface Epithelium Results in an Increase in Preneoplastic Changes." *Experimental Cell Research* 313 (1): 133–45.

Clark SL, Rodriguez AM, Snyder RR, Hankins GDV and Boehning D. 2012. "Structure-Function Of The Tumor Suppressor BRCA1." *Computational and Structural Biotechnology Journal* 1 (1). https://www.ncbi.nlm.nih.gov/pubmed/22737296.

Cohen PE, Zhu L and Pollard JW. 1997. "Absence of Colony Stimulating Factor-1 in Osteopetrotic (csfmop/csfmop) Mice Disrupts Estrous Cycles and Ovulation." *Biology of Reproduction* 56 (1): 110–18.

Crow J, Amso NN, Lewin J and Shaw RW. 1994. "Physiology: Morphology and Ultrastructure of Fallopian Tube Epithelium at Different Stages of the Menstrual Cycle and Menopause." *Human Reproduction* 9 (12): 2224–33.

Davidson B, Holth A, Hellesylt E, Tan TZ, Huang RYJ, Tropé C, Nesland JM and Thiery JP. 2015. "The Clinical Role of Epithelial-Mesenchymal Transition and Stem Cell Markers in Advanced-Stage Ovarian Serous Carcinoma Effusions." *Human Pathology* 46 (1): 1–8.

Davis BJ, Lennard DE, Lee CA, Tiano HF, Morham SG, Wetsel WE and Langenbach R. 1999.

"Anovulation in Cyclooxygenase-2-Deficient Mice Is Restored by Prostaglandin E2 and Interleukin-1beta." *Endocrinology* 140 (6): 2685–95.

Derynck R and Zhang YE. 2003. "Smad-Dependent and Smad-Independent Pathways in TGF-Beta Family Signalling." *Nature* 425 (6958): 577–84.

Díaz-López A, Moreno-Bueno G and Cano A. 2014. "Role of microRNA in Epithelial to Mesenchymal Transition and Metastasis and Clinical Perspectives." *Cancer Management and Research* 6: 205.

Doherty MR, Cheon H, Junk DJ, Vinayak S, Varadan V, Telli ML, Ford JM, Stark GR and Jackson MW. 2017. "Interferon-Beta Represses Cancer Stem Cell Properties in Triple-Negative Breast Cancer." *Proceedings of the National Academy of Sciences of the United States of America* 114 (52): 13792–97.

Eming SA, Martin P and Tomic-Canic M. 2014. "Wound Repair and Regeneration: Mechanisms, Signaling, and Translation." *Science Translational Medicine* 6 (265): 265sr6.

Fang Y, Wang J, Wang G, Zhou C, Wang P, Zhao S, Zhao S, et al. 2017. "Inactivation of p38 MAPK Contributes to Stem Cell-like Properties of Non-Small Cell Lung Cancer." *Oncotarget* 8 (16): 26702–17.

Fathalla MF. 1971. "Incesssant Ovulation – a Factor in Ovarian Neoplasia?" *Lancet* 2 (7716): 163.

Flesken-Nikitin A, Hwang CI, Cheng CY, Michurina TV, Enikolopov G and Nikitin AY. 2013. "Ovarian Surface Epithelium at the Junction Area Contains a Cancer-Prone Stem Cell Niche." *Nature* 495 (7440): 241–45.

Futagami A, Ishizaki M, Fukuda Y, Kawana S and Yamanaka N. 2002. "Wound Healing Involves Induction of Cyclooxygenase-2 Expression in Rat Skin." *Laboratory Investigation; a Journal of Technical Methods and Pathology* 82 (11): 1503–13.

Gamwell LF, Collins O and Vanderhyden BC. 2012. "The Mouse Ovarian Surface Epithelium Contains a Population of LY6A (SCA-1) Expressing Progenitor Cells That Are Regulated by Ovulation-Associated Factors." *Biology of Reproduction* 87 (4): 80, 1–10.

Gaytán M, Sánchez MA, Morales C, Bellido C, Millán Y, Martín de Las Mulas J, Sánchez-Criado JE and Gaytán F. 2005. "Cyclic Changes of the Ovarian Surface Epithelium in the Rat." *Reproduction* 129 (3): 311–21.

George RJ, Sturmoski MA, Anant S and Houchen CW. 2007. "EP4 Mediates PGE Dependent Cell Survival through the PI3 Kinase/AKT Pathway." *Prostaglandins & Other Lipid Mediators* 83 (1-2): 112–20.

Goren I, Lee SY, Maucher D, Nüsing R, Schlich T, Pfeilschifter J and Frank S. 2015. "Inhibition of Cyclooxygenase-1 and-2 Activity in Keratinocytes Inhibits Pge2 Formation and Impairs Vascular Endothelial Growth Factor Release and Neovascularisation in Skin Wounds." *International Wound Journal* 14 (1): 53–63.

Grande MT, Sánchez-Laorden B, López-Blau C, De Frutos CA, Boutet A, Arévalo M, Rowe RG, Weiss SJ, López-Novoa JM and Nieto MA. 2015. "Snail1-Induced Partial Epithelial-to-Mesenchymal Transition Drives Renal Fibrosis in Mice and Can Be Targeted to Reverse Established Disease." *Nature Medicine* 21 (9): 989–97.

Gumbiner BM and Kim NG. 2014. "The Hippo-YAP Signaling Pathway and Contact Inhibition of Growth." *Journal of Cell Science* 127 (Pt 4): 709–17.

Guo S and Dipietro LA. 2010. "Factors Affecting Wound Healing." *Journal of Dental Research* 89 (3): 219–29.

Guo W, Keckesova Z, Donaher JL, Shibue T, Tischler V, Reinhardt F, Itzkovitz S, et al. 2012. "Slug and Sox9 Cooperatively Determine the Mammary Stem Cell State." *Cell* 148 (5): 1015–28.

Guo X and Wang XF. 2009. "Signaling Cross-Talk between TGF-beta/BMP and Other Pathways." *Cell Research* 19 (1): 71–88.

Hakem R, de la Pompa JL, Sirard C, Mo R, Woo M, Hakem A, Wakeham A, et al. 1996. “The Tumor Suppressor Gene Brca1 Is Required for Embryonic Cellular Proliferation in the Mouse.” *Cell* 85 (7): 1009–23.

Hales DB, Zhuge Y, Lagman JAJ, Ansenberger K, Mahon C, Barua A, Luborsky JL and Bahr JM. 2008. “Cyclooxygenases Expression and Distribution in the Normal Ovary and Their Role in Ovarian Cancer in the Domestic Hen (Gallus Domesticus).” *Endocrine* 33 (3): 235–44.

Hay ED. 1995. “An Overview of Epithelio-Mesenchymal Transformation.” *Cells, Tissues, Organs* 154 (1): 8–20.

Hirano K. Nagata S, Yamaguchi S, Nakagawa M, Okita K, Kotera H, Ainscough J and Tada T. 2012. “Human and Mouse Induced Pluripotent Stem Cells Are Differentially Reprogrammed in Response to Kinase Inhibitors.” *Stem Cells and Development* 21 (8): 1287–98.

Hodgkinson K, Forrest LA, Vuong N, Garson K, Djordjevic B and Vanderhyden BC. 2018. “GREB1 Is an Estrogen Receptor-Regulated Tumour Promoter That Is Frequently Expressed in Ovarian Cancer.” *Oncogene* 37: 5837 – 5886.

Huang R, Wong MK, Tan TZ, Kuay KT, Ng AHC, Chung VY, Chu YS, et al. 2013. “An EMT Spectrum Defines an Anoikis-Resistant and Spheroidogenic Intermediate Mesenchymal State That Is Sensitive to E-Cadherin Restoration by a Src-Kinase Inhibitor, Saracatinib (AZD0530).” *Cell Death & Disease* 4: e915.

Iczkowski KA. 2010. “Cell Adhesion Molecule CD44: Its Functional Roles in Prostate Cancer.” *American Journal of Translational Research* 3 (1): 1–7.

Inman GJ, Nicolás FJ, Callahan JF, Harling JD, Gaster LM, Reith AD, Laping NJ and Hill CS. 2002. “SB-431542 Is a Potent and Specific Inhibitor of Transforming Growth Factor-Beta Superfamily Type I Activin Receptor-like Kinase (ALK) Receptors ALK4, ALK5, and ALK7.” *Molecular Pharmacology* 62 (1): 65–74.

Jayson GC, Kohn EC, Kitchener HC and Ledermann JA. 2014. “Ovarian Cancer.” *The Lancet* 384 (9951): 1376–88.

Jockusch HS, Voigt S and Eberhard D. 2003. “Localization of GFP in Frozen Sections from Unfixed Mouse Tissues: Immobilization of a Highly Soluble Marker Protein by Formaldehyde Vapor.” *The Journal of Histochemistry and Cytochemistry* 51 (3): 401–4.

Johnson J, Canning J, Kaneko T. Pru JK and Tilly JL. 2004. “Germline Stem Cells and Follicular Renewal in the Postnatal Mammalian Ovary.” *Nature* 428 (6979): 145–50.

Jolly MK, Boareto M, Huang B. Jia D, Lu M, Ben-Jacob E, Onuchic JN and Levine H. 2015. “Implications of the Hybrid Epithelial/Mesenchymal Phenotype in Metastasis.” *Frontiers in Oncology* 5: 155.

Jolly MK, Jia D. Boareto M, Mani SA, Pienta KJ, Ben-Jacob E and Levine H. 2015. “Coupling the Modules of EMT and Stemness: A Tunable ‘Stemness Window’ Model.” *Oncotarget* 6 (28): 25161–74.

Joshua B, Kaplan MJ, Doweck I, Pai R, Weissman IL, Prince ME and Ailles LE. 2012. “Frequency of Cells Expressing CD44, a Head and Neck Cancer Stem Cell Marker: Correlation with Tumor Aggressiveness.” *Head & Neck* 34 (1): 42–49.

Kalluri R and Weinberg RA. 2009. “The Basics of Epithelial-Mesenchymal Transition.” *The Journal of Clinical Investigation* 119 (6): 1420–28.

Karin M and Clevers H. 2016. “Reparative Inflammation Takes Charge of Tissue Regeneration.” *Nature* 529 (7586): 307.

Karst AM and Drapkin R. 2012. “Primary Culture and Immortalization of Human Fallopian Tube Secretory Epithelial Cells.” *Nature Protocols* 7 (9): 1755–64.

Kawahara T, Yamashita M, Ikegami K, Nakamura T, Yanagita M, Yamada S, Kitamura M and Murakami S. 2015. “TGF-Beta Negatively Regulates the BMP2-Dependent Early

Commitment of Periodontal Ligament Cells into Hard Tissue Forming Cells." *PloS One* 10 (5): e0125590.

Kim T, Veronese A, Pichiorri F, Lee TJ, Jeon YJ, Volinia S, Pineau P, Marchio A, Palatini J, Suh SS, Alder H, Liu CG, Dejean A and Croce CM. 2011. "p53 Regulates Epithelial-Mesenchymal Transition Through MicroRNAs Targeting ZEB1 and ZEB2." *Journal of Experimental Medicine* 208 (5): 875.

Klonisch T, Wiechec E, Hombach-Klonisch S, Ande SR, Wesselborg S, Schulze-Osthoff K and Los M. 2008. "Cancer Stem Cell Markers in Common Cancers–therapeutic Implications." *Trends in Molecular Medicine* 14 (10): 450–60.

Knight PG and Glister C. 2006. "TGF-β Superfamily Members and Ovarian Follicle Development." *Reproduction* 132 (2): 191–206.

Kondo T and Ishida Y. 2010. "Molecular Pathology of Wound Healing." *Forensic Science International* 203 (1-3): 93–98.

Kruk PA, Uitto VJ, Firth JD, Dedhar S and Auersperg N. 1994. "Reciprocal Interactions between Human Ovarian Surface Epithelial Cells and Adjacent Extracellular Matrix." *Experimental Cell Research* 215 (1): 97–108.

Kujubu DA, Fletcherlln BS, Varnum BC, Lim RW and Herschman HR. 1991. "TIS10, a Phorbol Ester Tumor Promoter-Inducible mRNA from Swiss 3T3 Cells, Encodes a Novel Prostaglandin Synthase/Cyclooxygenase Homologue." *Planning Perspectives: PP* 12866: 12872.

Lamouille S, Subramanyam D, Blelloch R and Derynck R. 2013. "Regulation of Epithelial-Mesenchymal and Mesenchymal-Epithelial Transitions by microRNAs." *Current Opinion in Cell Biology* 25 (2): 200–207.

Lamouille S, Xu J and Derynck R. 2014. "Molecular Mechanisms of Epithelial-Mesenchymal Transition." *Nature Reviews Molecular Cell Biology* 15 (3): 178–96.

Leibovich SJ and Ross R. 1975. "The Role of the Macrophage in Wound Repair. A Study with Hydrocortisone and Antimacrophage Serum." *The American Journal of Pathology* 78 (1): 71.

Leoni G, Neumann PA, Sumagin R, Denning TL and Nusrat A. 2015. "Wound Repair: Role of Immune-Epithelial Interactions." *Mucosal Immunology* 8 (5): 959–68.

Liang WC, Fu WM, Wong CW, Wang Y, Wang WM, Hu GX, Zhang L, et al. 2015. "The lncRNA H19 Promotes Epithelial to Mesenchymal Transition by Functioning as miRNA Sponges in Colorectal Cancer." *Oncotarget* 6 (26): 22513–25.

Lim E, Vaillant F, Wu D, Forrest NC, Pal B, Hart AH, Asselin-Labat ML, et al. 2009. "Aberrant Luminal Progenitors as the Candidate Target Population for Basal Tumor Development in BRCA1 Mutation Carriers." *Nature Medicine* 15 (8): 907–13.

Lim H, Paria BC, Das SK, Dinchuk JE, Langenbach R, Trzaskos JM and Dey SK. 1997. "Multiple Female Reproductive Failures in Cyclooxygenase 2–deficient Mice." *Cell* 91 (2): 197–208.

López-Novoa JM and Nieto MA. 2009. "Inflammation and EMT: An Alliance towards Organ Fibrosis and Cancer Progression." *EMBO Molecular Medicine* 1 (6-7): 303–14.

Lord CJ and Ashworth A. 2016. "BRCAness Revisited." *Nature Reviews. Cancer* 16 (2): 110–20.

Lucas T, Waisman A, Ranjan R, Roes J, Krieg T, Müller W, Roers A and Eming SA. 2010. "Differential Roles of Macrophages in Diverse Phases of Skin Repair." *Journal of Immunology* 184 (7): 3964–77.

Ma L, Young J, Prabhala H, Pan E, Mestdagh P, Muth D, Teruya-Feldstein J, et al. 2010. "miR-9, a MYC/MYCN-Activated microRNA, Regulates E-Cadherin and Cancer Metastasis." *Nature Cell Biology* 12 (3): 247–56.

Mani SA, Guo W, Liao MJ, Eaton EN, Ayyanan A, Zhou AY, Brooks M, et al. 2008. "The Epithelial-Mesenchymal Transition Generates Cells with Properties of Stem Cells." *Cell* 133 (4): 704–15.

McCloskey CW, Goldberg RL, Carter LE, Gamwell LF, Al-Hujaily EM, Collins O, Macdonald EA, et al. 2014. “A New Spontaneously Transformed Syngeneic Model of High-Grade Serous Ovarian Cancer with a Tumor-Initiating Cell Population.” *Frontiers in Oncology* 4: 53, 1–10.

Migone FF, Cowan RG, Williams RM, Gorse KJ, Zipfel WR and Quirk SM. 2016. “In Vivo Imaging Reveals an Essential Role of Vasoconstriction in Rupture of the Ovarian Follicle at Ovulation.” *Proceedings of the National Academy of Sciences of the United States of America* 113 (8): 2294–99.

Mo JS, Park HW and Guan KL. 2014. “The Hippo Signaling Pathway in Stem Cell Biology and Cancer.” *EMBO Reports* 15 (6): 642–56.

Molyneux G, Geyer FC, Magnay FA, McCarthy A, Kendrick H, Natrajan R, Mackay A, et al. 2010. “BRCA1 Basal-like Breast Cancers Originate from Luminal Epithelial Progenitors and Not from Basal Stem Cells.” *Cell Stem Cell* 7 (3): 403–17.

Morel AP, Lièvre M, Thomas C, Hinkal G, Ansieau S and Puisieux A. 2008. “Generation of Breast Cancer Stem Cells through Epithelial-Mesenchymal Transition.” *PloS One* 3 (8): e2888.

Moustakas A, and Heldin CH. 2005. “Non-Smad TGF-Beta Signals.” *Journal of Cell Science* 118 (Pt 16): 3573–84.

Murdoch WJ and Martinchick JF. 2004. “Oxidative Damage to DNA of Ovarian Surface Epithelial Cells Affected by Ovulation: Carcinogenic Implication and Chemoprevention.” *Experimental Biology and Medicine* 229 (6): 546–52.

Murdoch WJ and McDonnel AC. 2002. “Roles of the Ovarian Surface Epithelium in Ovulation and Carcinogenesis.” *Reproduction* 123 (6): 743–50.

Neil JR, Johnson KM, Nemenoff RA and Schiemann WP. 2008. “Cox-2 Inactivates Smad Signaling and Enhances EMT Stimulated by TGF- through a PGE2-Dependent Mechanisms.” *Carcinogenesis* 29 (11): 2227–35.

Ng A and Barker N. 2015. “Ovary and Fimbrial Stem Cells: Biology, Niche and Cancer Origins.” *Nature Reviews. Molecular Cell Biology* 16 (10): 625–38.

Ng A, Tan S, Singh G, Rizk P, Swathi Y, Tan TZ, Huang RYJ, Leushacke M and Barker N. 2014. “Lgr5 Marks Stem/progenitor Cells in Ovary and Tubal Epithelia.” *Nature Cell Biology* 16 (8): 745–57.

Nieto MA, Huang RYJ, Jackson RA and Thiery JP. 2016. “EMT: 2016.” *Cell* 166 (1): 21–45.

Ohtake H, Katabuchi H, Matsuura K and Okamura H. 1999. “A Novel in Vitro Experimental Model for Ovarian Endometriosis: The Three-Dimensional Culture of Human Ovarian Surface Epithelial Cells in Collagen Gels.” *Fertility and Sterility* 71 (1): 50–55.

Pacchiarotti J, Maki C, Ramos T, Marh J, Howerton K, Wong J, Pham J, Anorve S, Chow YC and Izadyar F. 2010. “Differentiation Potential of Germ Line Stem Cells Derived from the Postnatal Mouse Ovary.” *Differentiation; Research in Biological Diversity* 79 (3): 159–70.

Paik DY, Janzen DM, Schafenacker AM, Velasco VS, Shung MS, Cheng D, Huang J, Witte ON and Memarzadeh S. 2012. “Stem-Like Epithelial Cells Are Concentrated in the Distal End of the Fallopian Tube: A Site for Injury and Serous Cancer Initiation.” *Stem Cells* 30: 2487–97.

Peinado H, Olmeda D and Cano A. 2007. “Snail, Zeb and bHLH Factors in Tumour Progression: An Alliance against the Epithelial Phenotype?” *Nature Reviews. Cancer* 7 (6): 415–28.

Pimentel H, Bray NL, Puente S, Melsted P and Pachter L. 2017. “Differential Analysis of RNA-Seq Incorporating Quantification Uncertainty.” *Nature Methods* 14 (7): 687–90.

Pode-Shakked N, Metsuyanim S, Rom-Gross E, Mor Y, Fridman E, Goldstein I, Amariglio N, Rechavi G, Keshet G and Dekel B. 2009. “Developmental Tumourigenesis: NCAM as a Putative Marker for the Malignant Renal Stem/progenitor Cell Population.” *Journal of Cellular and Molecular Medicine* 13 (8b): 1792–1808.

Proia TA, Keller PJ, Gupta PB, Klebba I, Jones AD, Sedic M, Gilmore H, et al. 2011. “Genetic

Predisposition Directs Breast Cancer Phenotype by Dictating Progenitor Cell Fate." *Cell Stem Cell* 8 (2): 149–63.

Puisieux A, Brabletz T and Caramel J. 2014. "Oncogenic Roles of EMT-Inducing Transcription Factors." *Nature Cell Biology* 16 (6).

Radisky ES and Radisky DC. 2010. "Matrix Metalloproteinase-Induced Epithelial-Mesenchymal Transition in Breast Cancer." *Journal of Mammary Gland Biology and Neoplasia* 15 (2): 201–12.

Reid BM, Permuth JB and Sellers TA. 2017. "Epidemiology of Ovarian Cancer: A Review." *Cancer Biology and Medicine* 14 (1): 9–32.

Rodgers LH, Ainmhire EO, Young AN and Burdette JE. 2016. "Loss of PAX8 in High-Grade Serous Ovarian Cancer Reduces Cell Survival despite Unique Modes of Action in the Fallopian Tube and Ovarian Surface Epithelium." *Oncotarget* 7 (22): 32785–95.

Rolfe KJ and Grobbelaar AO. 2012. "A Review of Fetal Scarless Healing." *ISRN Dermatology* 2012: 698034.

Ruff M, Leyme A, Le Cann F, Bonnier D, Le Seyec J, Chesnel F, Fattet L, Rimokh R, Baffet G and Théret N. 2015. "The Disintegrin and Metalloprotease ADAM12 Is Associated with TGF-β-Induced Epithelial to Mesenchymal Transition." *PloS One* 10 (9): e0139179.

Salamanca CM, Maines-Bandiera SL, Leung PCK, Hu YL and Auersperg N. 2004. "Effects of Epidermal Growth Factor/hydrocortisone on the Growth and Differentiation of Human Ovarian Surface Epithelium." *Journal of the Society for Gynecologic Investigation* 11 (4): 241–51.

Savagner P. 2015. "Epithelial-Mesenchymal Transitions: From Cell Plasticity to Concept Elasticity." *Current Topics in Developmental Biology* 112: 273–300.

Savagner P, Kusewitt DF, Carver EA, Magnino F, Choi C, Gridley T and Hudson LG. 2005. "Developmental Transcription Factor Slug Is Required for Effective Re-Epithelialization by Adult Keratinocytes." *Journal of Cellular Physiology* 202 (3): 858–66.

Schmidt JM, Panzilius E, Bartsch HS, Irmler M, Beckers J, Kari V, Linnemann JR, et al. 2015. "Stem-Cell-like Properties and Epithelial Plasticity Arise as Stable Traits after Transient Twist1 Activation." *Cell Reports* 10 (2): 131–39.

Schneider A, Guan YF, Zhang Y, Magnuson MA, Pettepher C, Loftin CD, Langenbach R and Breyer RM. 2004. "Generation of a Conditional Allele of the Mouse Prostaglandin EP Receptor." *Genesis* 40: 7–14.

Shaw TJ and Martin P. 2016. "Wound Repair: A Showcase for Cell Plasticity and Migration." *Current Opinion in Cell Biology* 42: 29–37.

Shintani Y, Maeda M, Chaika N, Johnson KR and Wheelock MJ. 2008. "Collagen I Promotes Epithelial-to-Mesenchymal Transition in Lung Cancer Cells via Transforming Growth Factor-Beta Signaling." *American Journal of Respiratory Cell and Molecular Biology* 38 (1): 95–104.

Singavarapu R, Buchinsky N, Cheon DJ, Orsulic S. 2010. "Whole Ovary Immunohistochemistry for Monitoring Cell Proliferation and Ovulatory Wound Repair in the Mouse." *Reproductive Biology and Endocrinology: RB&E* 8: 98.

Smith WL, DeWitt DL and Garavito RM. 2000. "Cyclooxygenases: Structural, Cellular, and Molecular Biology." *Annual Review of Biochemistry* 69: 145–82.

Starita LM and Parvin JD. 2003. "The Multiple Nuclear Functions of BRCA1: Transcription, Ubiquitination and DNA Repair." *Current Opinion in Cell Biology* 15 (3): 345–50.

Stewart CA and Behringer RR. 2012. "Mouse Oviduct Development." *Results and Problems in Cell Differentiation* 55: 247–62.

Sugimoto Y and Narumiya S. 2007. "Prostaglandin E Receptors." *Journal of Biological Chemistry* 282 (16): 11613–17.

Suster NK, Smrkolj S and Virant-Klun I. 2017. “Putative Stem Cells and Epithelial-Mesenchymal Transition Revealed in Sections of Ovarian Tumor in Patients with Serous Ovarian Carcinoma Using Immunohistochemistry for Vimentin and Pluripotency-Related Markers.” *Journal of Ovarian Research* 10 (1): 11.

Szotek PP, Chang HL, Brennand K, Fujino A, Pieretti-Vanmarcke R, Lo Celso C, Dombkowski D, et al. 2008. “Normal Ovarian Surface Epithelial Label-Retaining Cells Exhibit Stem/progenitor Cell Characteristics.” *Proceedings of the National Academy of Sciences of the United States of America* 105 (34): 12469–73.

Takaishi S, Okumura T, Tu S, Wang SSW, Shibata W, Vigneshwaran R, Gordon SAK, Shimada Y and Wang TC. 2009. “Identification of Gastric Cancer Stem Cells Using the Cell Surface Marker CD44.” *Stem Cells* 27 (5): 1006–20.

Tan OL and Fleming JS. 2004. “Proliferating Cell Nuclear Antigen Immunoreactivity in the Ovarian Surface Epithelium of Mice of Varying Ages and Total Lifetime Ovulation Number Following Ovulation.” *Biology of Reproduction* 71 (5): 1501–7.

Tan TZ, Miow QH, Miki Y, Noda T, Mori S, Huang RYJ and Thiery JP. 2014. “Epithelial-Mesenchymal Transition Spectrum Quantification and Its Efficacy in Deciphering Survival and Drug Responses of Cancer Patients.” *EMBO Molecular Medicine* 6 (10): 1279–93.

Tessner TG, Muhale F, Riehl TE, Anant S and Stenson WF. 2004. “Prostaglandin E2 Reduces Radiation-Induced Epithelial Apoptosis through a Mechanism Involving AKT Activation and Bax Translocation.” *The Journal of Clinical Investigation* 114 (11): 1676–85.

Thériault BL, Shepherd TG, Mujoomdar ML and Nachtigal MW. 2007. “BMP4 Induces EMT and Rho GTPase Activation in Human Ovarian Cancer Cells.” *Carcinogenesis* 28 (6): 1153–62.

Thiery JP, Acloque H, Huang RYJ and Nieto MA. 2009. “Epithelial-Mesenchymal Transitions in Development and Disease.” *Cell* 139 (5): 871–90.

Thiery JP and Sleeman JP. 2006. “Complex Networks Orchestrate Epithelial-Mesenchymal Transitions.” *Nature Reviews Molecular Cell Biology* 7 (2): 131–42.

Tian Y, Pan Q, Shang Y, Zhu R, Ye J, Liu Y, Zhong X, et al. 2014. “MicroRNA-200 Cluster Regulation by Ascl2: Impact on the Epithelial-Mesenchymal Transition in Colon Cancer Cells.” *The Journal of Biological Chemistry* 289 (52): 36101 – 36115.

Tonary AM, Macdonald EA, Faught W, Senterman MK and Vanderhyden BC. 2000. “Lack of Expression of c-KIT in Ovarian Cancers Is Associated with Poor Prognosis.” *International Journal of Cancer* 89 (3): 242–50.

Turner N, Tutt A and Ashworth A. 2004. “Hallmarks of ‘BRCAness’ in Sporadic Cancers.” *Nature Reviews. Cancer* 4 (10): 814–19.

Varelas X, Samavarchi-Tehrani P, Narimatsu M, Weiss A, Cockburn K, Larsen BG, Rossant J and Wrana JL. 2010. “The Crumbs Complex Couples Cell Density Sensing to Hippo-Dependent Control of the TGF-β-SMAD Pathway.” *Developmental Cell* 19 (6): 831–44.

Verdoodt F, Kjaer SK and Friis S. 2017. “Influence of Aspirin and Non-Aspirin NSAID Use on Ovarian and Endometrial Cancer: Summary of Epidemiologic Evidence of Cancer Risk and Prognosis.” *Maturitas* 100: 1–7.

Virant-Klun I, Rozman P, Cvjeticanin B. Vrtacnik-Bokal E, Novakovic S, Rülicke T, Dovc P and Meden-Vrtovec H. 2009. “Parthenogenetic Embryo-like Structures in the Human Ovarian Surface Epithelium Cell Culture in Postmenopausal Women with No Naturally Present Follicles and Oocytes.” *Stem Cells and Development* 18 (1): 137–49.

Virant-Klun I, Skutella T, Stimpfel M and Sinkovec J. 2011. “Ovarian Surface Epithelium in Patients with Severe Ovarian Infertility: A Potential Source of Cells Expressing Markers of Pluripotent/multipotent Stem Cells.” *Journal of Biomedicine & Biotechnology* 2011: 381928.

Virant-Klun I, Zech N, Rozman P, Vogler A, Cvjeticanin B, Klemenc P, Malicev E and Meden-

Vrtovec H. 2008. “Putative Stem Cells with an Embryonic Character Isolated from the Ovarian Surface Epithelium of Women with No Naturally Present Follicles and Oocytes.” *Differentiation; Research in Biological Diversity* 76 (8): 843–56.

Vuong NH, Cook DP, Forrest LA, Carter LE, Robineau-Charette P, Kofsky JM, Hodgkinson KM and Vanderhyden BC. 2018. “Single-Cell RNA-Sequencing Reveals Transcriptional Dynamics of Estrogen-Induced Dysplasia in the Ovarian Surface Epithelium.” *PLoS Genetics* 14:11.

Wang WM, Lee S, Steiglitz BM, Scott IC, Lebares CC, Allen ML, Brenner MC, Takahara K and Greenspan DS. 2003. “Transforming Growth Factor-β Induces Secretion of Activated ADAMTS-2: A Procollagen III N-Proteinase.” *The Journal of Biological Chemistry* 278 (21): 19549–57.

Wang Y, Sacchetti A, van Dijk MR, van der Zee M, van der Horst PH, Joosten R. Burger CW, Grootegoed JA, Blok LJ and Fodde R. 2012. “Identification of Quiescent, Stem-like Cells in the Distal Female Reproductive Tract.” *PloS One* 7 (7): e40691.

Warzecha CC and Carstens RP. 2012. “Complex Changes in Alternative Pre-mRNA Splicing Play a Central Role in the Epithelial-to-Mesenchymal Transition (EMT).” *Seminars in Cancer Biology* 22 (5-6): 417–27.

White YAR, Woods DC, Takai Y, Ishihara O, Seki H and Tilly JL. 2012. “Oocyte Formation by Mitotically Active Germ Cells Purified from Ovaries of Reproductive-Age Women.” *Nature Medicine* 18 (3): 413–21.

Wilgus TA, Bergdall VK, Tober KL, Hill KJ, Mitra S, Flavahan NA and Oberyszyn TM. 2004. “The Impact of Cyclooxygenase-2 Mediated Inflammation on Scarless Fetal Wound Healing.” *The American Journal of Pathology* 165 (3): 753–61.

Wilgus TA, Vodovotz Y, Vittadini E, Clubbs EA and Oberyszyn TM. 2003. “Reduction of Scar Formation in Full-Thickness Wounds with Topical Celecoxib Treatment.” *Wound Repair and Regeneration* 11 (1): 25–34.

Xu J, Lamouille S and Derynck R. 2009. “TGF-β-Induced Epithelial to Mesenchymal Transition.” *Cell Research* 19 (2): 156–72.

Zamah AM, Hassis ME, Albertolle ME and Williams KE. 2015. “Proteomic Analysis of Human Follicular Fluid from Fertile Women.” *Clinical Proteomics* 12 (1): 5.

Zavadil J, Cermak L, Soto-Nieves N and Böttinge EP. 2004. “Integration of TGF-β/Smad and Jagged1/Notch Signalling in Epithelial-to-mesenchymal Transition.” *The EMBO Journal* 23 (5): 1155–65.

Zhou F, Shi LB and Zhang SY. 2017. “Ovarian Fibrosis: A Phenomenon of Concern.” *Chinese Medical Journal* 130 (3): 365–71.

Zhu Y, Nilsson M and Sundfeldt K. 2010. “Phenotypic Plasticity of the Ovarian Surface Epithelium: TGF-Beta 1 Induction of Epithelial to Mesenchymal Transition (EMT) in Vitro.” *Endocrinology* 151 (11): 5497–5505.

Zou K, Yuan Z, Yang Z, Luo H, Sun K, Zhou L, Xiang J, et al. 2009. “Production of Offspring from a Germline Stem Cell Line Derived from Neonatal Ovaries.” *Nature Cell Biology* 11 (5): 631–36.

Zou K, Yuan Z, Yang Z, Luo H, Sun K, Zhou L, Xiang J, et al. 2009. “Production of Offspring from a Germline Stem Cell Line Derived from Neonatal Ovaries.” *Nature Cell Biology* 11 (5): 631–36.